Study of Molecular Order and Dynamics in Calamitic and Discotic Liquid Crystals by ^{2}H NMR

BY

XIAODONG SHEN

A Thesis

Submitted to the Faculty of Graduate Studies

in Partial Fulfillment of the Requirements

for the Degree of

DOCTOR OF PHILOSOPHY

Department of Physics and Astronomy

The University of Manitoba

© August, 1998

National Library
of Canada

Bibliothèque nationale
du Canada

Acquisitions and
Bibliographic Services

Acquisitions et
services bibliographiques

395 Wellington Street
Ottawa ON K1A 0N4
Canada

395, rue Wellington
Ottawa ON K1A 0N4
Canada

0-612-32889-9

Canada

THE UNIVERSITY OF MANITOBA

FACULTY OF GRADUATE STUDIES
*****
COPYRIGHT PERMISSION PAGE

STUDY OF MOLECULAR ORDER AND DYNAMICS
IN CALAMITIC AND DISCOTIC LIQUID CRYSTALS
BY ^{2}H NMR

BY

XIAODONG SHEN

A Thesis/Practicum submitted to the Faculty of Graduate Studies of The University

of Manitoba in partial fulfillment of the requirements of the degree

of

DOCTOR OF PHILOSOPHY

Shen Xiaodong   ©1998

Abstract

Deuterium nuclear magnetic resonance (NMR) spectroscopy was used to explore molecular motions in the mesophases of calamatic liquid crystals $4-n-$pentyloxybenzylidene$-4'-$heptylaniline(5O.7), p-(methoxybenzylidine)-p-n-butylaniline(MBBA or 1O.4), 4-n-hexyloxy-4'-cyanobiphenyl (6OCB), a mixture of 6OCB and 4-n-octyloxy-4'-cyanobiphenyl (8OCB), and discotic liquid crystals hexakis(n-hexyloxy)triphenylene(HAT6). The Zeeman and quadrupolar spin$-$lattice relaxation times were measured as a function of temperature at 15.1 MHz and 46 MHz using a broadband multiple$-$pulse sequence. In addition, quadrupolar splittings were measured for 6OCB, 6OCB/8OCB mixture and columnar phase of HAT6. The TZ model was used to interpret the deuteron relaxation of biaxial molecules in the uniaxial medium. For 5O.7, the analysis of the relaxation data in the nematic and smectic A phases supports a model which includes director fluctuations and rotational diffusion of an asymmetric rigid rotor in a biaxial potential of mean torque. The molecular biaxiality of the molecule is found, based on the relaxation data, to give a small positive molecular biaxial order parameter $S_{xx} - S_{yy}$. In addition, the activation energy for the tumbling motion of the molecule is found to be larger than that for the spinning motion. For MBBA, the zero-frequency spectral densities $J_0(0)$ data is quantitatively interpreted using a model that includes director fluctuations and rotational diffusion of symmetric rotors in a nematic phase. The contribution to $J_0(0)$ from director fluctuations has mainly a second-order component, whereas the first-order contribution to $J_1(\omega)$ is suppressed in the megahertz region(Larmor frequencies are 15.1 and 46 MHz) due to the high-frequency cutoff, which is estimated to be around 3-10 MHz for MBBA. For 6OCB and 6OCB/8OCB mixture, the data analyses were carried out for both samples in order to achieve a consistent physical picture. The additive potential method is employed to model the quadrupolar

splittings of 6OCB, from which the potential of mean torque is parametrized, and the order parameter tensor for an "average" conformer is determined. A decoupled model is used to describe correlated internal motions of the end chain, which are independent of the molecular reorientation. The latter motion is treated using the small-step rotational diffusion model of Tarroni and Zannoni, while the former motion is described using a master rate equation. In comparing the NMR results of the pure 6OCB sample and of the 6OCB/8OCB mixture, both the dynamic and static behaviours appear to be similar, and there are no dramatic changes upon entering the reentrant nematic phase of 6OCB/8OCB, supporting the belief that the effects driving the reentrancy in this mixture are very subtle. The tumbling motion of 6OCB molecules shows quite different behaviours in the two studied samples. Both 6OCB and 8OCB possess a strong terminal electric dipole and tend to form "loose" dimers. The degree of dimerization can be inferred from the tumbling motion of 6OCB molecules and their internal chain dynamics. For discotic HAT6, a similar analysis procedure to 6OCB was carried out in the columnar phase. It is found that the tumbling motion of the molecular core is slightly faster than its spinning motion, in contrast with the findings in the calamitic liquid crystals. The decoupled model of Dong for correlated internal rotations in the end chains is used for the first time in a discotic liquid crystal. The usefullness of the global target analysis approach was demonstrated throughout this thesis.

Acknowledgments

Table of Contents

List of Tables

List of Figures

Chapter 1

Introduction to Liquid Crystals and Thesis Outline

1.1 Introduction

Liquid crystals are those compounds exhibiting more than one transition in passing from solid to liquid. For this reason they are known to show mesophases, from the Greek word mesos meaning middle. The earlier discoveries of these kinds of materials were near the end of 19th century(Reinitzer and Lehmann[1.1]). An essential requirement for mesomorphism is that the molecule must be highly anisotropic in its geometry. In those mesophases between the solid state and liquid state, the molecules show some degree of orientational order and/or positional order. The liquid crystalline phases possess liquid properties, like fluidity, etc., and solid features such as birefringence and other anisotropic properties.

The organic molecules which are to be investigated in this thesis have a rod-like or disk-like shape and form different liquid crystal phases. They usually consist of a rigid core to which flexible chains

are attached. The liquid crystalline phases are classified according to the molecular ordering. The nematic phase is the most common phase in liquid crystals, which is mainly encountered in this study. The smectic A phase is also studied. It is noted that both nematic and smectic A phases are uniaxial phases, that is, only one phase symmetry axis exists. Discotic liquid crystals form more ordered phases known as columnar phases, although discotic nematic phases may exist.

1.2 Classification of Mesophases Involved in the Present Study

Nematic Phase:

This nematic phase has the lowest ordering of all the mesophases and, if present, precedes the transition to the isotropic liquid at the clearing point. The molecules making up the nematic phase are arranged in such a manner that there is no positional order of their centers of mass, like in the isotropic liquid, but is characterized by the presence of a long range orientational order, in which the molecules tend to align parallel to each other. The molecules tend to orient on the average along a preferred direction within a large cluster of molecules. The prefered direction defines a symmetry axis called the director $\vec{n}$.

Smectic Phase:

In smectic phases, molecules not only have the long range orientational order, but also possess a certain degree of translational ordering resulting in a layered structure. The molecular centers of mass are, on the average, arranged in equidistant planes. There exist several different types of smectic phases, labelled S_A, S_B, ..., S_I. The most common type is smectic A, which is studied in this thesis. In the smectic A phase, the molecules within the layer are on the average aligned parallel to the layer's normal.

Reentrant Nematic Phase:

There is a special nematic phase called reentrant nematic phase. Some samples, when cooling down from the isotropic phase, possess two or more nematic phases, with one or more smectic phase(s) in between. The reentrant nematic phase refers to the lower temperature phase below a more ordered phase like smectic A. The 6OCB/8OCB mixture sample, for the composition ranging between approximately 25 and 31 wt. % 6OCB, exhibits a reentrant nematic (RN) phase at atmospheric pressure, i.e., one observes a transition from the smectic A phase to a nematic phase on either heating or cooling the system. The collective packing of the chains, which enhances the stability of the S_A phase, is frustrated in a reentrant phase.

Discotic Phase:

Liquid crystal phases exist also in systems composed of disk-like molecules. The columnar mesophases are built up with bi-dimensional central rigid part, in contrast with the rod-like mesophases. The first evidence of existence of discotic liquid crystals was reported by S. Chandrasekhar[1.2] in 1977. The diamagnetic susceptibility tensor $\tilde{\chi}$ in a uniaxial medium has two principal components $\chi_\parallel$ and $\chi_\perp$, which are along and normal to the director, respectively. The diamagnetic susceptibility anisotropy $\Delta\chi(= \chi_\parallel - \chi_\perp)$ is positive for most rod-like molecules resulting in the director being aligned parallel to the external magnetic field, whereas the discotics have negative $\Delta\chi$ such that the director is aligned perpendicular to the external magnetic field.(see the next section)

1.3 Effects of External Fields on Liquid Crystals

The diamagnetic susceptibility anisotropy $\Delta\chi = \chi_\parallel - \chi_\perp$ can be associated primarily with the

3

π electrons of the aromatic rings, so the diamagnetism is particularly strong when the molecule contains an aromatic core. When those molecules are placed in a magnetic $\vec{B}$ field, it costs less energy for the magnetic field to lie in the plane of the ring. In this case, the nematogen has a positive diamagnetic susceptibility anisotropy. The magnetic contribution to the Gibbs free energy density[1.3] is

$$ f_m = -\frac{1}{2\mu_0}\chi_- B^2 - \frac{1}{2\mu_0}\Delta\chi \left(\hat{n} \cdot \vec{B}\right)^2 \tag{1.1} $$

Hence, if $\Delta\chi > 0$, the magnetic free energy density is minimized when the director is colinear with the $\vec{B}$ field. When $\Delta\chi < 0$, the director is aligned normal to the $\vec{B}$ field in order to minimize the magnetic free energy density.

Consider the competing effects of a wall (surface alignment) and of a magnetic field on the alignment of a nematic sample. Deformation of surface alignment away from the wall in the presence of a homogeneous magnetic field can take place over a characteristic distance ξ, which is a measure of the length of the region over which the orientation changes from parallel to perpendicular when the $\vec{B}$ field is normal to the wall surface. Near the wall there is a transition layer in which the director undergoes elastic deformations, which are described by elastic constants splay (K_{11}), twist (K_{22}) and bend (K_{33}) in the Oseen-Frank theory of nematics[1.4, 1.5]. The equilibrium configuration is determined by minimizing the free energy density, then the "coherence length" ξ is given by[1.6]

$$ \xi = \left(\frac{\mu_0 K}{\Delta\chi}\right)^{1/2} \frac{1}{B} \tag{1.2} $$

where K is some average of K_{11}, K_{22} and K_{33}. The static distortions in liquid crystals are due to the response of bulk samples to external disturbances. Now it is appropriate to regard the liquid crystal as a continuum medium with curvature elasticity. Deformational fluctuations in liquid crystals are described by a director field $\hat{n}(\vec{r})$. The average (macroscopic) director $\hat{n}_0$ is simply the spatial

4

average $<\hat{n}(\vec{r})>$. Three fundamental deformations are illustrated in Fig. 1.1. At any point $\vec{r}$ in the liquid crystal sample, a coordinate system with its Z_D axis along $\hat{n}_0$ is chosen. The local director $\hat{n}(\vec{r})$ may be expressed as $\hat{n}_0 + \delta \vec{n}$ with $\delta \vec{n}$ being given by two small components $n_x(\vec{r})$ and $n_y(\vec{r})$ along the X_D and Y_D axis, respectively. The six components of curvature strain at this point are defined by

$$
\begin{aligned}
a_1 &= \frac{\partial n_x}{\partial x}. & a_5 &= \frac{\partial n_y}{\partial y}. \\
a_2 &= \frac{\partial n_x}{\partial y}. & a_4 &= \frac{\partial n_y}{\partial x}. \\
a_3 &= \frac{\partial n_x}{\partial z}. & a_6 &= \frac{\partial n_y}{\partial z}.
\end{aligned}
\tag{1.3}
$$

The splay (K_{11}) deformation is described by a_1 and a_5 and gives a nonzero $\nabla \cdot \hat{n}(\vec{r})$: the twist ($K_{22}$) deformation is described by a_2 and a_4 and gives a nonzero $\hat{n}(\vec{r}) \cdot \nabla \times \hat{n}(\vec{r})$: the bend ($K_{33}$) deformation is described by a_3 and a_6 and gives a nonzero $\hat{n}(\vec{r}) \times [\nabla \times \hat{n}(\vec{r})]$. The Fourier transformations of $n_x(\vec{r})$ and $n_y(\vec{r})$ are

$$
n_\alpha(\vec{r}) = \frac{1}{V} \sum_{\vec{q}} n_\alpha(\vec{q}) \exp[-i\vec{q} \cdot \vec{r}]
\tag{1.4}
$$

where V is the sample volume and the mode amplitudes are

$$
n_\alpha(\vec{q}) = \int n_\alpha(\vec{r}) \exp[i\vec{q} \cdot \vec{r}] d^3r
\tag{1.5}
$$

The $n_\alpha(\vec{q})$ are transverse modes responsible for bringing the instantaneous director $\hat{n}$ to its equilibrium orientation. They relax with exponential damping[1.10, 1.11] according to

$$
\frac{\partial}{\partial t} n_\alpha(\vec{q}) = -\frac{1}{\tau_\alpha(\vec{q})} n_\alpha(\vec{q})
\tag{1.6}
$$

where $\alpha = 1, 2$ and the time constants $\tau_\alpha(\vec{q})$ are proportional to the viscosities $\eta_\alpha(\vec{q})$ which depend on the wave vector $\vec{q}$ and are closely related to the twist viscosity.

5
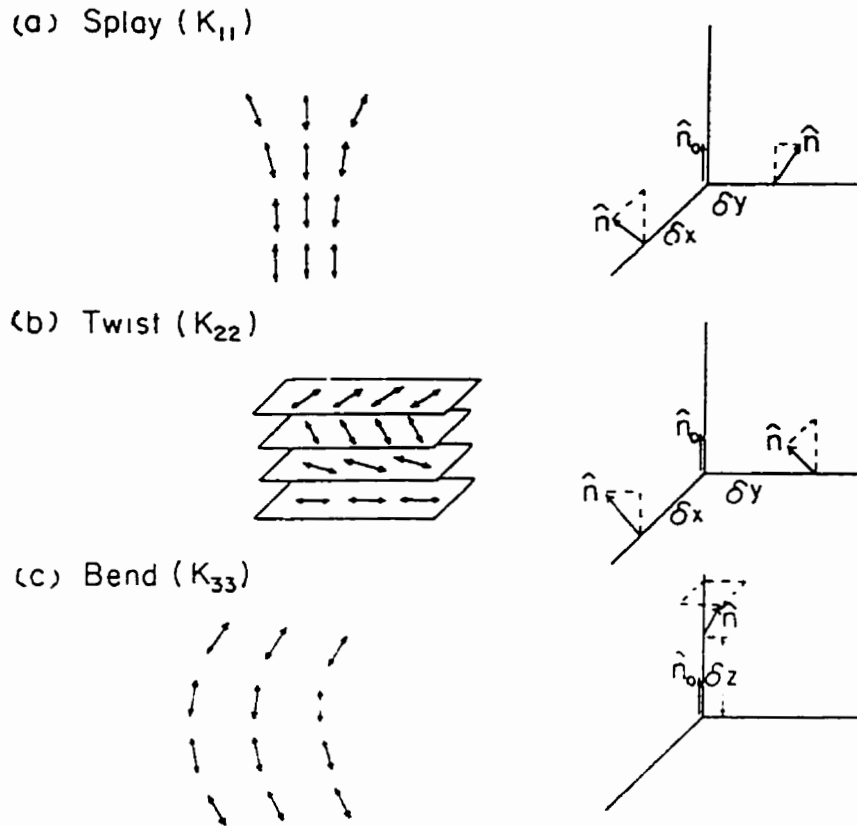
Figure 1.1 Three types of deformation in a director field (a) splay, (b) twist, and (c) bend. The double arrows are used to emphasize the apolar nature of nematics. $\hat{n}_0$ is chosen along the Z_D axis of the director frame.

1.4 Liquid Crystal Samples

The following liquid crystalline solvents are used

(1) 5O.7-d_1 and 5O.7-d_4:

4-n-pentyloxybenzylidene-d_1-4$'$-heptylaniline

4-n-pentyloxybenzylidene-4$'$-heptylaniline-2,3,5,6-d_4 (see Fig. 1.2)

5O.7-d_1 was purchased from Merck Sharp and Dohme Canada Ltd. in Montreal, and 5O.7-d_4 was kindly provided by Dr. J. W. Doane, Kent State University, U.S.A.. Those 2 samples were used without further purification.

(a)

(b)
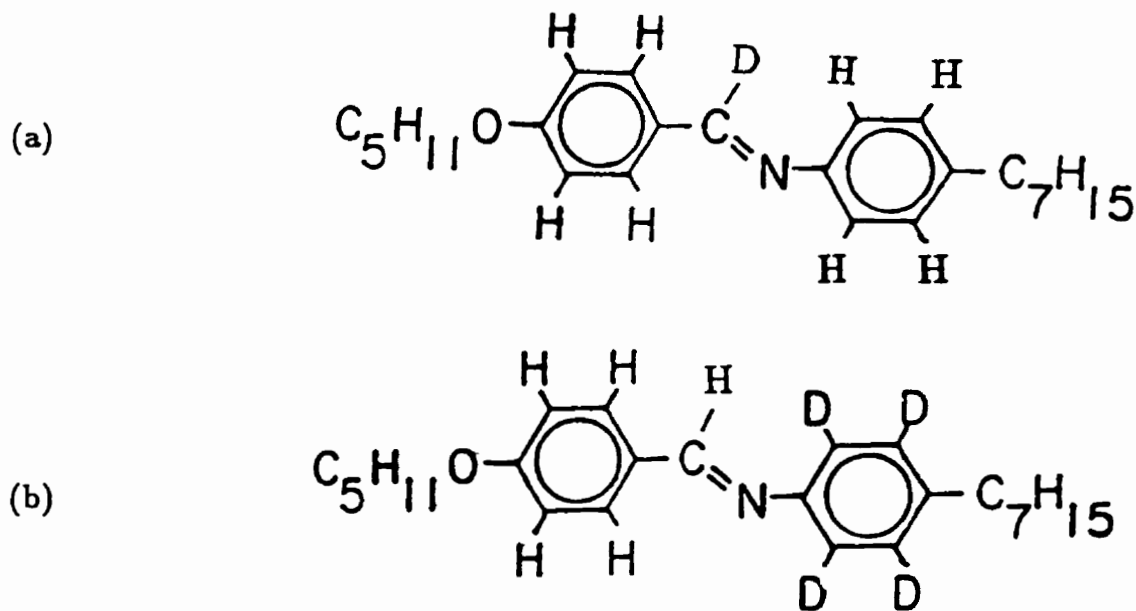
Figure 1.2 The molecular structure of (a) 5O.7-d_1 and (b) 5O.7-d_4.

For NMR studies of liquid crystals[1.7], deuterons have often been used as spin probes to measure the Zeemen(T_{1Z}) and quadrupolar (T_{1Q}) spin-lattice relaxation times. These two relaxation times

7

can be simultaneously determined in a Jeener-Broekaert type[1.8 and see Chapter 2] experiment and allow a seperation of the two spectral densities of motion $J_1(\omega_0)$ and $J_2(2\omega_0)$, where $\omega/2\pi$ is the Larmor frequency. On the other hand, these spectral densities can be calculated for liquid crystals using a model which employs a rotational diffusion mechanism as well as a relaxation mechanism due to director fluctuations[see Chapter 5]. The rotational diffusion model[1.9, 1.10] assumes a stochastic Markov process for molecular reorientation in which each molecule moves in time as a sequence of small angular steps caused by collisions with its neighboring molecules and under the influence of an anisotropic potential set up by these neighbors. Nordio and co-works[1.10] considered reorientation of cylindrical molecules in uniaxial phases. Each molecule is characterized by a rotational diffusion tensor $\overline{D}$, normally defined in a frame fixed on the molecule. The principal components of $\overline{D}$ are $D_x = D_y$ and D_z. A number of models of increasing complexity has been proposed[1.11-1.15] for rigid molecules reorienting in uniaxial and biaxial liquid crystalline phases. As an extension to the Nordio model, reorientation of asymmetric molecules in uniaxial phases has been considered by several groups, including the rigorous treatment by Tarroni and Zannoni[1.13]. However, applications of the latter theoretical model to interpret NMR data remain scarce[1.12]. In order to address this problem in liquid crystal, we consider the experimental data[1.16] of 4-n-pentyloxybenzylidene-4′-heptylaniline (50.7). The data were analyzed previously based on either the third-rate model[1.17] or Nordio model[1.10]. The deuteration of 50.7 samples at methine and aniline ring sites allows us to treat the molecule as a "rigid" rotor. As a result of the present work[see Chapter 7], the analysis of the relaxation data in the nematic and smectic A phases of 50.7 supports a model which includes director fluctuations and rotational diffusion of an asymmetric rigid rotor in a potential of mean torque which reflects the molecular biaxiality. The molecule is found, based on the relaxation data, to show a small positive order parameter $S_{yy} - S_{xx}$.

(2) MBBA-d_{13} (or 10.4):

p-(methoxybenzylidine)-p-n-butylaniline (see Fig. 1.3)

This MBBA sample was purchased from Merck Sharp and Dohme Canada Ltd. and used without

further purification.
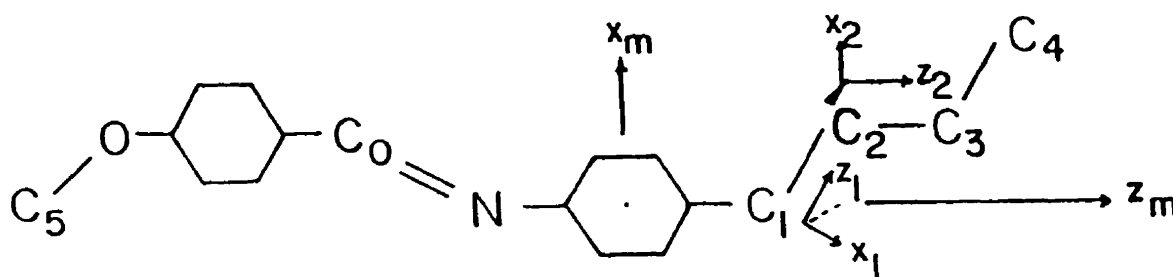
Figure 1.3 The molecular structure of MBBA, showing the carbon labelling.

Director fluctuations are unique and important sources of nuclear spin relaxation in liquid crystals[1.7, 1.18 and see Chapter 5]. These fluctuations involve collective motions of a large number of molecules. Studies of director fluctuations can provide information on molecular properties such as elastic constants and viscosities. This dynamic process was fisrt used to explain light scattering experiments in liquid crystals by Chatelain[1.19]. de Gennes[1.20] was first to recognize that director fluctuations consists of long-range collective modes of motion in liquid crystals. Pincus[1.21] derived a $\omega^{1/2}$ frequency relation for the nuclear spin-lattice relaxation rate. Lubensky[1.22] noted the square of the nematic order parameter in the spin-lattice relaxation rate. When using a small angle (θ) approximation, where θ is the angle between the instantaneous director and its equilib-

rium orientation, the director fluctuations contribute a $\omega^{1/2}$ term in the spectral density $J_1(\omega)$ and have zero contributions in $J_2(2\omega)$ and $J_0(0)$. Whereas for the second order director fluctuations ($\propto \theta^2$), the frequency dependence in J_2 is calculated to be generally small, but J_0 is predicated to be quite large as $\omega \to 0$[1.23]. Although director fluctuations normally give small contributions in the megahertz region, there are at least two liquid crystals 5O.7[see Chapter 7] and 4O.8[1.24] in which director fluctuations have been used to account for part of $J_1(\omega)$. For these two liquid crystals, the high-frequency cutoffs appear to be on the order of 10^2 MHz, while for p-(methoxybenzylidine)-p-n-butylaniline (MBBA or 1O.4), there is no detectable contribution from director fluctuations to the deuteron spin-lattice relaxation in the megahertz region[1.25]. The same conclusion was made by Vilfan et al.[1.26] on the basis of their proton NMR study. The spin-spin relaxation data of MBBA show, however, that there is a substantial contribution from director fluctuations to $J_0(0)$. We believe that a possible explanation of the different behaviours among the studied liquid crystals of $nO.m$ series may due to their high-frequency cutoffs, which has motivated us to measure the spin-spin relaxation time T_2 by the modified Carr-Purcell pulse sequence[see Chapter 2]. In combination with J_1 and J_2, the experimental J_0 values can be obtained[see Chapter 2]. Our T_1 and T_2 data support the idea that MBBA has a relative low value for the high-frequency cutoff (around 3-10 MHz). The contribution to $J_0(0)$ from director fluctuations has mainly a second-order component($35\% - 50\%$), whereas the first-order contribution to $J_1(\omega)$ is suppressed in the megahertz region($< 10\%$) since our Larmor frequencies are 15.3 and 46MHz.

(3) 6OCB-d_{21} and 6OCB/8OCB mixture

4-n-hexyloxy-4'-cyanobiphenyl (6OCB) (see Fig. 1.4)

4-n-octyloxy-4'-cyanobiphenyl (8OCB)

The 6OCB-d_{21} was purchased from Merck, Sharp and Dohme Canada and used without further purification. The 6OCB/8OCB mixture has 28 wt. % of 6OCB. They were put together, melt thoroughly and evenly, de-gased and sealed.
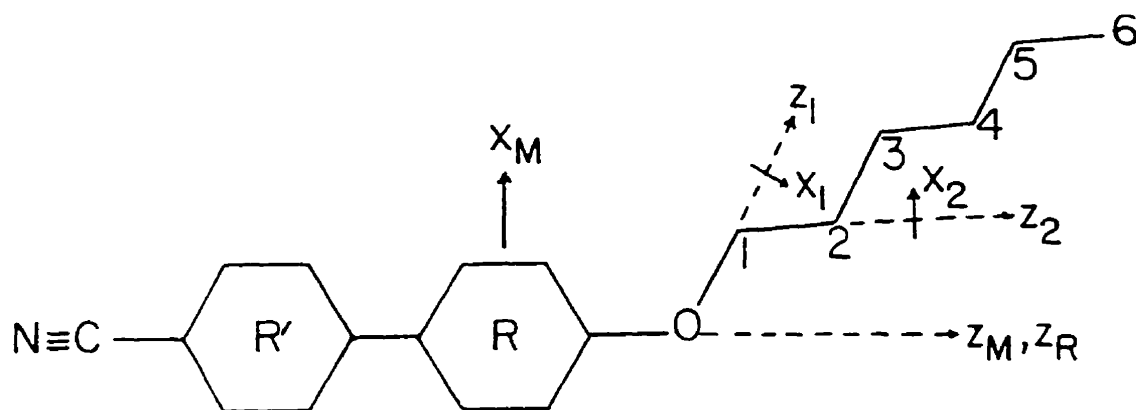
Figure 1.4 Schematic diagram of a 6OCB molecule and various coordinate systems used.

The constituent molecules of liquid crystals usually contain an aromatic core and one or more flexible pendant chains. Marcelja[1.27] was first to explicitly consider flexible end chains in the ordering process resulting from the molecular field of neighbour molecules, since the alkyl chains not only occupy space but also contribute to the anisotropic potential and interactions which are responsible for molecular ordering in liquid crystals. Deuterium NMR spectroscopy is also a powerful technique on providing valuable information on dynamical processes in liquid crystals, which include not only the molecular reorientations and collective motions known as director fluctuations, but also the internal rotations[1.28-1.31]. The molecular core is assumed to be relatively massive such that the internal bond rotations in the chain can be treated independent of the overall motion of the molecule, the so called decoupled model[1.29]. In order to test this model for longer alkyl chains in molecules, we chose the pure 6OCB and 6OCB/8OCB mixture with 28 wt. % of 6OCB. The pure

6OCB sample shows only a nematic phase, while the latter sample shows a nematic, smectic A and reentrant-nematic (RN) phases. We have carried out data analyses for both samples in order to achieve a consistent physical picture. In comparing the NMR results of pure 6OCB sample and of the 6OCB/8OCB mixture, both the dynamic and static behaviors appear to be similar, and there are no dramatic changes upon entering the RN phase of 6OCB/8OCB, supporting the belief that the effects driving the reentrancy in this mixture are very subtle. The tumbling motion of 6OCB molecules, however, shows quite different behaviors in the two studied samples. Both 6OCB and 8OCB possess a strong terminal dipole and tend to form "loose" dimers. The hope that the degree of dimerization may be inferred from the tumbling motion of 6OCB molecules and their internal chain dynamics is realized in the present study.
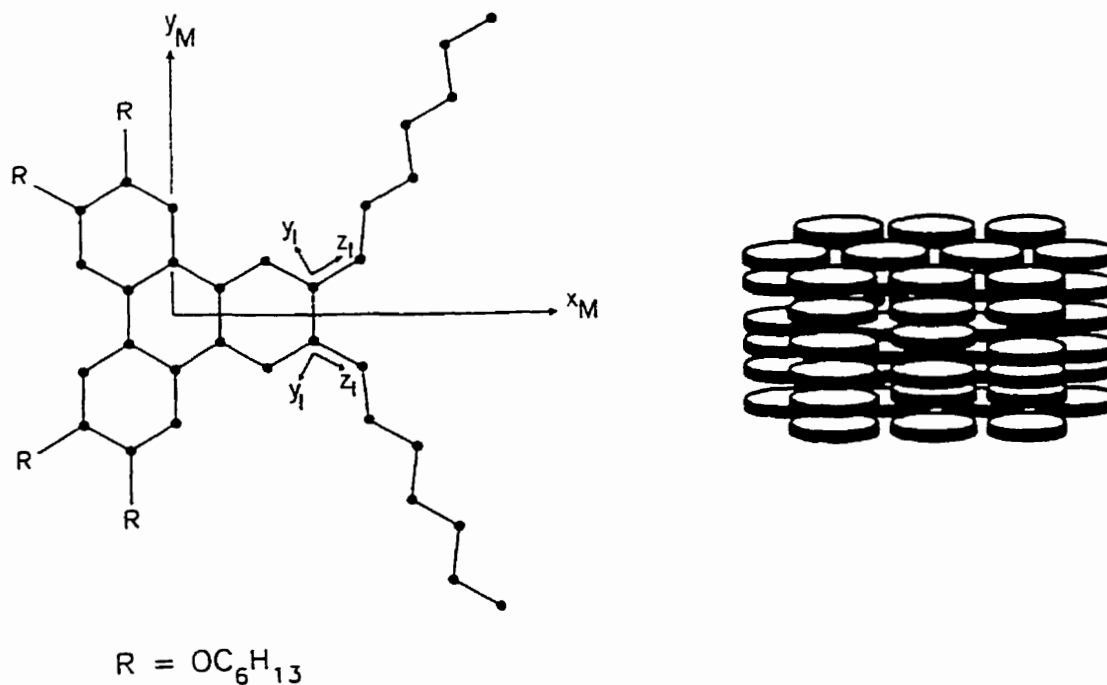
Figure 1.5 Hexakis(n-hexyloxy)triphenylene (HAT6) shown with coordinate systems used in the text, and a schematic view of its columnar D_h mesophase.

(4) HAT6

hexakis(n-hexyloxy)triphenylene (see Fig. 1.5)

Chain deuterated HAT6

Ring deuterated HAT6

Both HAT6 samples were kindly provided by Prof. N. Boden, Center for Self-Organising Molecular Systems, The University of Leeds, Leeds, The United Kingdom.

The disc-like molecules such as the hexakis(alkyloxy)triphenylenes (HATn) can form columnar phases[1.32]. These disc-like molecules are stacked, with only short-range positional order, into columns which are arranged on a two-dimensional lattice, typically hexagonal. Deuterated HATn molecules have been studied using proton and deuteron NMR by Luz and co-works[1.33-1.36] more than 10 years ago. To explain[1.37] the spectral densities of aromatic deuterons in HAT6, Nordio model[1.10] was used and rotational diffusion constants for HAT6 molecules were derived. The quadrupolar splittings of the chain deuterons were also modeled[1.38] using additive potential (AP) method which was pioneered by Marcelja[1.27]. These earlier attempts for the homologous series HATn unfortunately contained numerical errors and good fits were therefore fortuitive. In the present study, the decoupled model[1.29] is applied for the first time to deal with the dynamics of internal bond rotations of discotic liquid crystal. The geometric factors of this disk-like molecule are re-adjusted, and the interaction tensors for both disk-shaped core and cigar-shaped C-C bond are treated appropriately. The AP method is used to model the quadrupolar splittings, from which the potential of mean torque is parameterized, and the order parameter tensor for an 'average' conformer is determined. The small step rotational diffusion model is used to find the rotational diffusion constants $D_{\parallel}$ and $D_{\perp}$ for the spinning and tumbling motions of molecular core. It is found

that D_- is slightly larger than $D_\parallel$ in constrast with the findings in calamitic liquid crystals. The jump constants for internal bond rotations are also derived.

1.5 Thesis Outline

Chapter 1 gives the introduction to liquid crystals and samples used in this study as well as the motivation and anticipated significances of this thesis. Chapter 2 presents the basic NMR theory and the experimental details. The broadband pulse sequence can be used to simultaneously measure the spin-lattice relaxation times T_{1Z} and T_{1Q}, and the modified Carr-Purcell pulse sequence is used to measure the spin-spin relaxation time T_2. An outline of the theoretical framework of additive potential (AP) method involved in describing orientational order of flexible mesogens is given in Chapter 3. Chapters 4-6 are presentations of the existing theories of the molecular dynamics of liquid crystals necessary for the current study, i.e., molecular reorientations of biaxial molecules in the uniaxial phases, described by the Tarroni-Zannoni (TZ) model, is given in Chapter 4, director fluctuations, the unique dynamic property of liquid crystals, is outlined in Chapter 5, and Chapter 6 presents the decoupled model of internal and overall motions for the flexible chain dynamics. Chapters 7 through 10 contain the experimental results and discussion for the studied liquid crystal samples. The final chapter gives an overview of various findings from the various systems, and makes comparison of molecular properties where possible.

References

1.1 F. Reinitzer. *Monatsh.* **9**. 421. 1888; O. Lehmann. *Z. Phys. Chem.* 4. 1889.

1.2 S. Chandrasekhar. B.K. Sadashiva. K.A. Suresh. *Pramana* **9**. 471. 1977.

1.3 P.G. de Gennes. In *The Physics of Liquid Crystals* Clarendon. Oxford. 1975.

1.4 P.G. de Gennes. In *The Physics of Liquid Crystals* Oxford University. London. 1974.

1.5 E.B. Priestley. P.J. Wojtowica. P. Sheng. In *Introduction to Liquid Crystals* Plenum. New York. 1975.

1.6 P.G. de Gennes. In *Proceedings of the 2nd International Liquid Crystal Conference*. edited by G.H. Brown. Gordon and Breach. New York. 1969. p. 531.

1.7 R.Y. Dong. *Nuclear Magnetic Resonance of Liquid Crystals*. 2nd ed.. Springer-verlag. New York. 1997; *Nuclear Magnetic Resonance of Liquid Crystals*. edited by J.W. Emsley. Reidel. Dordrecht. 1985.

1.8 J. Jeener. P. Broekaert. *Phys. Rev..* **157**. 232. 1967; R.L. Vold. W.H. Dickerson. R.R. Vold. *J. Magn. Reson..* **43**. 213. 1981; R.Y. Dong. *Bull. Magn. Reson.* **14**. 134. 1992.

1.9 J.H. Freed. J. Chem. Phys.. 41. 2077. 1964; W. Huntress. *Jr. Adv. Magn. Reson..* **4**. 1. 1970.

1.10 P.L. Nordio. P. Busolin. J. Chem. Phys. 55. 5485. 1971; P.L. Nordio. G. Rigatti. U. Segre. *Mol. Phys..* **25**. 129. 1973.

1.11 J.M. Bernassau. E.P. Black. D.M. Grant. *J. Chem. Phys..* **76**. 253. 1982.

1.12 J. Bulthuis. L. Plomp. *J. Phys. (Paris)* **51**. 2581. 1990.

1.13 R. Tarroni. C. Zannoni. *J. Chem. Phys.*, **95**. 4550. 1991.

1.14 E. Berggren. R. Tarroni. C. Zannoni. *J. Chem. Phys.*, **99**. 6180. 1993.

1.15 E. Berggren. C. Zannoni. *Mol. Phys.*, **85**. 299. 1995.

1.16 R.Y. Dong. X. Shen. *Phys. Rev. E*. **49**. 538. 1994.

1.17 R.R. Vold. R.L. Vold. *J. Chem. Phys.*, **88**. 1443. 1988.

1.18 R.L. Vold. R.R. Vold. in *The Molecular Dynamics of Liquid Crystals*. G.R. Luckhurst. C.A. Veracini. Eds. Kumer Academic. Dordrecht. 1994: C.G. Wade. *Annu. Rev. Phys. Chem.*. **28**. 47. 1977.

1.19 P. Chatelain. *Acta Crystallogr.*. **1**. 315. 1948.

1.20 P.G. de Gennes. *Compt. Rend.*. **226B**. 15. 1968.

1.21 P. Pincus. *Solid State Commun.*. **7**. 415. 1969.

1.22 T. Lubensky. *Phys. Rev. A*. **2**. 2497. 1970.

1.23 R.L. Vold. R.R. Vold. M.J. Warner. *J. Chem. Soc.. Faraday Trans. 2*. **84**. 997. 1988.

1.24 R.Y. Dong. *J. Phys. Chem.*. **100**. 15663. 1996: T.M. Barbara. R.R. Vold. R.L. Vold. M.E. Neubert. *J. Chem. Phys.*. **82**. 1612. 1985.

1.25 R.Y. Dong. L. Friesen. G.M. Richards. *Mol. Phys.*. **81**. 1017. 1994.

1.26 M. Vilfan. R. Blinc. J.W. Doane, *Solid State Commun.*. **11**. 1073. 1972.

1.27 S. Marcelja. *J. Chem. Phys.*, **60**. 3599, 1974.

1.28 P.A. Beckmann. J.W. Emsley. G.R. Luckhurst. D.L. Turner. *Mol. Phys.*. **59**. 97. 1986.

1.29 R.Y. Dong. G.M. Richards. *Chem. Phys. Lett.*. **171**. 389. 1990; R.Y. Dong. *Phys. Rev. A*. **43**. 4310. 1991.

1.30 A. Ferrarini. G.J. Moro. P.L. Nordio. *Liq. Cryst.*. **8**. 593. 1990.

1.31 R.Y. Dong. X. Shen. G.M. Richards. *Phys. Rev. E*. **52**. 1753. 1995; R.Y. Dong. G. Ravindranath. *Liq. Cryst.*. **17**. 47. 1994.

1.32 S. Chandrasekhar. G.S. Raganath. *Rep. Prog. Phys.*. **53**. 57. 1990.

1.33 R.Y. Dong. D. Goldfarb. M. Moseley. Z. Luz. H. Zimmermann. *J. Phys. Chem.*. **88**. 3148. 1984.

1.34 D. Goldfarb. Z. Luz. H. Zimmermann. *J. Phys. (Paris)*. **42**. 1303. 1981.

1.35 D. Goldfarb. Z. Luz. H. Zimmermann. *J. Chem. Phys.*. **78**. 7065. 1983.

1.36 D. Goldfarb. R.Y. Dong. Z. Luz. H. Zimmermann. *Mol. Phys.*. **54**. 1185. 1985.

1.37 G.M. Richards. R.Y. Dong. *Liq. Crys.*. **5**. 1011. 1989.

1.38 G.Q. Cheng. R.Y. Dong. *J. Chem. Phys.*. **89**. 3308. 1988.

Chapter 2

Basic ^{2}H NMR Theory and

Experimental Methods

2.1 Introduction

A nucleus in an external magnetic field has two or several spin energy levels which are produced by the interactions between the magnetic moment and the applied field. Figure 2.1 gives the explanatory diagram of energy levels for a deuteron spin ($I = 1$) in a large external magnetic field. When a collection of nuclei is irradiated with the characteristic resonant frequency of the nuclei, the population of each spin state is changed due to the excitation by the applied alternating field. After the rf-pulse the spin system relaxes back to its equilibrium state, and the induced magnetization could be detected. Various theories and experiments have been developed to study the relaxation process since it can give information about the "lattice" and the dynamics of the nuclei. The lattice is defined as all degrees of freedom excluding those of a spin system. Several experiments under different circumstances and observations of different nuclei in the same system are often needed in order to obtain a consistent molecular picture; correspondingly, different theories and models are

required to account for the diversity of various circumstances and observations of different nuclei.

The theoretical treatment of nuclear relaxation in a non-isolated spin system started with Bloember-gen, Purcell and Pound who treated nuclear spin relaxation in a liquid[2.1]. The rate of statistical fluctuation in the interaction with the surrounding system defines the correlation time of the nuclei. Later the Wangsness-Bloch theory[2.2, 2.3] gave a possibility to calculate the decay constants of the transverse and the longitudinal relaxations.
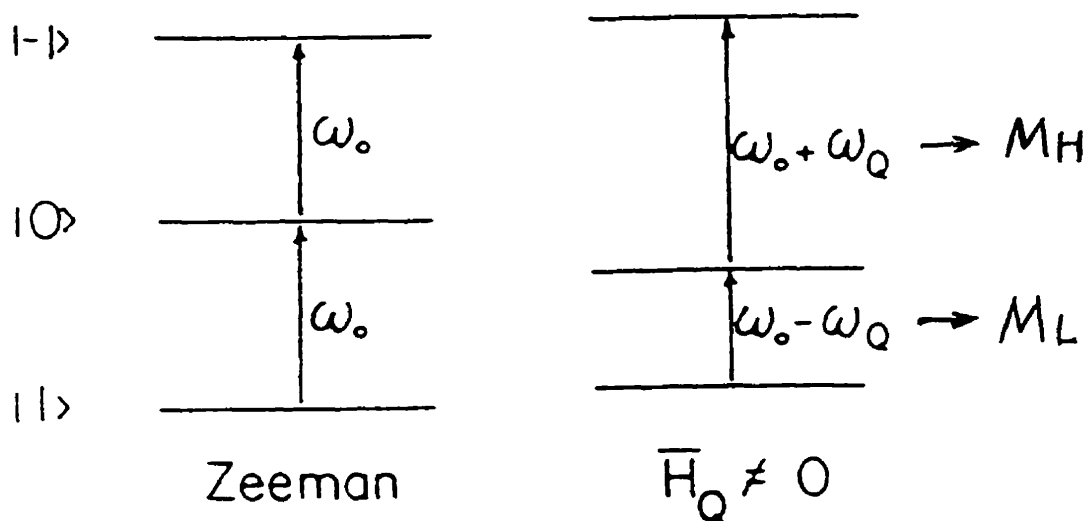
Figure 2.1 Energy level diagram of deuteron ($\eta = 0$ assumed) in a large external magnetic field. $\omega_0/2\pi$ is the Larmor frequency.

2.2 ^{2}H NMR

There are two main contributions to the energy for a deuterium(^2H) nucleus in a magnetic field; Zeeman energy and quadrupole energy. The spin Hamiltonian may be written as

$$\mathcal{H} = \mathcal{H}_Z + \mathcal{H}_Q \tag{2.1}$$

where $\mathcal{H}_Z$ is the Zeeman Hamiltonian and $\mathcal{H}_Q$ is the quadrupolar Hamiltonian. $\mathcal{H}_Z$ describes the interaction of the nuclear magnetic moment $\vec{\mu}$ with the static magnetic field $\vec{H_0}$.

$$\mathcal{H}_Z = -\vec{\mu} \bullet \vec{H_0} = -\gamma \hbar \vec{I} \bullet \vec{H_0} = -\gamma \hbar I_Z H_0 \tag{2.2}$$

where γ is the gyromagnetic ratio. $\vec{I}$ is the nuclear spin operator and the field $\vec{H}_0$ is taken along the Z_L direction of a laboratory frame. The Larmor frequency, ω_0, equals γH_0.

The quadrupolar Hamiltonian $\mathcal{H}_Q$ arises from an electrostatic interaction of the nuclear quadrupole moment $(Q_{\alpha\beta})$ with the electric field gradient (efg). $V_{\alpha\beta}(= \nabla \vec{E})$ at the position of the nucleus. $V_{\alpha\beta}$ and $Q_{\alpha\beta}$ are second order tensors and are defined as

$$Q_{\alpha\beta} = e \sum_{\kappa(protons)} (3x_{\alpha\kappa}x_{\beta\kappa} - \delta_{\alpha\beta}r_{\kappa}^2) \tag{2.3}$$

$$V_{\alpha\beta} = \left(\frac{\partial^2 V}{\partial x_\alpha \partial x_\beta} \right)_{nuclei} \tag{2.4}$$

Since the field is sourceless, V satisfies the Laplace's equation giving $V_{xx} + V_{yy} + V_{zz} = 0$. In the principal axis coordinate system (PAS) of the efg, all off diagonal terms are zero and the quadrupolar Hamiltonian is:

$$\mathcal{H}_Q = \frac{eQ}{4I(2I-1)} \left[V_{ZZ}(3I_Z^2 - I(I+1)) + \frac{1}{2}(V_{XX} - V_{YY})(I_+^2 + I_-^2) \right] \tag{2.5}$$

The asymmetry parameter η is customarily introduced as

$$\eta = \frac{V_{XX} - V_{YY}}{V_{ZZ}} \tag{2.6}$$

20

Generally, the efg asymmetry parameter is small for deuterons, $\eta \leq 0.06$, with the principal z axis being along the direction of the $C -^2 H$ bond, and can usually be neglected.
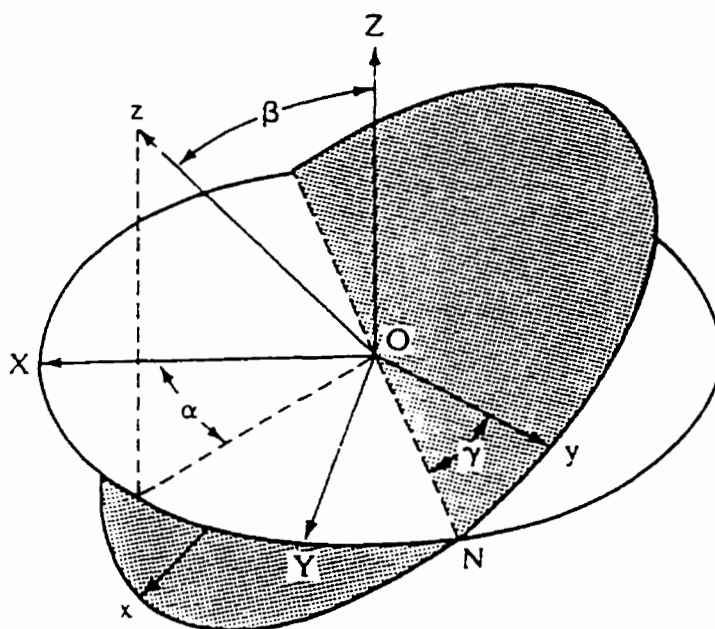
Figure 2.2 Rotations used in the definition of the Euler angles.

Usually the elements $V_{\alpha\beta}$ are known in a fixed molecular coordinate system but the spin operators I_x, I_y and I_z are quantized along the laboratory fixed magnetic field. Therefore it is necessary to rotate efg tensor through a coordinate transformation. This is done by making successive rotations through Euler angles α, β, γ(Fig. 2.2) [2.4]. A natural choice of basis is the spherical basis where efg tensor can be expressed in terms of its irreducible components V_m^2, ($m = 0, \pm 1, \pm 2$). In the principal

axis coordinate system

$$V_0^{-2} = \sqrt{\frac{3}{2}} V_{ZZ}$$

$$V_{\pm 1}^{-2} = V_{ZX} + iV_{ZY} = 0 \quad (in \; PAS)$$

$$V_{\pm 2}^{-2} = \frac{1}{2}(V_{XX} - V_{YY}) \pm iV_{XY} = \frac{1}{2}\eta V_{ZZ} \quad (in \; PAS) \tag{2.7}$$

The transformation from one frame to another simply involves the Wigner rotation matrices $D_{mm'}^2$.

$$V_{m'}^{-2} = \sum_{m=-2}^{2} D_{mm'}^2(\alpha, \beta, \gamma) V_m^{-2} \tag{2.8}$$

2.3 Relaxation

The phenomenon of evolution towards the statistical equilibrium of a macroscopic system is given the name 'relaxation'. In nuclear magnetic resonance the whole system consists of two weakly coupled parts: 1. the spin system consisting of all degrees of freedom dependent on the spin-operators of the nuclei, and 2. the lattice consisting of all other degrees of freedom associated with the molecular rotations and translations. Nuclear magnetic relaxation is the evolution of the spin system towards its thermal equilibrium with the lattice, and is called spin-lattice relaxation. Since the lattice temperature is not affected measurably by the exchange of energy with the spin system taking place during relaxation, it is considered to be an 'infinite' bath. Relaxation times are connected to well defined characteristics of the dynamics of molecular motions and translations. In general, the only physical quantities considered in nuclear magnetic relaxation are the components of nuclear polarization.

The longitudinal relaxation time T_1, is due to the change in the magnetization component along the axis parallel to the applied magnetic field (the Z_L axis of the laboratory frame). Any change in

22

the Z_L-magnetization is accompanied by an energy flow between the nuclear spin system and other degrees of freedom of system(the lattice). T_1 is also called the spin-lattice relaxation time. When a static field is applied along the Z_L axis, the longitudinal magnetization M_Z has a non-vanishing value M_0, whereas the transverse components M_X and M_Y vanish, at thermal equilibrium. Starting from a non-equilibrium state, the evolution of M_Z towards M_0 modifies the energy of the spin system, which corresponds to an exchange of energy with the lattice, whereas the decrease in transverse magnetization components does not produce such an exchange of energy. The transverse relaxation time, T_2, is defined by the relaxation of the magnetization components on the $X_L Y_L$-plane. The T_2-mechanism arises from the spread in precession rates caused by the magnetic field that one nucleus produces at another; T_2 is also referred to as the spin-spin relaxation time. In constrast to the longitudinal decay, the transverse relaxation conserves the spin energy in the static magnetic field.

The spin system needs a 'spin-lattice interaction' to exchange energy with the lattice and in the case of the deuteron, the dominant mechanism is invariably the coupling of the electric field gradient with the quadrupolar moment of the nucleus. Since the orientation of the electric field gradient with respect to the main external field is randomly modulated as a function of time by the molecular motions, there is a relaxation Hamiltonian whose average value vanishes. T_1 gives information on relatively fast dynamical molecular processes having correlation times in the vicinity of approximately 10^{-9}s. This is because longitudinal relaxation involves an exchange of either one or two quanta of nuclear energy between the spins and the lattice. Thus T_1 involves the spectral density $J(\omega)$ of the spin-lattice interactions in the vicinity of frequency ω_0 and $2\omega_0$, where Larmor frequency $\omega_0/2\pi$ depends on the static magnetic field strength and is either 15MHz or 46MHz in the present study. T_2 is the relaxation time associated with the increasing dispersion of phase accumulated by

the nuclear spins due to thermally driven fluctuations in the quadrupolar splitting. Fast motions that contribute to T_1 also contribute to T_2 so $T_2 \leq T_1$ is always satisfied. Slow motions which satisfy the condition that $(\omega_0 \tau_c)^2 \gg 1$, where τ_c is the correlation time, contribute appreciably to T_2, but not to T_1. Therefore when $T_2 \ll T_1$, the significance of slow motions can be recognized.

2.4 ^{2}H NMR Relaxation Rate

How a nuclear spin system achieves thermal equilibrium by exchanging energy with its surrounding medium or the 'lattice' is governed by the NMR relaxation rates. Pulsed NMR provides a highly versatile and flexible tool to determine spin relaxation rates, which can probe the entire spectrum of molecular motions. These include the molecular rotations, the translational self-diffusion, the "coherent" rotational motion, and the internal motion in non-rigid molecules. However, several nuclear interactions may simultaneously all contribute to the relaxation of the spin system. These may include the magnetic dipole-dipole interaction, the quadrupole interaction, the spin-rotation interaction, the scalar coupling, and the chemical shift anisotropy interaction. Due to the need of estimating certain nuclear couplings and/or correlation times associated with molecular motions, considerable uncertainty may exist in identifying and separating these contributions. Following the ideas of Redfield[2.5], the Bloch-Wangsness-Redfield theory[2.6] developed on the basis of density matrix method, gives a semi-classical treatment, simply because it uses time correlation functions which are classical.

The most difficult problem in any relaxation theory is the calculation of correlation functions or spectral densities of motion. It is often possible to determine the mean square spin interaction

$\langle H_q^2(t) \rangle$. where $H_q(t)$ is a component of the spin Hamiltonian which fluctuates randomly in time owing to molecular motions. The time dependence of correlation function $\langle H_q(t)H_{q'}(t - \tau) \rangle$ can often be approximated by an exponential decay function of τ. i.e.

$$\langle H_q(t)H_{q'}(t - \tau) \rangle = \langle H_q(t)H_{q'}(t) \rangle \, e^{-\tau/\tau_c} \qquad (2.9)$$

where the angle brackets denote an ensemble average. and the correlation time τ_c for the motion can be determined with the help of experiments. In NMR. the coupling between the lattice and Zeeman reservoir of the nuclear spin system is magnetic in all cases except one. The exception is the quadrupolar coupling between the nuclear quadrupole moment (for spin angular momentum $I > \frac{1}{2}$) and the lattice via an electric field gradient. which is electrical in nature. When this coupling exists. it is generally more efficient than any magnetic coupling. Deuteron (spin $I = 1$) has a small quadrupole moment with a coupling constants e^2qQ/h typically 150-250 kHz. large enough so that relaxation is dominated by the quadrupole interaction and small enough so that the perturbation theory is applicable.

Suppose that an assembly of N identical spin systems is considered. This allows a quantum statistical description of a spin system. If the spin system is in a state of wavefunction or ket $| \psi_k \rangle$. the expectation value of a physical observable given by its operator Q is

$$\langle Q \rangle_k = \langle \psi_k | Q | \psi_k \rangle \qquad (2.10)$$

NMR spectroscopy deals with the observation of macroscopic observables. Thus. one needs to perform an average over the N systems in the ensemble:

$$\langle Q \rangle = \sum_{k=1}^{N} \langle Q \rangle_k / N \qquad (2.11)$$

25

In genaral. the ket $\mid \psi_k \rangle$ is time dependent and may be expanded using a complete orthonormal basis set of m stationary kets $\mid \phi_j \rangle \equiv \mid j \rangle$

$$\mid \psi_k \rangle = \sum_{j=1}^{m} C_j^k(t) \mid j \rangle \tag{2.12}$$

where the expansion coefficient C_j^k are time dependent. This leads to

$$\langle Q \rangle = \sum_{\alpha,j} \langle j \mid Q \mid \alpha \rangle \sigma_{\alpha j}(t) \tag{2.13}$$

where the σ is defined as density operator. whose matrix elements in the orthonormal basis $\mid \alpha \rangle$ are

$$\sigma_{\alpha j} = \langle \alpha \mid \sigma \mid j \rangle = \overline{C_\alpha(t)C_j^*(t)} \tag{2.14}$$

and the bar denotes an ensemble average. The equation of motion for σ is obtained from the Schrödinger equation for $\mid \psi \rangle$

$$\frac{d}{dt} \mid \psi \rangle = -iH \mid \psi \rangle \tag{2.15}$$

where H is an appropriate spin Hamiltonian (in angular frequency units) for the spin system. The equation for the time dependence of the density operator σ is obtained by evaluating $d\sigma_{\alpha j}/dt$ to give

$$\frac{d\sigma}{dt} = -i[H.\sigma(t)] \tag{2.16}$$

A spin system with the Hamiltonian given by

$$H = H_0 + H'(t) \tag{2.17}$$

is now taken. where H_0 is the static Hamiltonian and $H'(t)$ represents time-dependent spin-lattice coupling. H' is a random function of time with vanishing time average [i.e. $\overline{H'(t)} = 0$]. and H_0 includes the Zeeman interactions, static averages of dipolar and quadrupole couplings. and time-dependent radiofrequency (rf) interactions. Writing σ and H' as $\tilde{\sigma}$ and $\widetilde{H}'$ in the *interaction*

26

representation and using the second-order perturbation theory, the time evolution of the density operator can be shown to obey

$$\frac{d\tilde{\sigma}}{dt} = -\int_0^t dt' \overline{\left[\tilde{H}'(t).[\tilde{H}'(t-t').(\tilde{\sigma}(t) - \sigma_{eq})]\right]}\qquad(2.18)$$

where the bar is now used to indicate an average over all identical molecules in the sample. Using the eigenket basis of the static Hamiltonian H_0 (i.e. $H_0 \mid \alpha \rangle = \alpha \mid \alpha \rangle$), Redfield has obtained a set of linear differential equations:

$$\frac{d}{dt}\tilde{\sigma}_{\alpha\alpha'} = \sum_{\beta\beta'} \exp\left[-i(\omega_{\alpha\alpha'} - \omega_{\beta\beta'})t\right] R_{\alpha\alpha'\beta\beta'}\left[\tilde{\sigma}_{\beta\beta'}(t) - \tilde{\sigma}_{\beta\beta'}(\infty)\right]\qquad(2.19)$$

where $\omega_{\alpha\beta} = \alpha - \beta(\hbar = 1)$. $\tilde{\sigma}_{\beta\beta'}(\infty)$ corresponds to the matrix elements $\tilde{\sigma}_{\beta\beta'}$ at thermal equilibrium, and the terms $R_{\alpha\alpha'\beta\beta'}$ are elements of the Redfield relaxation supermatrix[2.7], which are given by

$$R_{\alpha\alpha'\beta\beta'} = U_{\alpha\alpha'\beta\beta'} + U_{\beta\beta'\alpha\alpha'} - \delta_{\alpha'\beta'}\sum_{\gamma} U_{\gamma\gamma\beta\alpha} - \delta_{\alpha\beta}\sum_{\gamma} U_{\beta'\alpha'\gamma\gamma}\qquad(2.20)$$

This treatment is closely related to the relaxation theory of Wangsness and Bloch[2.6]. The U functions are further simplified by examining, for example, $U_{\alpha\alpha'\beta\beta'}$.

$$\begin{aligned}
U_{\alpha\alpha'\beta\beta'} &= \int_0^{\Delta t} d\tau \exp(-i\omega_{\alpha'\beta'}\tau)G_{\alpha\beta\alpha'\beta'}(\tau)\\
&\times \left\{\frac{\exp[i(\alpha - \beta - \alpha' + \beta')(\Delta t - \tau)] - 1}{i(\alpha - \beta - \alpha' + \beta')\Delta t}\right\}
\end{aligned}\qquad(2.21)$$

where $G_{\alpha\beta\alpha'\beta'}(\tau)$ denote correlation functions of a stationary random function $H'(t)$, which is by definition independent of the origin of time, and

$$G_{\alpha\beta\alpha'\beta'}(\tau) = \overline{H'^*_{\alpha'\beta'}(t)H'_{\alpha\beta}(t+\tau)}\qquad(2.22)$$

where $H'_{\alpha\beta}(t) = \langle \alpha \mid H'(t) \mid \beta \rangle$. Note that the integrand is large only if $\tau \ll \tau_c$, the correlation time for $G_{\alpha\beta\alpha'\beta'}(\tau)$. Thus, the upper limit (Δt) of the integral can be set to infinity. The bracket in the

27

integrand is a constant ($\Delta t \gg \tau$) and equal to 1. In this limit, $U_{\alpha\alpha'\beta\beta'} = J_{\alpha\beta\alpha'\beta'}(\omega_{\beta'\alpha'})$, the spectral densities which are given by

$$J_{\alpha\beta\alpha'\beta'}(\omega_{\alpha'\beta'}) = \int_0^\infty d\tau \exp(-i\omega_{\alpha'\beta'}\tau)G_{\alpha\beta\alpha'\beta'}(\tau) \tag{2.23}$$

and the relaxation matrix elements are now given by

$$\begin{aligned}
R_{\alpha\alpha'\beta\beta'} &= J_{\alpha\beta\alpha'\beta'}(\omega_{\alpha'\beta'}) + J_{\alpha\beta\alpha'\beta'}(\omega_{\alpha\beta}) - \delta_{\alpha'\beta'}\sum_\gamma J_{\gamma\beta\gamma\alpha}(\omega_{\gamma\alpha}) \\
&- \delta_{\alpha\beta}\sum_\gamma J_{\gamma\alpha'\gamma\beta'}(\omega_{\gamma\alpha'})
\end{aligned} \tag{2.24}$$

Because of the large heat capacity of the lattice relative to that of the nuclear spins, the lattice may be considered at all times to be in thermal equilibrium, while the time-varying spin states, in the absence of a rf field, evolve to thermal equilibrium because of the spin-lattice interactions. When the exponential argument $(\omega_{\alpha\alpha'} - \omega_{\beta\beta'})$ in Eq. (2.19) is significantly larger than the spin relaxation rates, the exponential term oscillates rapidly in comparison with the slow variation in the density matrix due to relaxation. As a consequence, the impact of these terms becomes zero. The so-called secular approximation $(\omega_{\alpha\alpha'} = \omega_{\beta\beta'})$ effectively simplifies the equation of motion to

$$\frac{d}{dt}\tilde{\sigma}_{\alpha\alpha'} = {\sum}' R_{\alpha\alpha'\beta\beta'} [\tilde{\sigma}_{\beta\beta'}(t) - \tilde{\sigma}_{\beta\beta'}(\infty)] \tag{2.25}$$

where the prime on the summation indicates that only terms that satisfy $\omega_{\alpha\alpha'} = \omega_{\beta\beta'}$ are kept. Now the exponentials in front of those $R_{\alpha\alpha\beta\beta}$ in Eq. (2.19) are clearly secular. These $R_{\alpha\alpha\beta\beta}$ parameters control the spin-lattice relaxation and are associated with the diagonal elements $\sigma_{\alpha\alpha}$, which specify the probabilities (P_α) that spin states $|\alpha\rangle$ are occupied. The exponentials in front of $R_{\alpha\beta\alpha\beta}$ are also secular. These $R_{\alpha\beta\alpha\beta}$ parameters control the spin-spin relaxation. When only spin-lattice relaxation is considered, the important Redfield terms in the eigenbase representation are limited

to the following two types:

$$R_{\alpha\alpha\beta\beta} = 2J_{\alpha\beta\alpha\beta}(\omega_{\alpha\beta}) - 2\delta_{\alpha\beta}\sum_{\gamma} J_{\gamma\beta\gamma\alpha}(\omega_{\gamma\beta})$$

$$R_{\alpha\alpha\alpha\alpha} = -2\sum_{\gamma\neq\alpha} J_{\gamma\alpha\gamma\alpha}(\omega_{\gamma\alpha}) = -\sum_{\gamma\neq\alpha} R_{\gamma\gamma\alpha\alpha} \tag{2.26}$$

The $H'(t)$ in Eq. (2.17) determines what is called the relaxation mechanism. The quadrupolar Hamiltonian with an axially symmetric ($\eta = 0$) electric field gradient tensor is given by

$$H'_{\lambda}(t) = \sum_{m_L} \sqrt{3/8}(e^2 qQ/\hbar) T_{2,m_L} \left\{ D^2_{m_L,0}[\Omega(t)] - \overline{D^2_{m_L,0}} \right\} \tag{2.27}$$

where the time dependence arises via Euler angles Ω in the Wigner rotation matrices $D^2_{m,n}(\Omega)$, and T_{2,m_L}, the spin operator in the laboratory frame, are given for a deuteron by

$$T_{2,0} = \frac{1}{\sqrt{6}}\left(3I_z^2 - I^2\right)$$

$$T_{2,\pm 1} = \mp\frac{1}{2}\left(I^{\pm}I_z + I_z I^{\pm}\right)$$

$$T_{2,\pm 2} = \frac{1}{2}\left(I^{\pm}\right)^2 \tag{2.28}$$

When the cross products between spin Hamiltonian matrix elements of different m_L values can be ignored (e.g. in liquids) where m_L is the projection index of a rank L (=2) interaction Hamiltonian, the spectral densities of Eq. (2.23) becomes

$$J_{\alpha\beta\alpha'\beta'}(\omega_{\alpha\beta}) = \frac{3}{8}\left(\frac{e^2 qQ}{\hbar}\right)^2 \sum_{m_L} \langle \alpha \mid T_{2,m_L} \mid \beta \rangle \langle \alpha' \mid T_{2,m_L} \mid \beta' \rangle^* J_{m_L}(\omega_{\alpha\beta}) \tag{2.29}$$

where

$$J_{m_L}(\omega) = \int_0^{\infty} G_{m_L}(\tau) e^{-\omega\tau} d\tau \tag{2.30}$$

with

$$G_{m_L}(\tau) = \left\langle \left\{ D^2_{m_L,0}[\Omega(t)] - \overline{D^2_{m_L,0}} \right\} \left\{ D^{2*}_{m_L,0}[\Omega(t-\tau)] - \overline{D^{2*}_{m_L,0}} \right\} \right\rangle \tag{2.31}$$

29

It should be noted that the $J_{m_L}(\omega)$ are quantities that are obtained from experiments without reference to any molecular dynamics model. Now, Eq. (2.19) can be transformed back to the Schrödinger representation:

$$\frac{d}{dt}\sigma_{\alpha\alpha'}(t) = i\,[\sigma, H_0] + \sum_{\beta\beta'} R_{\alpha\alpha'\beta\beta'}\,[\sigma_{\beta\beta'}(t) - \sigma_{\beta\beta'}(\infty)] \qquad (2.32)$$

The first term on the right-hand side describes spin precessions and is only important for spin-spin relaxation. According to Redfield, the above equation is valid provided that the relaxation elements are small in comparison to the inverse correlation time τ_c^{-1} of the thermal motion, i.e.

$$\frac{1}{R_{\alpha\alpha'\beta\beta'}} \gg \Delta t \gg \tau_c \qquad (2.33)$$

where Δt represents the time interval over which the density matrix of the spin system has not appreciably changed.

The following gives the application of the Redfield theory to a deuteron with its quadrupolar moment experiencing a fluctuating electric field gradient owing to molecular motions in an anisotropic liquid crystal. As in Fig. 2.1, $\overline{H_Q} \neq 0$, this static average of quadrupolar interaction is included in the static Hamiltonian H_0. The density operator matrix for a deuteron spin is of the dimension 3×3 and the corresponding Redfield relaxation supermatrix has the dimension of $3^2 \times 3^2$. When only nuclear spin-lattice relaxation is considered, the spin precession term in Eq. (2.32) is set to zero and the diagonal elements $\sigma_{\alpha\alpha}$ ($\alpha = 1, 2, 3$) satisfy

$$\frac{d}{dt}P_\alpha(t) = \sum_\beta R_{\alpha\beta}\,[P_\beta(t) - P_\beta(\infty)] \qquad (2.34)$$

where $P_1 \equiv P_1$, $P_2 \equiv P_0$, and $P_3 \equiv P_{-1}$ are the populations in spin states $|1\rangle$, $|0\rangle$ and $|-1\rangle$, respectively (see Fig. 2.1), and $R_{\alpha\beta} = R_{\alpha\alpha\beta\beta}$ given in Eq. (2.26). $R_{\alpha\beta}$ represents the transition

probability per second from the spin state β to the spin state α and $R_{\alpha\beta} = R_{\beta\alpha}$. Thus, nuclear spin-lattice relaxation involves transitions between nuclear states of different energies induced by time-dependent spin interactions. Letting $\overrightarrow{P}(t)$ be a vector with components $P(t) - P(\infty)$, Eq. (2.34) may be expressed in matrix form:

$$\frac{d}{dt}\overrightarrow{P}(t) = \mathbf{R}\overrightarrow{P}(t) \tag{2.35}$$

whose formal solution is simply given by

$$\overrightarrow{P}(t) = \exp[\mathbf{R}t]\overrightarrow{P}(0) \tag{2.36}$$

The matrix elements of $\mathbf{R}$ can now be obtained from Eqs. (2.26) and (2.30). For instance, the off-diagonal element R_{12} is

$$
\begin{aligned}
R_{12} &= 2J_{12}(\omega_0) \\
&= \frac{3}{4}\left(\frac{e^2qQ}{\hbar}\right)^2 \sum_{m_L} \langle 1 \mid T_{2,m_L} \mid 0 \rangle \langle 1 \mid T_{2,m_L} \mid 0 \rangle^* J_{m_L}(\omega_0) \tag{2.37}
\end{aligned}
$$

where $\omega_0 = \omega_{12}$ and the Hamiltonian matrix element is non-zero only if $m_L = 1$, i.e.

$$\langle 1 \mid T_{2,m_L} \mid 0 \rangle = -\frac{1}{\sqrt{2}} \tag{2.38}$$

Hence, $R_{12} = K_Q J_1(\omega_0)$ with $K_Q = (3\pi^2/2)(e^2qQ/h)^2$. Similarly, the diagonal elements can be obtained, e.g.

$$
\begin{aligned}
R_{11} &= 2J_{11}(0) - 2\sum_{\gamma=1}^{3} J_{\gamma 1\gamma 1}(\omega_{\gamma 1}) \\
&= K_Q\left[-J_1(\omega_0) - 2J_2(2\omega_0)\right] \tag{2.39}
\end{aligned}
$$

where $\omega_{31} = 2\omega_0$ and the Redfield relaxation matrix in Eq. (2.35) is

$$
\mathbf{R} = K_Q \begin{pmatrix} -J_1(\omega_0) - 2J_2(2\omega_0) & J_1(\omega_0) & 2J_2(2\omega_0) \\ \\ J_1(\omega_0) & -2J_1(\omega_0) & J_1(\omega_0) \\ \\ 2J_2(2\omega_0) & J_1(\omega_0) & -J_1(\omega_0) - 2J_2(2\omega_0) \end{pmatrix}
$$

(2.40)

Now $\mathbf{R}$ may be diagonalized through a similarity transformation and Eq. (2.36) can be expressed in terms of linear combinations of the eigenstate population P_α.

$$
\begin{pmatrix} P_1(t) + P_0(t) + P_{-1}(t) \\ \\ P_1(t) - P_{-1}(t) \\ \\ -P_1(t) + 2P_0(t) - P_{-1}(t) \end{pmatrix} = \begin{pmatrix} 1 & 0 & 0 \\ \\ 0 & \exp(-t/T_{1Z}) & 0 \\ \\ 0 & 0 & \exp(-t/T_{1Q}) \end{pmatrix}
$$

$$
\times \begin{pmatrix} P_1(0) + P_0(0) + P_{-1}(0) \\ \\ P_1(0) - P_{-1}(0) \\ \\ -P_1(0) + 2P_0(0) - P_{-1}(0) \end{pmatrix}
$$

(2.41)

where the deuteron spin-lattice relaxation times T_{1Z} and T_{1Q} are for relaxation of the Zeeman and quadrupolar orders, respectively.

$$
T_{1Z}^{-1} = K_Q \left[J_1(\omega_0) + 4J_2(2\omega_0) \right]
$$

$$
T_{1Q}^{-1} = 3 K_Q J_1(\omega_0)
$$

(2.42)

In the above equations, ω_Q is assumed to be vanishing small, otherwise one needs to replace $J_m(m\omega_0)$ by $\frac{1}{2}\left[J_m(m\omega_0 - \omega_Q) + J_m(m\omega_0 + \omega_Q) \right]$[2.8], where ω_Q is shown in Fig. 2.1. In aligned liquid crystal samples, both T_{1Z} and T_{1Q} can be simultaneously measured using the modified Jeener-Broekaert pulse sequence $90^\circ_x - \tau - 45^\circ_y - t - 45^\circ_y$[2.9][see Section 2.7].

The applicable terms of spin-spin relaxation in the present study are the off-diagonal elements $\sigma_{\alpha\beta}$ of the density operator matrix. Suppose a selective excitation experiment is considered using $90^\circ - \tau - 180^\circ$ spin echo sequence with the 90° pulse selectively irradiating the $1 \to 2$ ($|1\rangle \to |0\rangle$) transition at $\omega_0 - \omega_Q$ (see Fig. 2.1). The single transition (or fictitious spin-$\frac{1}{2}$) operators may be used in the eigenbase of H_0[2.10]. The complete set of single transition operators for a deuteron[2.11] is represented by the nine generalized Pauli spin matrices. For example, the operator $I_-^{(12)} = I_x^{(12)} + iI_y^{(12)}$ gives

$$I_-^{(12)} = \begin{pmatrix} 0 & 1 & 0 \\ 0 & 0 & 0 \\ 0 & 0 & 0 \end{pmatrix} \tag{2.43}$$

and the transverse magnetization $\langle I_-^{(12)} \rangle = Tr(\sigma I_-^{(12)}) = \sigma_{12}$. From Eq. (2.32), the following is obtained:

$$\begin{aligned} \frac{d}{dt}\sigma_{12} &= i\left[\sigma, H_0\right]_{12} + \sum_{\jmath\jmath'} R_{12\jmath\jmath'}\left[\sigma_{\jmath\jmath'}(t) - \sigma_{\jmath\jmath'}(\infty)\right] \\ &= -i\omega_{12}\sigma_{12} + R_{1212}\left[\sigma_{12} - \sigma_{12}(\infty)\right] + R_{1223}\left[\sigma_{23} - \sigma_{23}(\infty)\right] \end{aligned} \tag{2.44}$$

where other terms in the double sum involve zero Rs. Since the other component of the doublet is not irradiated, $\sigma_{23} = \sigma_{23}(\infty) = 0$ and the selective spin-spin relaxation rate is

$$T_2^{-1} = -R_{1212} = K_Q\left[\frac{3}{2}J_0(0) + \frac{3}{2}J_1(\omega_0) + J_2(2\omega_0)\right] \tag{2.45}$$

It is noted that the 180° pulse in the selective spin echo experiment reverses dephasing from both magnetic field inhomogeneities and a distribution of the order parameter[2.12].

2.5 ^{2}H NMR in Liquid Crystals

NMR is one of many techniques employed in the experimental investigation of liquid crystals. Recently internal dynamics of mesogenic molecules have attracted much efforts; both experimental and theoretical studies have been carried out. Experimentally, deuterium NMR can be used to probe relations among the NMR observables. The measurements usually yield parameters that are averages over both internal and external molecular motions. The spectroscopic timescale for ^2H NMR, $\tau_s \approx 3 \times 10^{-6}s$, is long enough to render appreciable motional-averaging due to molecular motions. Thus NMR occupies a unique place among spectroscopic techniques. The slow motions, which have correlation time $\tau_c \gg \tau_s$, have negligible influence on the spectrum of liquid crystals. The fast motions, i.e., $\tau_c \ll \tau_s$, have a large influence on the spectrum due to motion-averaging of spin interaction over fast motions. The site specificity of deuterons is often evident in the ^2H NMR spectrum, and the thermally driven molecular motion can be studied by spin relaxation time measurements.

2.6 Apparatus

The home-built pulse NMR spectrometer must transmit an rf pulse to a sample and receive its resulting response. A large sensitivity scale should be taken into account. For example, the rf pulse transmitted to the sample is relatively large, but the resulting response from the sample is quite small. Thus, the spectrometer must work in such a way that it protects the sensitive parts of the spectrometer which are used to detect weak signals from the sample, while large rf pulses are being sent to the sample. The spectrometer is controlled, or activated, by signals sent from a pulse programmer controlled by the GE 1280 computer. A block diagram of the spectrometer is shown in Fig. 2.3.
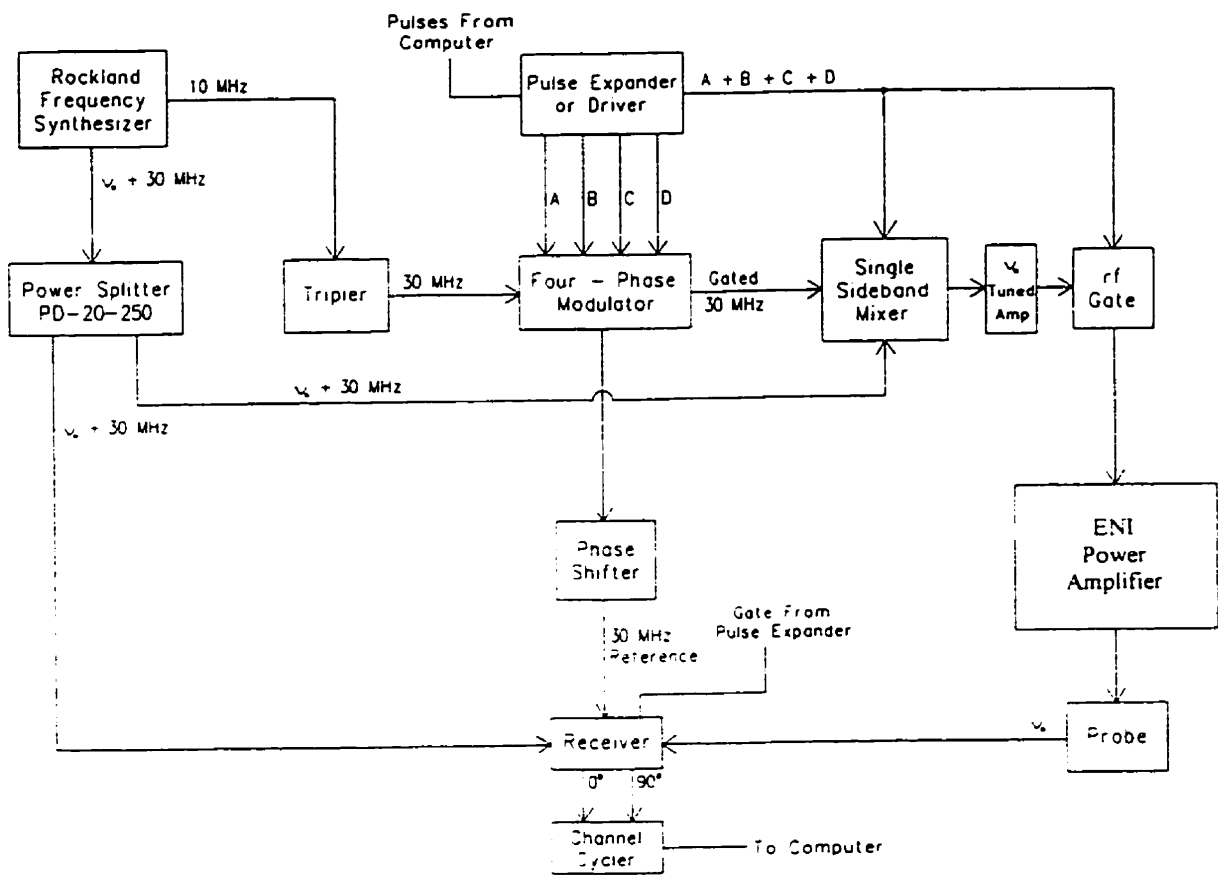
Figure 2.3 Block diagram for a heterodyne spectrometer

Frequency Synthesizer

The frequency synthesizer generates two initial radio frequency (rf) signals: One is the intermediate frequency (IF) signal with a frequency of the Larmor frequency plus 30MHz, and the other is a 10MHz signal whose frequency is multiplied by three to provide a reference signal for the receiver. The IF frequency can range from 0.1 to 160 MHz. This frequency is set at the value of the Larmor frequency of the nuclear moment being studied plus 30MHz and is expressed as $\nu_0 + 30$MHz. This intermediate frequency (IF) is chosen because many of the spectrometer's components operate at a frequency of 30MHz. In particular, manipulation of rf phases is done at 30MHz. It will be seen later that the combination of $\nu_0 + 30$MHz and 30MHz signals in the spectrometer produces an appropriate signal at the Larmor frequency, which is sent to the sample.

0° Power Splitter

The power splitter splits the $\nu_0 + 30$MHz frequency into two signals with the same frequency and phase as the incoming signal. One of them is carried to the single sideband mixer, while the other goes to the receiver. Both components are discussed below.

Frequency Tripler

The 10MHz signal from the frequency synthesizer enters the frequency tripler to produce a 30MHz signal. The 10 MHz signal which enters the tripler, is initially sent through a 0° power splitter. One of these split signals is then passed through a frequency doubler to give a signal with a frequency of 20 MHz. This signal is sent through a 20 MHz filter in order to remove unwanted frequencies produced by the frequency doubler. The resulting signal, along with the other 10 MHz signal from the power splitter, is fed into a double-balanced mixer to produce a signal with a frequency of 30

36

MHz. Since the mixer also produces the difference in the two signals (20 MHz−10 MHz) as well as leakages from the input signals (10 MHz and 20 MHz), a 30 MHz filter is used to remove those frequencies other than the 30 MHz. The 30 MHz continuous signal from the frequency tripler enters the four-phase modulator, or shifter. Since the other input signals for the four-phase modulator come from the pulse expander/driver, it is discussed as follows.

Pulse Expander/Driver

The computer program of the spectrometer controls the phase of the rf pulses which will be sent to the sample. The four-phase modulator generates four phases, which are $0°$, $90°$, $180°$ and $270°$. The phase chosen for the rf pulse sent to the sample determines the direction in which the torque will rotate the total magnetization (M) of the sample. The signals from the computer's pulse pro-grammer are not the actual rf pulses sent to sample, but merely determine which phase channel is activated in the spectrometer to give an rf pulse of a given pulse duration. The computer also controls timing of the spectrometer functions, triggering certain components at appropriate times. Since the signals from the pulse programmer do not have the power required to drive the compo-nents of the spectrometer, the pulse expander/driver is used to increase their power such that they will be capable of driving the spectrometer's components.

Four-Phase Modulator

The four-phase modulator has four different channels which generate rf signals of different phases ($0°$, $90°$, $180°$, $270°$) at 30MHz. The 30 MHz input signal is first amplified, and then split by a $0°$ power splitter into two output signals. One of these two signals is fed to the phase shifter which allows precise phase adjustment to provide the reference signal for the receiver. The other

37

signal is again split into two signals by a 90° power splitter. The frequency of two signals remains unchanged, but their phases become 0° and 90°. Both signals are fed into 180° power splitters. The input signal with 0° phase is split into two signals with phases of 0° and 180°, while the 90° signal is split into two signals with phases of 90° and 270° with respect to the 30MHz signal used for the reference phase of the receiver. Each signal then passes through circuitry which allows small adjustment of the phase to produce the precise phase required for each signal. It then enters an electric attenuator for the precise adjustment of its amplitude. These signals are continuous sinusoidal signals and have identical amplitudes and precise rf phases. The rf pulses are accomplished by feeding the continuous rf signals into four double-balanced mixers, each of which is connected to one of the channels (0, 1, 2, or 3) from the pulse expander/driver. A gating signal received from the pulse expander can trigger (or turn on) one of the mixers, which will allow the signal with the desired phase to pass through the circuitry at the proper time for a duration of the gating signal. From here, all of the rf pulse signals enter a 0° power combiner. This combines all the signals so that they leave the four-phase modulator as a single output. The output is amplified and fed into another electronic attenuator for further adjustment of the rf amplitude.

In principle, the dials on the front panel of the four-phase modulator allow independent adjustment of the amplitudes and phases of the four rf channels. However, it is found that adjustment of either the phase or the amplitude of a rf signal produces a change in the other parameter. Thus care is required in making adjustments to the phases and amplitudes of the four rf channels such that the 90° pulse widths for these channels are precisely the same.

Single Sideband Mixer

To minimize rf leakages, the output of the four-phase modulator is made to pass through another rf gate. This produces a gated rf signal of a frequency 30MHz and a phase ϕ, which may be represented by 30MHz+ϕ. The 30MHz+ϕ signal and the IF from the synthesizer are then fed to the single sideband mixer in order to convert the signal to the Larmor frequency ν_0, while retaining the phase information, ϕ, obtained from the four-phase modulator. Each of these signals is split by two 90° power splitters. The gated 30MHz+ϕ signal and the continuous ν_0+30MHz signal, both with 0° phase, are then sent to a mixer. Similarly, the corresponding signals of 90° phase are also fed to another mixer. These mixers combine the two signals such that the frequencies are summed and subtracted. Only the signals producing the difference in frequencies for the two pairs of signals are desired and they are recombined in a combiner to give a gated signal of ν_0+ϕ. This ν_0+ϕ signal leaves the single sideband mixer, then passes through a pre-amplifier to remove any frequency distortion. This pre-amplifier has a narrow bandwidth about ν_0 and allows only the desired frequency to pass on to the next component, the RF Gate.

RF Gate

The RF gate removes the distortion at the edges of the rf square pulse which leaves the single sideband mixer. The gate is triggered by the sum pulse (sum of gating signals from channel 0-3) from the pulse expander/driver. The gate allows no signal from the single sideband mixer to pass through until the sum pulse arrives and turns the gate on. Thus, the RF gate allows only the desired square pulses to pass to the next component and any distortion in the pulse shape is removed.

Power Amplifier

The signal which leaves the RF Gate is of the correct phase and frequency to be sent to the sam-

ple. However, its power is not great enough to noticeably excite the sample. The desired power is obtained by first feeding the rf pulses to a high power (ENI amplifier, 1 kW) power amplifier.

Sample Probe

The sample probe receives its input from the power amplifier and sends its output to the receiver. The probe withstands the large input rf voltage and recovers quickly to sensitively detect the weak nuclear, or FID, signal generated in the sample. Pairs of antiparallel diodes are used with the power amplifier and the receiver. Since current can only flow in one direction of the diodes and the two diodes are antiparallel, it would appear that current may always flow through this circuitry in either direction. However, diodes are non-linear elements and do not conduct, or allow current flow, until the barrier potential is overcome. Thus, a pair of crossed diodes in series circuit allows current to pass in either direction if the incoming signals are large. If the signals are small, the circuit acts like a poor conductor and current does not pass through. Conversely, a pair of crossed diodes in parallel with the circuitry, or parallel crossed diodes, performs the function of a shunt for large signals and has no effects on small signals. Obviously, series crossed diode circuits may be used to remove equipment which produces large signals from small signals which are being fed back, while parallel crossed diode circuits may be used to protect equipment, which receives small signals, from large signals.

The sample under study is put in the rf coil. The rf coil is connected with a capacitor to form an LC, or inductor-capacitor, circuit tuned to the Larmor frequency. The series crossed diodes act like a switch and are required to isolate the power amplifier from the output nuclear signals. The parallel crossed diodes also act like a switch and are required to protect the sensitive receiver from

the large input rf signals. Thus, the input rf signal from the power amplifier first passes through a series crossed diode circuit, and then is fed to the sample probe. The output FID signal detected from the sample can enter the receiver without being affected by a parallel crossed diode circuit to ground just in front of the receiver. It is important that the cable connecting the series and parallel crossed diodes circuits has a length equivalent to one quarter the transmitted wavelength.

According to the transmission theory, a line which has a length of one quarter of the transmitted wavelength ($\lambda/4$) acts like impedance transformer. The transformation is given by

$$Z_i Z_o = |Z|^2$$

where Z_i =input impedance, Z_o =output impedance and $|Z|^2$ =real squared resultant impedance. The transformed impedance is a characteristic of the specific cable used. If the input is shorted ($Z_i = 0$), then the output impedence becomes infinity($Z_o \rightarrow \infty$). It can be seen that connecting a $\lambda/4$ line to a shorted input has the same effect as connecting nothing to the output, i.e., it is an open circuit. When the power amplifier is on and the rf signal is being sent to the probe, the impedance of the parallel crossed diodes is very small (Z_i approaches zero). The $\lambda/4$ line then transforms this low input impedance to a very high output impedance and as a result, no current is allowed to pass through the $\lambda/4$ line to the receiver. Any current which may pass through the line does not reach the receiver since the parallel crossed diode circuitry acts as a shunt. Thus, the sensitive receiver is protected from the damaging large rf signals used to excite the sample. When the power amplifier is off, both the series and parallel crossed diodes do not conduct (Z_i becomes very large). Thus, the nuclear signal emitted by the sample is not fed back to the amplifier and the $\lambda/4$ line transforms the very large impedance of the parallel crossed diodes to a very small output

41

impedance at the NMR probe, or LC, circuit. The parallel crossed diodes then have little or no effect on the nuclear signal and the receiver may detect the nuclear signal.

Receiver

The nuclei in the sample induce an emf in the inductor of the LC circuit of the probe. This signal from the probe is too small and is first amplified by pre-amplifiers in the receiver. In fact there are three narrowband filters, each tuned to the Larmor frequency, put in between the pre-amplifiers. The amplified signal now must be compared to the 30 MHz reference signal in order to obtain information regarding the sample. It has a frequency slightly different than the Larmor frequency $(\nu_0 \pm \Delta\nu)$. Now, one of the $\nu_0 + 30$MHz signal from the power splitter is put into the receiver. This signal is mixed with the signal from the sample $(\nu_0 \pm \Delta\nu)$, and the resultant NMR signal is obviously 30MHz$\pm\Delta\nu$, which is now compared to the reference 30MHz signal using a quadrature detector. Inside the quadrature detector, each signal is split into two signals. The phase of one of the two reference signals is then shifted by $90°$. Each of the two reference signals is then combined with one of the nuclear signals to produce signals which have amplitudes and phases equivalent to the differences in the amplitudes and phases of the reference and nuclear signals. The two output signals are in quadrature, i.e. their phases differ by $90°$. The two signals which leave the receiver are fed into a filter component which is composed of two filters, one for each of the signals from the receiver. Those filters remove noise from the signals by narrowing the observation bandwidth.

Channel Cycler

After passing through the filters, the $0°$ and $90°$ quadrature outputs enter the channel cycler. The $0°$ quadrature signal enters the A input of the cycler and the $90°$ quadrature signal enters the B

input of the cycler. The channel cycler has the ability to determine what are the A and B outputs to go to the computer memories. The cycler may either leave the inputs alone as outputs, or put the $0°$ quadrature signal in the B output and the $90°$ quadrature signal in the A output. The switching between the two options occurs after every fourth acquisition. And the rf phase must be shifted by $90°$ every four scans so that no mixing of the real and imaginary signals occurs in the computer. In reality, the phase difference of the two channels in the receiver may deviate from the desired value of $90°$ and the gains of these channels may not be exactly the same. These problems are solved by using phase cycling of both radiofrequency pulses and the receiver channels. The computer controls the four-phase modulator to produce rf phases at $0°$, $90°$, $180°$, $270°$. Each channel in the quadrature detector takes its turn in detecting the real and imaginary parts of the FID signals as the receiver phase is cycled between $0°$ and $90°$. As a result, the two channels equally share any error in quadrature or amplification. Then the computer collects the real and imaginary parts of the FID signal and sums them in two separate memories (one acquires the signals from the A output and the other acquires the signals from the B output). Thus the imperfections in rf phases and in the quadrature detector of the receiver are compensated[2.13-2.15].

The above home-built superheterodyne coherent pulse NMR spectrometer has performed many deuterium NMR experiments[2.16-2.19]. This home-built spectrometer was operated at either 15.1 MHz using a Varian 15 electromagnet or at 46.05 MHz using a 7.1 Tesla Oxford Instruments superconducting magnet for deuterium nuclei. The sample was placed in a NMR probe whose temperature was regulated in the superconducting magnet by air flow with a Bruker BST-1000 temperature controller, while in the electromagnet by an external oil bath circulator. The temperature gradient across the sample was estimated to be better than 0.3 $°C$. The $\pi/2$ pulse width of about $3.8\mu s$ was

produced by a ENI power amplifier. Pulse control and signal collection were executed by a General Electric 1280 mini-computer[2.18, 2.19]. Fourier transformation and data processing were done by Spectral Calc and Micro Calc Origin software on a IBM-PC computer.

2.7 Pulse Sequence

In order to observe relaxation effects, the spin system has to be disturbed from equilibrium. In NMR this is done by applying an oscillating magnetic field for a short period. This oscillating field carries a frequency at or near the Larmor frequency ω_0 of the spin. For all pulse sequences 8 cyclops phase cycling was used to minimize errors due to instrumental imperfections. The repetition times were chosen to be at least $5T_1$ to ensure the sample had returned to equilibrium before applying the next pulse trian. Modified Jeener Broekaert pulse sequence, the so called broadband J-B (Wimperis) sequence[2.20-2.22], with phase cycling was used to measure the Zeeman and quadrupolar spin-lattice relaxation rates. See below and Tables 2.1 and 2.2.

Jeener Broekaert sequence $(t \geq 5T_1)$

$$90_{\phi_1} - \tau_1 - 45_{\phi_2} - \tau_2 - 45_{\phi_3} - t - 45_{\phi_4} - t-$$

The first three pulses in this pulse sequence[2.9] allows the creation of "spin alignment" and the observation of a stimulated echo[2.23] for a spin-1 system. Each deuteron gives rise to a doublet due to incomplete averaging of the quadrupole coupling. The intensities of the two lines of this doublet, named 'L' and 'H', depend on the time τ_2 as

$$M_L + M_H \quad \propto \quad C + \exp(-\tau_2/T_{1Z}) \tag{2.46}$$

44

$$M_H - M_L \quad \propto \quad \exp(-\tau_2/T_{1Q}) \qquad\qquad (2.17)$$

where C is the constant related to the equilibrium magnetization (M_0). τ_1 is chosen to maximize the quadrupolar order for a particular doublet splitting.

TABLE 2.1

J-B Sequence with Phase-cycling

ϕ_1	ϕ_2	ϕ_3	Aqu T	ϕ_4	Aqu T	Receiver Phase(*)
x	y	x	-			0
-y	x	y	-			90
x	y	-x	-			0
-y	x	-y	-			90
				y	-	90
				x	-	0
				-y	-	90
				-x	-	0
				-x	-	0
				-y	-	90
				x	-	0
				y	-	90
x	-y	-y	-			90
-y	-x	-x	-			0
x	-y	y	-			90
-y	-x	x	-			0

TABLE 2.2

Broadband J-B Sequence with Phase-cycling

ϕ_1	ϕ_2	ϕ_3	ϕ_4	ϕ_5	Aqu T	ϕ_6	Aqu T	receiver Phase(*)
x	-y	y	y	x	-			0
-y	-x	x	x	y	-			90
x	-y	y	y	-x	-			0
-y	-x	x	x	-y	-			90
						y	-	90
						x	-	0
						-y	-	90
						-x	-	0
						-x	-	0
						-y	-	90
						x	-	0
						y	-	90
x	y	-y	-y	-y	-			90
-y	x	-x	-x	-x	-			0
x	y	-y	-y	y	-			90
-y	x	-x	-x	x	-			0

(*) +/- during aquisition (Aqu) denotes addition to or subtraction of the signal from computer memory; cycling of the receiver phase minimized the quadrature images.

The modified J-B pulse sequence (Table 2.1) has included an additional monitoring $45^\circ_{\phi_4}$ pulse to minimize any long-term instability of the spectrometer. This pulse was phase cycled to have a net effect of subtracting the equilibrium magnetization (M_0) signal from the J-B signal, making $C = 0$ in the Eq. (2.46). After the spin system has been put in a non-equilibrium state by the first two pulses of the sequence, the relaxation to its equilibrium state is monitored by a detection pulse at various time τ_2.

Modified Broadband Jeener Broekaert ($t \geq 5T_1$)

$$90_{\phi_1} - 2\tau_1 - 67.5_{\phi_2} - 2\tau_1 - 45_{\phi_3} - \tau_1 - 45_{\phi_4} - \tau_2 - 45_{\phi_5} - t - 45_{\phi_6} - t -$$

The broadband J-B sequence can also be used to simultaneously measure T_{1Z} and T_{1Q} with the appropriate phase-cycling of radiofrequency and receiver phases [Table 2.2]. This avoids the necessity of matching the pulse separation between the first two pulses in the traditional J-B method to the quadrupolar splitting of the observed deuteron.

Modified Carr-Purcell

$$90_{\phi_1} - \tau - 90_{\phi_2} - (2\tau - 90_{\phi_2})_n - t -$$

This echo pulse train, with an eight-step phase cycling scheme was used to measure T_2[2.24,2.25]. Free induction decays (FIDs) after the last $90°$ pulse for different n were recorded with quadrature detection and then fast Fourier-transformed to obtain deuterium NMR spectra. In measuring T_2 at

46.05 MHz. FID signals were averaged over 24 scans or less with a repetition time of 400 ms. Each T_2 experiment consisted of 32 different n($=1,4,8\cdots.128$) values and sample heating was found to be minimal($< 0.5°$). A plot of the peak intensity of a quadrupolar doublet versus $2n\tau$ was used to determine T_2. It has been shown that[2.25] the measured T_2 depends on the pulse spacing. Two limiting cases produce different linear combinations of spectral densities $J_0(0)$, $J_1(\omega_0)$ and $J_2(2\omega_0)$, where $\omega_0/2\pi = 46.05$ MHz. When the pulse spacing τ is small such that $\tau < 1/\nu_Q$ with $2\nu_Q$ being the quadrupolar splitting of the deuteron in measurement, the deuteron spin relaxes as if the splitting is absent. This limit is not experimentally feasible because of rather large quadrupolar splittings in liquid crystals and the the problem of over-heating the sample by the rf pulse train. The another limit corresponds to $\tau > 1/\nu_Q$ when the two lines of the doublet relax independently and the deuteron spin-spin relaxation rate $1/T_2$ is given in Eq. (2.45).

References

2.1 N. Bloembergen. E.M. Purcell. R. Pound. *Phys. Rev.* **73**. 679. 1948.

2.2 R.K. Wangsness. F. Bloch. *Phys. Rev.* **89**. 728. 1953.

2.3 F. Bloch. *Phys. Rev.* **102**. 104. 1956.

2.4 M.E. Rose. In *Elementary Theory of Angular Momentum* John Wiley & Sons. Inc.. New York. 1957.

2.5 A.G. Redfield. *IBM J. Res. Dev.* **1**. 19. 1957.

2.6 R.K. Wangsness. F. Bloch. *Phys. Rev.* **89**. 728. 1953: F. Bloch. *ibid.*. **102**. 104. 1956.

2.7 A.G. Redfield. *Adv. Magn. Reson..* **1**. 1. 1965.

2.8 D. Petit. J.P. Korb. A. Delville. *J. Magn. Reson..* **96**. 252. 1992.

2.9 J. Jeener. P. Broekaert. *Phys. Rev.* **157**. 232. 1967.

2.10 A. Abragam. *Principles of Nuclear Magnetism*. Clarendon. Oxford. 1961.

2.11 M. Mehring. E.K. Wolff. M.E. Stoll. *J. Magn. Reson..* **37**. 475. 1980.

2.12 R.R. Vold. R.L. Vold. *J. Chem. Phys..* **66**. 4018. 1977.

2.13 R.L. Vold. W.H. Dickerson. R.R. Vold. *J. Magn. Reson.* **43**. 213. 1981.

2.14 T.M. Barbara. R.L. Vold. R.R. Vold. *J. Magn. Reson.* **59**. 478. 1984.

2.15 Eiichi Fukushima, Stephen B.W. Roedar. In *Experimental Pulse NMR* Addison Wesley Publishing Company, Inc., 1981.

2.16 L. Friesen. *B.Sc. Thesis*. Brandon University. 1992.

2.17 X. Shen. *M.Sc. Thesis*. the University of Manitoba. 1994.

2.18 R.Y. Dong. G.M. Richards. *J. Chem. Soc. Faraday Trans. II*. **84**. 1053. 1988.

2.19 R.Y. Dong. L. Friesen. G.M. Richards. *Mol. Phys.*. **81**. 1017. 1994.

2.20 S. Wimperis. *J. Magn. Reson.* **86**. 46. 1990.

2.21 S. Wimperis. *J. Magn. Reson.* **83**. 509. 1989.

2.22 S. Wimperis. G. Bodenhausen. *Chem. Phys. Lett.* **132**. 194. 1986.

2.23 H.W. Spiess. *J. Chem. Phys.* **72**. 6755. 1980.

2.24 H.Y. Carr. E.M. Purcell. *Phys. Rev.* **94**. 630. 1954.

2.25 S.B. Ahmad. K.J. Packer and J.M. Ramsden. *Mol. Phys.* **33**. 857. 1977.

Chapter 3

Theory: Orientational Order

For a mesophase of cylindrical symmetry formed by symmetric and elongated objects, the orientational order was defined by Tsvetkov[3.1] 50 years ago, i.e.,

$$S = < (3\cos^2 \vartheta - 1)/2 > \tag{3.1}$$

where ϑ is the angle between the molecular and mesophase symmetry axes, and the angular brackets indicate a statistical average. This order parameter has the nice feature of being zero when the molecular axes are randomly distributed with respect to the laboratory axes, i.e., when the phase is an isotropic liquid. It also becomes unity when the molecular axes are completely aligned with respect to the director or a laboratory direction.

More generally, the purely orientational distribution can be expanded using the Wigner rotation matrices

$$P(\Omega) = \sum_{L,m,n} p_{Lmn} D_{mn}^L (\Omega) \tag{3.2}$$

where $\Omega = (\alpha, \beta, \gamma)$, the Euler angles, specify the orientation of a molecule with respect to the

director.

3.1 Cylindrical Molecules in Uniaxial Phase

To treat samples with uniaxial phases(i.e.. nematics or smectic A). the assumption is that the axis of the cylindrical symmetry(the director) is along the laboratory Z_L axis. Thus no observable property will change by rotating the sample about the Z_L axis. The probability for a molecule to have orientation (α, β, γ) should be the same whatever the α, since the angle α describes a rotation around the Z_L axis. Also for the molecules possessing uniaxial symmetry, the distribution should not depend on the angle γ which involves a rotation around the molecular z_M axis, so that

$$P(\alpha, \beta, \gamma) \propto P(\beta) \tag{3.3}$$

with the normalization condition

$$\int_0^\pi \sin\beta P(\beta) d\beta = 1 \tag{3.4}$$

In identifying a set of parameters that we can use in lieu of $P(\beta)$, the distribution is expanded in a basis set of orthogonal functions. Such a set is that of the Legendre polynomials $P_L(\cos\beta)$, for which

$$\int_0^\pi \sin\beta P_L(\cos\beta) P_N(\cos\beta) d\beta = \frac{2}{2L+1}\delta_{LN} \tag{3.5}$$

Clearly these functions correspond to a special subset of the Wigner rotation matrices used in the general expansion. The explicit forms of the first few Legendre polynomials are

$$P_0(\cos\beta) = 1$$

$$P_1(\cos\beta) = \cos\beta$$

51

$$P_2(\cos\beta) = (3\cos^2\beta - 1)/2$$

$$P_3(\cos\beta) = (5\cos^3\beta - 3\cos\beta)/2$$

$$P_4(\cos\beta) = (35\cos^4\beta - 30\cos^2\beta + 3)/8 \tag{3.6}$$

Legendre polynomials are either even functions or odd functions of $\cos\beta$, corresponding to either the rank L is even or odd, i.e.,

$$P_L(\cos\beta) = (-)^L P_L[\cos(\pi - \beta)] \tag{3.7}$$

If the molecules are unable to distinguish head from tail in a macroscopic sample, this corresponds to the experimental finding that on turning the aligned sample upside down no observable property changes. One has

$$P(\beta) = P(\pi - \beta) \tag{3.8}$$

Thus only even L terms need to be retained when expanding the distribution $P(\beta)$

$$P(\cos\beta) = \sum_{L=0}^{\infty} p_L P_L(\cos\beta) \quad L \text{ even} \tag{3.9}$$

The coefficient p_L is easily found as

$$p_L = \frac{2L + 1}{2} \langle P_L \rangle \tag{3.10}$$

with

$$\langle P_L \rangle = \int_0^{\pi} \sin\beta P_L(\cos\beta) P(\beta) d\beta \tag{3.11}$$

It is apparent that the knowledge of the infinite set of $\langle P_L \rangle$ completely defines the distribution and that the averages of Legendre polynomials $\langle P_L \rangle$ represent a set of orientational order parameters.

$$P(\beta) = \frac{1}{2} + \frac{5}{2}\langle P_2 \rangle P_2(\cos\beta) + \frac{9}{2}\langle P_4 \rangle P_4(\cos\beta) + \cdots \qquad (3.12)$$

The first non-trivial term contains the second rank order parameter

$$\langle P_2 \rangle = \left\langle (3\cos^2\beta - 1)/2 \right\rangle \qquad (3.13)$$

which is the same as described by Tsvetkov[3.1].

3.2 Non-Cylindrical Molecules in Uniaxial Phase

Here the assumption is that the rigid molecules of interest are still in a uniaxial phase, but the cylindrical symmetry for the molecules is removed. Since rotation around the molecular z_M axis changes the orientational distribution, the angle γ is needed in describing the system. Thus, the probability of finding the molecule at a specific orientation, $P(\Omega)$, which is related to the two Euler angles β, γ, can be expressed in a complete basis set of spherical harmonics as:

$$P(\beta, \gamma) = \sum_{Ln} p_{Ln} D_L^{0n}(\beta, \gamma) \qquad (3.14)$$

where $D_L^{0n}(\beta, \gamma)$ is the Wigner rotation matrix. The coefficients p_{Ln} can be determined using the orthogonality of the basis and the normalization condition. Thus,

$$P(\beta, \gamma) = \frac{1}{4\pi} \sum_{L=0}^{\infty} \sum_{n=-L}^{L} (2L + 1) < D_L^{0n} > D_L^{0n}(\beta, \gamma) \qquad (3.15)$$

Since the set of averaged Wigner rotation matrices $< D_L^{0n} >$ allows a complete characterization of $P(\beta, \gamma)$, the generally complex quantities $< D_L^{0n} >$ are called orientational order parameters. The complex conjugate of a Wigner function is $D_{L^*}^{mn}(\Omega) = (-1)^{m-n} D_L^{-m-n}(\Omega)$ and the $P(\beta, \gamma)$ is real.

then

$$< D_{L^*}^{0n} > = (-)^n < D_L^{0n} > \qquad (3.16)$$

and the number of independent quantities is correspondingly reduced.

When we choose the molecular frame with three C_2 symmetry axes, turning the biaxial particle upside down does not change anything. We need to retain the functions that are invariant under the transformation $\beta \rightarrow (\pi - \beta)$. In this operation, the spherical harmonics $D_{0n}^L(\beta, \gamma)$ have the following relation

$$D_{0n}^L(\beta\gamma) = (-)^L D_{0n}^L(\pi - \beta, \gamma) \tag{3.17}$$

Therefore, we only need to expand in Wigner rotation matrices of even rank L. The first few are

$$
\begin{aligned}
D_{00}^0(\beta, \gamma) &= 1 \\[2mm]
D_{00}^2(\beta, \gamma) &= P_2(\cos\beta) \\[2mm]
D_{0\pm2}^2(\beta, \gamma) &= \sqrt{\frac{3}{8}} \sin^2\beta \exp(\mp i2\gamma) \\[2mm]
D_{00}^4(\beta, \gamma) &= P_4(\cos\beta) \\[2mm]
D_{0\pm2}^4(\beta, \gamma) &= \sqrt{10}\left(14\cos^6\frac{\beta}{2} - 14\cos^4\frac{\beta}{2} + 3\cos^2\frac{\beta}{2}\right)\sin^2\frac{\beta}{2}\exp(\mp i2\gamma) \\[2mm]
D_{0\pm4}^4(\beta, \gamma) &= \sqrt{70}\cos^4\frac{\beta}{2}\sin^4\frac{\beta}{2}\exp(\mp i4\gamma)
\end{aligned}
\tag{3.18}
$$

The rank L order parameters can be calculated from

$$< D_{0n}^L > = \delta_{m0}\int d\Omega \, P(\Omega) D_{mn}^L(\Omega) \tag{3.19}$$

At second rank level, $L = 2$, and in the general case of biaxial molecules, there are at most five independent order parameters $< D_{0n}^2 >$, which could be chosen as the independent components of Cartesian ordering matrix S first introduced by Saupe[3.2]

54

$$S = \begin{pmatrix} < \frac{3}{2}\sin^2 \beta \cos^2 \gamma - \frac{1}{2} > & < \sin^2 \beta \cos \gamma \sin \gamma > & < \sin \beta \cos \beta \cos \gamma > \\ < \sin^2 \beta \cos \gamma \sin \gamma > & < \frac{3}{2}\sin^2 \beta \sin^2 \gamma - \frac{1}{2} > & < \sin \beta \cos \beta \sin \gamma > \\ < \sin \beta \cos \beta \cos \gamma > & < \sin \beta \cos \beta \sin \gamma > & < \frac{3}{2}\cos^2 \beta - \frac{1}{2} > \end{pmatrix} \qquad (3.20)$$

This order matrix is traceless and symmetric. Also it can be easily converted from the Saupe to the Wigner rotation matrix form[3.3].

$$S = \begin{pmatrix} \frac{\sqrt{6}}{2}Re < D_{02}^2 > -\frac{1}{2} < D_{00}^2 > & -\sqrt{\frac{3}{2}}Im < D_{02}^2 > & -\sqrt{\frac{3}{2}}Re < D_{01}^2 > \\ -\sqrt{\frac{3}{2}}Im < D_{02}^2 > & -\frac{\sqrt{6}}{2}Re < D_{02}^2 > -\frac{1}{2} < D_{00}^2 > & \sqrt{\frac{3}{2}}Im < D_{02}^2 > \\ -\sqrt{\frac{3}{2}}Re < D_{01}^2 > & \sqrt{\frac{3}{2}}Im < D_{01}^2 > & < D_{00}^2 > \end{pmatrix} \qquad (3.21)$$

We call the ordering matrix frame the principal axis system (PAS) of S when S is diagonal. The number of independent parameters is reduced to 2 in the PAS, $< D_{00}^2 >$, and $Re < D_{02}^2 >$, or S_{zz}, and $S_{xx} - S_{yy}$.

$$S_{xx} - S_{yy} = \sqrt{6}Re < D_{02}^2 > \quad and \quad S_{zz} =< D_{00}^2 > \qquad (3.22)$$

While $< D_{00}^2 >$ measures the alignment of the molecular z_M axis with respect to the director as in the case of cylindrical molecules, the non-zero $Re < D_{02}^2 >$ is caused by the molecular biaxiality. It provides the difference in ordering of the x_M and y_M axes for the molecule in the liquid crystal solvent. When the molecules have the cylindrical symmetry, then biaxiality parameter $S_{xx} - S_{yy} = 0$ and only one independent order parameter survives, i.e., $S_{zz} =< D_{00}^2 >=< (3\cos^2 \beta - 1)/2 >$, the same as described by Eq. (3.1). The molecular biaxiality may be due to either the rigid non-cylindrical part of molecules or the flexible parts of chain which are attached to the aromatic core. These order parameters $< D_{00}^2 >$ and $< D_{02}^2 >$ are very important in both modelling the quadrupo-

lar splittings and spectral density calculations using theoretical models.

The quadrupolar splitting $\Delta\nu_0$ of the C_0 deuteron, whose $C - D$ bond is fixed in the molecular (PAS) frame, is given by($\eta = 0$)

$$\Delta\nu_0 = -\frac{3}{2}q_{bb}^{(0)}\left[d_{00}^2(\theta_{bz}) < P_2 > +\frac{1}{2}(S_{xx} - S_{yy})(\cos^2\theta_{bx} - \cos^2\theta_{by})\right] \qquad (3.23)$$

where θ_{bx} and θ_{by} are angles between the C-D bond (the principal b axis of the EFG tensor) and the molecular x_M and y_M axes, respectively, and $\theta_{bz} = \theta$ is defined as the angle between the C-D bond and the molecular z_M axis. For the deuteron at methine site of 50.7 and MBBA, the $q_{bb}^{(0)}$ is taken as 185kHz. The above equation can be expressed in terms of the polar angle θ and azimuthal angle ϕ of the $C - D$ bond in the PAS of S

$$\Delta\nu_0 = -\frac{3}{2}q_{bb}^{(0)}\left[d_{00}^2(\theta) < P_2 > +\frac{1}{2}(S_{xx} - S_{yy})\sin^2\theta\cos 2\phi\right] \qquad (3.24)$$

If $\eta \neq 0$, the quadrupolar splitting is given by[3.4]

$$\begin{aligned}
\Delta\nu &= -\frac{3}{2}q_{bb}S_{zz}\{[d_{00}^2(\theta_{bz}) + \frac{1}{2}\eta(\cos^2\theta_{az} - \cos^2\theta_{cz})] \\
&\quad +\frac{1}{2}(S_{xx} - S_{yy})[\cos^2\theta_{bx} - \cos^2\theta_{by} \\
&\quad +\frac{\eta}{3}(\cos^2\theta_{ax} - \cos^2\theta_{cx} - \cos^2\theta_{ay} + \cos^2\theta_{cy})]\}
\end{aligned} \qquad (3.25)$$

This is used for a C-D bond on a phenyl ring. Eqs. (3.24)-(3.25) are appropriate when the C-D bond does not participate in internal motions.

3.3 Molecular Field Theory of Flexible Molecules: The AP method

The constituent molecules of liquid crystals usually contain an aromatic core and one or more flexible side chains. NMR studies of order parameter profiles in these molecules have revealed that

56

the ordering of their rigid segments varies with respect to each other and with temperature. Since the flexible chains not only occupy space but also contribute to the anisotropic potential and interactions, they are partially responsible for molecular ordering in liquid crystals. In attempting to interpret the deuterium quadrupolar splittings $\Delta\nu_i$, which are both temperature dependent and site dependent, it is necessary to assume that molecular conformation is independent of molecular orientation, thereby separating the internal and overall motions. The additive potential (AP) method was first used by Marcelja[3.5] to explicitly take the alkyl chain into account in calculating physical properties of liquid crystals, and extended subsequently by Emsley, Luckhurst and Stockley[3.6]. Due to internal degrees of freedom, the chain therefore does not always exist in an all-trans conformation. An additional average is needed for flexible molecules because different conformational states are available to the molecules. In doing so, it is necessary to determine all of the allowed conformations and their relative weights $p_{eq}(n)$, the equilibrium probability for finding the molecule in the nth conformation. It is assumed that each molecular conformer is a perfect rigid entity. To do the conformational average, it requires all configurations generated by the rotational isomeric state (RIS) model of Flory[3.7]. In this model, the bond lengths are taken to be fixed and the only angle that is allowed to vary is the bond rotation angle φ. Rotation about each carbon-carbon (C-C') bond in the chain may take one of the three dihedral angles ($\varphi = 0, \pm 112°$). These correspond to the *trans* (t) and two symmetric *gauche* ($g^{\pm}$) states. In the RIS model, only states in the potential minima are assumed to be appreciably populated. This is due to the very steep potential barriers between these minima. The *gauche* states have higher internal energy in comparison to that of the *trans* state by an amount E_{tg}. When the chain contains a g^-g^- or a g^-g^- linkage, an additional internal energy $E_{g^{\pm}g^{\pm}}$ may be added because these linkages bring parts of the chain near to one another, the so-called "pentane effect". The E_{tg} values reported for gaseous alkanes lie between 2.1

and 3.2 kJ/mol, while the $E_{g=g^=}$ value is about three times larger[3.7]. For 6OCB and HAT6, the $O-C$ bond is fixed and each $C_i - C_{i-1}$ bond (i=1,$\cdots$,5) can take three positions corresponding to the potential minima, and the number of configurations is 3^5=243.

In modeling the quadrupolar splittings ($\Delta \nu_i$) for the methylene C_i deuterons, one uses

$$\Delta \nu_i = \frac{3}{2} q_{CD}^{(i)} P_2(\cos \Theta) S_{CD}^{(i)} \qquad (3.26)$$

where $q_{CD}^{(i)} = (e^2 qQ/h)_i$ is the quadrupolar coupling constants for C_i deuterons and is taken as 165 kHz and 185 kHz for methylene and ring deuterons, respectively. Θ is the angle between the director and the external magnetic field. $\Theta = 0$ for the 5O.7, 6OCB and MBBA liquid crystals samples where director is aligned along the external magnetic field. $\Theta = 90°$ for the columnar HAT6 sample where the director is perpendicular to the external field. In this case, there is a factor $\frac{1}{2}$ produced by the term $P_2(\cos \Theta)$. $S_{CD}^{(i)}$ is a weighted average of the segmental order parameter. Suppose that $S_{\alpha\beta}^{n}$ represents an order parameter tensor which describes the orientational order of the nth rigid conformer. Then in the principle axis (X, Y, Z) frame of the nuclear quadrupolar interaction, one has

$$S_{CD}^{(i)} = \sum_n p_{eq}(n) \left[S_{ZZ}^{n,i} + \frac{\eta^{(i)}}{3}(S_{XX}^{n,i} - S_{YY}^{n,i}) \right] \qquad (3.27)$$

where the sum is over all possible configurations in the chain, the C-D bond is taken to be along the axis Z (i.e., $q_{CD}^{(i)} = q_{ZZ}^{(i)} \equiv V_{ZZ}^{(i)}$). $\eta^{(i)}$, the asymmetry parameter of the electric field gradient, is defined by

$$\eta^{(i)} = \frac{q_{XX}^{(i)} - q_{YY}^{(i)}}{q_{ZZ}^{(i)}} \qquad (3.28)$$

and $p_{eq}(n)$ is the equilibrium probability which specifies fraction of molecules in the nth conformation. For the methylene deuterons, $\eta = 0$ is a very good approximation. η is taken as 0.064 for the

ring deuteron. To evaluate $p_{eq}(n)$, one needs both the internal energy $U_{int}(n)$ and external potential energy $U_{ext}(n,\omega)$ of the nth conformer. The internal energy is assumed to depend on the number of *gauche* linkages (N_g) and the number of $g^\pm g^\mp$ linkages ($N_{g^\pm g^\mp}$) in the chain of the nth conformer:

$$U_{int}(n) = N_g E_{tg} + N_{g^\pm g^\mp} E_{g^\pm g^\mp} \tag{3.29}$$

while the external potential energy depends also on the orientation ω of the director in a molecular frame of the nth conformer.

The potential of mean torque $U_{ext}(n,\omega)$ is responsible for the alignment of a conformer and results from the molecular field of its neighbors. It depends on the conformational state n of the molecule and on the polar angle ω of the director in a frame that is attached to a particular rigid segment of the conformer. To minimize the number of parameters, it is assumed that the molecule can be divided into a small number of rigid segments. Each segment is associated with an interaction tensor that is independent of the conformation. The interaction tensor of the molecule is calculated by transforming the tensors from their segmental axis systems into a common system and then adding them together. This is the basis of the additive potential (AP) method. The potential of mean torque for a particular conformation can be approximated by a second-rank term[3.8].

$$U_{ext}(n,\omega) = -\sum_m (-)^m \epsilon^n_{2,m} C_{2,-m}(\omega) \tag{3.30}$$

where $C_{2,-m}(\omega)$ is a modified spherical harmonic of rank 2. $\epsilon^n_{2,m}$, the interaction tensor for conformation n, is given by

$$\epsilon^n_{2,m} = \sum_j \epsilon^j_{2,m}(n) \tag{3.31}$$

where the sum over j is to add together interaction tensors of all rigid subunits. In the jth segmental axis frame, $\epsilon_{2,r}^j$ represents the local interaction of the jth rigid sub-unit and is assumed to be independent of the conformation. Let $\epsilon_{2,r}^a$ and $\epsilon_{2,r}^c$ represent the interaction tensors of aromatic core and of each C-C segment, respectively. If both of them are assumed to have cylindrical symmetry, the unique components of $\epsilon_{2,r}^a$ and $\epsilon_{2,r}^c$ are X_a and X_{cc}, respectively. In this simplification, the number of interaction parameters required to calculate the molecular interaction tensor is reduced to 2. The segmental interaction tensors $\epsilon_{2,m}^j(n)$ vary with conformation because their components need to be expressed in a common molecular frame. This dependence is expressed in

$$\epsilon_{2,m}^j(n) = \sum_r D_{m,r}^{2*}(\omega_j^n)\epsilon_{2,r}^j \qquad (3.32)$$

where $D_{m,r}^2(\omega_j^n)$ is a second-rank Wigner rotation matrix, and ω_j^n denotes the set of Euler angles needed to transform between axes in the jth segment and the common molecular frame. The $p_{eq}(n)$ is given by

$$p_{eq}(n) = \exp[-U_{int}(n)/k_BT]Q_n/Z \qquad (3.33)$$

where Q_n, the orientational partition function of conformation n, is

$$Q_n = \int \exp[-U_{ext}(n,\omega)/k_BT]d\omega \qquad (3.34)$$

and Z, the conformation-orientational partition function, is

$$Z = \sum_n \exp[-U_{int}(n)/k_BT]Q_n \qquad (3.35)$$

Now the order parameter for a particular direction k in the conformer n (in Eq. (3.27)) may be evaluated in the principal (x,y,z) frame of $U_{ext}(n,\omega)$ according to

$$S_{kk}^{n,i} = \sum_\alpha^{x,y,z} S_{\alpha\alpha}^n \cos^2 \theta_{\alpha k}^{n,i} \qquad (3.36)$$

60

where $\theta_{\alpha k}^{n,i}$ denote angles for the C_i-^2H bond between the $k(= X, Y, Z)$ axis and a principal axis $\alpha(= x, y, z)$. $S_{\alpha\alpha}^n$ is the principal components of the Saupe ordering matrix for the conformer n. may be written as[3.9]

$$
\begin{aligned}
S_{xx}^n &= \frac{1}{2}\left(\sqrt{6}\left\langle d_{0,2}^2 \cos 2\omega\right\rangle_n - \left\langle d_{0,0}^2\right\rangle_n\right) \\
S_{yy}^n &= -\frac{1}{2}\left(\sqrt{6}\left\langle d_{0,2}^2 \cos 2\omega\right\rangle_n + \left\langle d_{0,0}^2\right\rangle_n\right) \\
S_{zz}^n &= \left\langle d_{0,0}^2\right\rangle_n
\end{aligned}
\tag{3.37}
$$

In order to evaluate the averages of the reduced rotation matrices, it is advantageous to describe the director orientation in the principal axis system of $U_{ext}(n,\omega)$. Hence, the constructed interaction tensor $U_{ext}(n,\omega)$ is first diagonalized to obtain the interaction tensor components $X_{2,0}^n$ and $X_{2,-2}^n$ for the conformer n. In the principal frame

$$
U_{ext}(n,\omega) = -\left[X_{2,0}^n d_{0,0}^2(\theta) + 2X_{2,2}^n d_{0,2}^2(\theta) \cos 2\omega\right]
\tag{3.38}
$$

Using $a_n = X_{2,0}^n/k_BT$ and $b_n = 2X_{2,2}^n/k_BT$, the order parameters of the nth conformer can be evaluated according to[3.9]

$$
\begin{aligned}
\left\langle d_{0,0}^2\right\rangle_n &= 2\pi \int_0^\pi P_2(\cos\theta) I_0[b_n d_{0,2}^2(\theta)] \exp[a_n d_{0,0}^2(\theta)] \sin\theta d\theta/Q_n \\
\left\langle d_{0,2}^2 \cos 2\omega\right\rangle_n &= 2\pi \int_0^\pi d_{0,2}^2(\theta) I_1[b_n d_{0,2}^2(\theta)] \exp[a_n d_{0,0}^2(\theta)] \sin\theta d\theta/Q_n
\end{aligned}
\tag{3.39}
$$

and Q_n becomes

$$
Q_n = 2\pi \int_0^\pi I_0[b_n d_{0,2}^2(\theta)] \exp[a_n d_{0,0}^2(\theta)] \sin\theta d\theta
\tag{3.40}
$$

and $I_n(x)$, the nth order modified Bessel function is given by

$$
I_n(x) = \frac{1}{\pi} \int_0^\pi \cos n\varphi \exp[x \cos\varphi] d\varphi
\tag{3.41}
$$

61

Finally, using Eq. (3.33) and Eqs. (3.36)-(3.41) in Eq. (3.27), the AP method allows the order parameter profiles to be modeled along flexible chains of nematogens and some smectogens.

3.4 Applications

The AP method has been applied to study the orientational order profiles in flexible mesogens of 6OCB, MBBA and HAT6. To construct $U_{ext}(n, \omega)$, one needs to know the geometry of the chain. Both 6OCB and HAT6 have alkyloxy chain(s). It is known that the $\angle COC$ or $\angle CCC$ which specifies the direction of the chain relative to the molecular core plays an important role in the observed variations of segmental order and spin relaxation profiles. The molecular core, which includes the first $C_{ar} - O$ bond in the chain, is assumed to be a rigid subunit and has cylindrical symmetry with an interaction parameter X_a. This simplification is based on the picture that the core's rotation around its symmetry axis is rather fast. As an approximation, the bond interaction parameter of $O - C_1$ bond is taken to be identical to those of $C - C$ bonds, i.e. $X_{oc} = X_{cc}$, and the $C -^2 H$ segments were included in the $C - C$ bonds (i.e., united atoms). According to the model prediction of AP method[3.6,3.10], the ratio $\lambda_c = X_{cc}/X_a$ should be independent of temperature. Due to the different molecular shapes of rod-like and disk-like molecules, different procedures are needed to process them seperately.

3.4.1 Calamitic Mesogens: 6OCB and MBBA

For 6OCB, the $C_{ar} - O$ bond may be taken to be along the biphenyl para axis, while in MBBA, the $C_{ar} - C_1$ bond is taken parallel to the para axis of the aniline ring. The interaction tensor $\epsilon_{\alpha\beta}^a$

62

for this rod-shaped core is written as

$$X_a \begin{pmatrix} -\frac{1}{2} & 0 & 0 \\ 0 & -\frac{1}{2} & 0 \\ 0 & 0 & 1 \end{pmatrix} \tag{3.42}$$

Since both rod-like core and $C - C$ segment can be regarded as cigar shaped rigid submunits, the interaction tensor $\epsilon_{a,j}^{cc}$ is also given by

$$X_{cc} \begin{pmatrix} -\frac{1}{2} & 0 & 0 \\ 0 & -\frac{1}{2} & 0 \\ 0 & 0 & 1 \end{pmatrix} \tag{3.43}$$

The following geometry is used: $\angle CCC = 113.5°$, $\angle CCH = 107.5°$, $\angle HCH = 113.6°$, $\angle OCC = \angle CCC$[3.10], and $\angle COC = 126.4°$[3.11,3.12]. The $O - C_1$ bond was fixed on the ring plane to give 243 conformations in the hexyloxy chain. For MBBA, the first dihedral angle in the butyl chain is allowed to sample all three RIS giving 27 different conformations. In a local (1,2,3) frame where 3 axis is along the $C_j - C_{j-1}$ bond, the 1 axis is in the plane bisecting the HCH angle, and the 2 axis is chosen to complete a right-handed Cartesian coordinate system, the $C -^2 H$ vector is given by

$$\overrightarrow{V}_{CD} = \begin{pmatrix} a \\ b \\ c \end{pmatrix} \tag{3.44}$$

where $b = \sin(\angle HCH/2)$, $c = \cos(\angle CCH)$ and $a = \sqrt{1 - b^2 - c^2}$. For 6OCB, a common molecular frame is picked with the z_M axis along the *para* axis of the core, the x_M axis lying on the $C_{ar} - O - C_1$ plane[see Figure 9.2]; while for MBBA, the z_M axis is along the $C_{ar} - C_1$ bond and the x_M axis lying on this ring plane. Then the orientation of the $C_j -^2 H$ vector in the common molecular frame

63

is given by

$$\vec{V}^{M}_{CD} = R_{M,1}R_{1,2}\cdots R_{j-1,j}\vec{V}_{CD} \tag{3.45}$$

where $R_{j-1,j}$ is a rotation matrix that transforms between the jth local and the $(j-1)$th local frame, which consists of two consecutive rotations. One is the rotation around local y_j by angle $180° - \angle CCC$, which brings the z_j axis to coincide with the z_{j-1} axis; the other is the rotation around local z_{j-1} axis by angle $180° - \phi$, which brings x_j axis to coincide with the x_{j-1} axis. Finally, the rotation matrix can be expressed as

$$R_{j-1,j} = \begin{pmatrix} \cos\beta_j\cos\gamma_j & \sin\gamma_j & -\sin\beta_j\cos\gamma_j \\ -\cos\beta\sin\gamma_j & \cos\gamma_j & \sin\beta_j\sin\gamma_j \\ \sin\beta_j & 0 & \cos\beta_j \end{pmatrix} \tag{3.46}$$

where $\beta_j = 180° - \angle CCC$ and $\gamma_j = 180° - \phi$. ϕ is one of the three dihedral angles corresponding to the potential minima $(0,\pm112°)$. To obtain the direction cosine in Eq. (3.36), it is necessary to get the $C_j -^2 H$ vector in the principal frame of the total interaction tensor

$$\vec{V}^{P}_{CD} = R_{p,M}\vec{V}^{M}_{CD} \tag{3.47}$$

where the rotation matrix $R_{p,M}$ contains the eigenvectors ($\vec{r}$) obtained in diagonalizing the total interaction tensor $\epsilon^{n}_{\alpha\beta}$ for each conformer. The $\epsilon^{n}_{\alpha\beta}$ is obtained by

$$\epsilon^{n}_{\alpha\beta} = \epsilon^{a}_{\alpha\beta} + \sum_{j=2}^{7} R_{1,2}\cdots R_{j-1,j}\epsilon^{cc}_{\alpha\beta}R^{-1}_{j-1,j}\cdots R^{-1}_{1,2} \tag{3.48}$$

This is the interaction tensor for the nth conformer and is a Cartesian tensor. Once it is diagonalized, the $U_{ext}(n,\omega)$ can be obtained from Eq. (3.38). Note that Eq. (3.47) is also needed to find the direction cosines (or $\theta^{n,i}_{\alpha k}$) in Eq. (3.36) for modeling the ring deuteron splitting using the $\vec{V}^{M}_{CD}$ for the ring C-D bond. Eq. (3.27) is used for each of the two non-equivalent deuterons in the ring.

64

It is necessary to explicitly consider ring rotations, i.e., need to average these splittings due to the rapid internal ring rotations.

3.4.2 Discotic Mesogens: HAT6

The interaction tensor $\epsilon^a_{\alpha\beta}$ for this disk-shaped core can still be written as

$$X_a \begin{pmatrix} -\frac{1}{2} & 0 & 0 \\ 0 & -\frac{1}{2} & 0 \\ 0 & 0 & 1 \end{pmatrix} \qquad (3.49)$$

Since the core is disk-liked and $C - C$ segment is cigar-shaped, care is needed to distinguish one from another. Two different signs were taken for the interaction tensors of these 2 different cylindrically symmetric units. The interaction tensor for the rodlike $C - C$ segment is now given by

$$X_{cc} \begin{pmatrix} \frac{1}{4} & 0 & 0 \\ 0 & \frac{1}{4} & 0 \\ 0 & 0 & -\frac{1}{2} \end{pmatrix} \qquad (3.50)$$

A scaled factor $\frac{1}{2}$ was implemented in the above expression. The geometry for this molecule is set the same as that of 6OCB. A common molecular frame is picked with the z_M axis perpendicular to the core plane (see Figure 1.5), and the x_M axis on the plane bisecting two of the six pendent chains. Here we construct the total interaction tensor for HAT6 by explicitly considering two chains as shown. All the $O - C_1$ bond are fixed on the ring $(x_M y_M)$ plane. The $C_{ar} - O$ bonds are included in the core when writing down the $\epsilon^a_{\alpha\beta}$; also included are the remaining four pendent chains. Furthermore, the conformations of the two chosen chains are assumed to be identical and non-interacting. The local frames and the $C -^2 H$ vector $\overrightarrow{V}_{CD}$ are set as before. Now transformations

65

from the 1st local frame to the common molecular frame for the two pendant chains are different. Hence, one has the following $\epsilon_{\alpha,J}^n$:

$$\epsilon_{\alpha,J}^n = \epsilon_{\alpha,J}^a + R_{M,1}\lambda_{\alpha,J}^n R_{M,1}^{-1} + R'_{M,1}\lambda_{\alpha,J}^n R'^{-1}_{M,1} \tag{3.51}$$

where

$$\lambda_{\alpha,J}^n = \sum_{J=2}^{7} R_{1,2} \cdots R_{J-1,J} \epsilon_{\alpha,J}^{cc} R_{J-1,J}^{-1} \cdots R_{1,2}^{-1} \tag{3.52}$$

where $R_{M,1}$ and $R'_{M,1}$ are rotation matrices for the two chains which transform between their first local frames to the molecular frame. For obtaining the direction cosines in Eq. (3.36), we use again

$$\overrightarrow{V}_{CD}^{M} = R_{M,1} R_{1,2} \cdots R_{J-1,J} \overrightarrow{V}_{CD} \tag{3.53}$$

Finally, for the aromatic deuterons, a η value of 0.064 is assumed, and their splitting (in Eq. (3.26)) is calculated using Eqs. (3.27), (3.36) and (3.47).

References

3.1 V. Tsvetkov. *Acta Physicoch* U.S.S.R.. **10**. 557. 1939.

3.2 A. Saupe. *Angew. Chem.* (Int. Edn.). **7**. 97. 1968.

3.3 C. Zannoni. In *The Molecular Physics of Liquid Crystals* edited by G.R. Luckhurst. G.W. Gray. Academic Press. London. 1979. Chap. 3. p51.

3.4 J.W. Emsley. *Nuclear Magnetic Resonance of Liquid Crystals* edited by J.W. Emsley. Reidel Publishing. Dordrecht. 1985.

3.5 S. Marcelja. *J. Chem. Phys.* **60**. 3599. 1974.

3.6 J.W. Emsley. G.R. Luckhurst. C.P. Stockley. *Proc. R. Soc. London A* **381**. 117. 1982.

3.7 P.J. Flory. In *Statistical Mechanics of Chain Molecules.* Inter Science. New York. 1969.

3.8 M.A. Cotter. In *The Molecular Physics of Liquid Crystals.* edited by G.R. Luckkhurst. G.W. Gray. Academic Press. London. 1979. Chap. 8.

3.9 G.R. Luckhurst. C. Zannoni. P.L. Nordio. A. Segre. *Mol. Phys.* **30**. 1345. 1975.

3.10 C.J.R. Counsell. J.W. Emsley. N.J. Heaton. G.R. Luckhurst. *Mol. Phys.* **54**. 847. 1985.

3.11 C.J.R. Counsell. *Ph.D. thesis.* Southampton. 1983.

3.12 C.J.R. Counsell. J.W. Emsley. G.R. Luckhurst. H.S. Sachdev. *Mol. Phys.* **63**. 33. 1988.

Chapter 4

Theory: A Review of the Tarroni and Zannoni Model

4.1 Introduction

Since its introduction by Debye[4.1], the rotational diffusion model has been widely used to describe molecular reorientation, and its use in the interpretation of nuclear spin relaxation in isotropic liquids is well established[4.2]. More recently, rotational diffusion has been used extensively as a model to account for the nuclear spin relaxation behavior in thermotropic liquid crystals. Each molecule is characterized by a rotational diffusion tensor $\overline{D}$, normally defined in a frame fixed on the molecule. The principal components of $\overline{D}$ are D_{xx}, D_{yy} and D_{zz}. For a symmetric rotor reorienting in a uniaxial potential with rotational diffusion constants $D_{xx} = D_{yy} \neq D_{zz}$, solutions were first presented by Nordio and co-workers[4.3-4.4]. The Nordio model was used in numerous experimental studies including NMR. Freed and co-workers[4.5-4.6] subsequently developed a more general and powerful ESR line shape simulation technique based on the numerical solution of the stochastic Liouville equation. Nuclear spin relaxation in liquid crystals showing nematic and/or

smectic A phases can usually be dealt with in a simpler fashion because the molecular reorientation is fast on the NMR time scale. During the last couple of decades, a number of models of increasing complexity have been proposed by several groups, and useful solutions have been provided to the rotational diffusion equation with a variety of boundary conditions[4.7-4.9]; e.g., for the asymmetric rotor ($D_{xx} \neq D_{yy} \neq D_{zz}$) in a uniaxial potential[4.10-4.14], and also for the cylindrically symmetric rotor[4.15] and non-cylindrically symmetric rotor[4.16] in the biaxial phase.

There were some attempts to analyze the deuterium spin relaxation behavior of non-cylindrically symmetric molecules, e.g., several asymmetric planar rotors, as rotational diffusion of a symmetric top in a uniaxial potential[4.17-4.18], but worries persisted that the less than perfect fits were caused by using this approximation. More recently, Bulthuis and Plomp[4.13] attempted to interpret relaxation data for perdeuterated toluene in Licristal Phase 5 in terms of rotational diffusion of an asymmetric top in a uniaxial potential, but good fits were not achieved. However, their solutions to the rotational diffusion equation were obtained by truncating the Wigner basis set above rank 4, and this number of terms might not be sufficient. The rigorous treatment of the asymmetric rotor has been published by Tarroni and Zannoni[4.14] (TZ model), which included terms up to rank 40 in the Wigner basis set. There is a recent report in which the TZ model was applied to study the deuteron relaxation of a biaxial solute Fluorene-d_{10} in the Licristal Phase 5[4.19]. At the rest part of this chapter, a briefly theoretical review of TZ model is presented, followed by the application of this model to various situations in the study.

4.2 Correlation Functions

The rotational diffusional model assumes a stochastic Markov process[4.2, 4.3, 4.7] for molecular

reorientation in which each molecule moves in time as a sequence of small angular steps caused by collisions with its neighboring molecules and under the influence of an anisotropic potential set up by its neighbors. The orientational correlation function can be written as

$$G_{mn,m'n'}^{LL'}(t) = \int\int d\Omega_0 d\Omega P(\Omega_0) D_{mn}^{L*}(\Omega_0)$$
$$\times P(\Omega_0|\Omega t) D_{m'n'}^{L'}(\Omega) \tag{4.1}$$

where m and n represent the projection index in the laboratory frame and the projection index in the molecular frame, respectively. $\Omega \equiv (\alpha, \beta, \gamma)$ denotes the Euler angles. $P(\Omega_0|\Omega t)$ is the conditional probability of finding a molecule at orientation Ω at time t if the orientation of the molecule was Ω_0 at $t = 0$, and the equilibrium probability, $P(\Omega)$ is given by the Boltzmann distribution:

$$P(\Omega) = \frac{\exp[-U(\Omega)/kT]}{\int d\Omega \exp[-U(\Omega)/kT]} \tag{4.2}$$

where k is the Boltzmann constant and T is the temperature. $U(\Omega)$ is the potential of mean torque acting on the molecule[4.20], and its symmetry is determined by the symmetry of the molecule and that of the mesophase. In the long time limit, the orientational correlation function may be non-zero in an anisotropic medium, and is given by

$$G_{mn,m'n'}^{LL'}(\infty) = \left\langle D_{0n}^{L}(\Omega_0) \right\rangle \left\langle D_{0n'}^{L'}(\Omega) \right\rangle \delta_{m0} \delta_{m'0} \tag{4.3}$$

This long time plateau has to be substracted from $G_{mn,m'n'}^{LL'}(t)$ to ensure its decay to zero in equilibrium.

For cylindrical molecules in the uniaxial phase, the potential of mean torque is governed by the β angle only, i.e. $U(\Omega) = U(\beta)$. Here we deal with asymmetric molecules reorienting in a uniaxial

70

phase. and the potential of mean torque depends on two Euler angles. *i.e.*, $U(\Omega) = U(\beta, \gamma)$[4.21].

Now the effective anisotropic potential $U(\Omega)$ can be expanded in terms of Wigner matrices as

$$\frac{U(\beta, \gamma)}{kT} = \sum_{Jq} a_{Jq} D^J_{0q}(\beta, \gamma) \tag{4.4}$$

and the orientational order parameters, averages of the Wigner rotation matrices $D^L_{mn}(\Omega)$, are (see Chapter 3)

$$\left\langle D^L_{0n} \right\rangle = \int d\Omega P(\beta, \gamma) D^L_{0n}(\beta, \gamma) \tag{4.5}$$

If the molecular reorientation takes place through a sequence of small angular steps, the evolution of the conditional probability $P(\Omega_0|\Omega t)$ can be described[4.22] by a differential equation for the rotational diffusion process as

$$\frac{\partial P(\Omega_0|\Omega t)}{\partial t} = -\sum_{\alpha\beta} L_\alpha D_{\alpha\beta} \left[L_\beta + L_\beta \left(\frac{U(\Omega)}{kT} \right) \right] P(\Omega_0|\Omega t) \tag{4.6}$$

where $L_\beta (= L_x, L_y,$ or $L_z)$ is a component of a dimensionless angular momentum operator $\overrightarrow{L}$, and $\overline{D}$ is a rotational diffusion tensor. Here we choose a molecule-fixed frame in which $\overline{D}$ is diagonal

$$\overline{D} = \begin{pmatrix} D_{xx} & 0 & 0 \\ 0 & D_{yy} & 0 \\ 0 & 0 & D_{zz} \end{pmatrix} = \rho \begin{pmatrix} 1+\epsilon & 0 & 0 \\ 0 & 1-\epsilon & 0 \\ 0 & 0 & \eta \end{pmatrix} \tag{4.7}$$

where

$$\rho \equiv \frac{D_{xx} + D_{yy}}{2}, \quad \epsilon \equiv \frac{D_{xx} - D_{yy}}{D_{xx} + D_{yy}}, \quad \eta \equiv \frac{2D_{zz}}{D_{xx} + D_{yy}} \tag{4.8}$$

ϵ is an asymmetry parameter of the diffusion tensor, going from -1 to $+1$. η is the ratio between diffusion around z_M axis (spinning motion) and that of the z_M axis itself (tumbling motion) expressed by ρ. In the cylindrical symmetry limit (ρ becomes $D_\perp$, η becomes $D_\parallel/D_\perp$ and ϵ reduces to 0), the diffusion matrix is reduced to the Nordio's notation.

71

Now, back to the more general case with non-zero ϵ, the Eq. (4.6) becomes

$$\frac{1}{\rho}\frac{\partial P(\Omega_0|\Omega t)}{\partial t} = -(1+\epsilon)\left[L_x^2 + L_x\left(L_x\frac{U(\Omega)}{kT}\right)\right]P(\Omega_0|\Omega t)$$

$$-(1+\epsilon)\left[L_y^2 + L_y\left(L_y\frac{U(\Omega)}{kT}\right)\right]P(\Omega_0|\Omega t)$$

$$-\eta\left[L_z^2 + L_z\left(L_z\frac{U(\Omega)}{kT}\right)\right]P(\Omega_0|\Omega t)$$

$$\equiv \overrightarrow{\Gamma}P(\Omega_0|\Omega t) \tag{4.9}$$

where $\overrightarrow{\Gamma}$ is the diffusion operator which, for the purpose of numerical calculations, can be rewritten using a unitary transformation as

$$\hat{\Gamma} = P^{-1/2}(\Omega)\overrightarrow{\Gamma}P^{1/2}(\Omega)$$

$$= -\left\{\nabla^2 + \frac{1}{2}\left(\nabla^2\frac{U(\Omega)}{kT}\right) - \frac{1}{4}\left(L_-\frac{U(\Omega)}{kT}\right)\left(L_+\frac{U(\Omega)}{kT}\right) - \frac{1}{4}\eta\left(L_z\frac{U(\Omega)}{kT}\right)^2\right\}$$

$$-\epsilon\left\{\frac{1}{2}\left(L_+^2 + L_-^2\right) + \frac{1}{4}\left[\left(L_+^2 + L_-^2\right)\frac{U(\Omega)}{kT}\right] - \frac{1}{8}\left[\left(L_-\frac{U(\Omega)}{kT}\right)^2 + \left(L_+\frac{U(\Omega)}{kT}\right)^2\right]\right\} \tag{4.10}$$

where $P(\Omega)$ is the equilibrium distribution, the nobla operator $\nabla^2 = L_x^2 + L_y^2 + \eta L_z^2$ and $L_\pm = L_x \pm iL_y$ is the angular momentum step operator. When $\epsilon = 0$, the above operator $\hat{\Gamma}$ is the same as that used by Nordio and his co-workers. The diffusion equation in this symmetrized form is given by

$$\frac{1}{\rho}\frac{\partial \hat{P}(\Omega_0|\Omega t)}{\partial t} = \hat{\Gamma}\hat{P}(\Omega_0|\Omega t) \tag{4.11}$$

where

$$\hat{P}(\Omega_0|\Omega t) = P^{-1/2}(\Omega)P(\Omega_0|\Omega t)P^{1/2}(\Omega_0) \tag{4.12}$$

is the symmetrized form of the conditional probability. Now the symmetrized diffusion equation is easily solved using a matrix representation in a basis of normalized Wigner matrices given by:

$$\mathcal{D}_{mn}^L(\Omega) = \sqrt{\frac{2L+1}{8\pi^2}}D_{mn}^L(\Omega) \tag{4.13}$$

72

In particular.

$$\hat{P}(\Omega_0|\Omega t) = \sum_{Lmn} C_{Lmn}(\Omega_0, t)\mathcal{D}^L_{mn}(\Omega) \tag{4.14}$$

where the expansion coefficients, C_{Lmn}, are evaluated by using the initial condition $\hat{P}(\Omega_0|\Omega 0) = \delta(\Omega - \Omega_0)$ to give

$$C_{Lmn}(\Omega_0, 0) = \mathcal{D}^{L*}_{mn}(\Omega_0) \tag{4.15}$$

By substituting Eq. (4.14) in Eq. (4.11), multiplying both sides on the left by $\mathcal{D}^{L*}_{mn}(\Omega)$ and integrating over Ω, a system of linear differential equations is obtained:

$$\frac{1}{\rho}\dot{C}(t) = \hat{R}C(t) \tag{4.16}$$

where

$$\left(\hat{R}^m\right)_{L'n'Ln} = \int d\Omega \mathcal{D}^{L'*}_{mn'}(\Omega)\hat{\Gamma}\mathcal{D}^L_{mn}(\Omega)$$

In solving the above linear differential equations, a unitary eigenvector matrix $\widehat{X}^m$ which diagonalizes the self-adjoint diffusion matrix $\hat{R}^m$ should be introduced

$$\hat{R}^m\widehat{X}^m = \widehat{X}^m\tilde{r}^m \tag{4.17}$$

where $\tilde{r}^m$ is a diagonal matrix that contains the eigenvalues of $\hat{R}^m$. The formal solution is

$$C^m(t) = \widehat{X}^m \exp(t\rho\tilde{r}^m)(\widehat{X}^m)^T C^m(0) \tag{4.18}$$

Considering the matrix elements of $\widehat{X}^m$ and substituting the zero time coefficients, we obtain

$$C_{Jmp}(\Omega_0, t) = \sum_K \sum_{J'p'} (\widehat{X}^m)_{Jp,K} \exp(t\rho\tilde{r}^m_K)(\widehat{X}^m)^T_{J'p',K} \mathcal{D}^{J'*}_{mp'}(\Omega_0) \tag{4.19}$$

where K is used to label the eigenvalues of the diffusional matrix, $\hat{R}^m$. Using the un-normalized Wigner matrices here, the symmetrized conditional probability can be written as

$$\hat{P}(\Omega_0|\Omega t) = \frac{1}{8\pi^2}\sum_{Kq}\sum_{Jp}\sum_{J'p'}\sqrt{2J+1}\sqrt{2J'+1}(\widehat{X}^q)_{Jp,K}$$

73

$$\times \exp(t\rho \hat{r}_K^q)(\hat{X}^q)_{J'p',K} D_{qp}^J(\Omega) D_{qp'}^{J'*}(\Omega_0) \tag{4.20}$$

According to the asymptotic condition,

$$\lim_{t \to \infty} P(\Omega_0 | \Omega t) = P(\Omega) \tag{4.21}$$

all the exponentials in Eq. (20) decay to zero at infinite time except for the one corresponding to the zero eigenvalue, $\hat{r}_0^0$. The long time behavior of the symmetrized conditional probability is obtained as

$$
\begin{aligned}
\lim_{t \to \infty} \hat{P}(\Omega_0 | \Omega t) &= P^{1/2}(\Omega_0) P^{1/2}(\Omega) \\
&= \frac{1}{8\pi^2} \sum_{J''p''} \sum_{J'''p'''} \sqrt{2J''+1}\sqrt{2J'''+1} \\
&\quad \times (\hat{X}^0)_{J''p'',0} (\hat{X}^0)_{J'''p''',0} D_{0p''}^{J''}(\Omega) D_{0p'''}^{J'''*}(\Omega_0)
\end{aligned} \tag{4.22}
$$

Eq. (4.1) is rewritten as

$$
\begin{aligned}
G_{mnn'}^{LL'}(t) &= \int d\Omega_0 P^{1/2}(\Omega_0) D_{mn}^{L*}(\Omega_0) \\
&\quad \times \int d\Omega P^{1/2}(\Omega) \hat{P}(\Omega_0 | \Omega t) D_{m'n'}^{L'}(\Omega)
\end{aligned} \tag{4.23}
$$

Substituting Eq. (4.20) and Eq. (4.22) to Eq. (4.23), the correlation functions can be expressed as

$$
\begin{aligned}
G_{mnn'}^{LL'}(t) &= \sum_K \exp(t\rho \hat{r}_K^n) \sum_{Jp} \sum_{J'p'} \sum_{J''J'''} \frac{\sqrt{(2J+1)(2J'+1)(2J''+1)(2J'''+1)}}{(2L+1)(2L'+1)} \\
&\quad \times (\hat{X}^m)_{Jp,K} (\hat{X}^m)_{J'p',K} (\hat{X}^0)_{J'',n'-p;0} (\hat{X}^0)_{J''',n-p';0} C(J''',J',L;0,m) \\
&\quad \times C(J''',J',L;n-p',p') C(J'',J,L';0,m) C(J'',J,L';n'-p,p) \\
&= \sum_K (b_{mnn'}^{LL'})_K \exp[t(a_{mnn'}^{LL'})_K] \tag{4.24}
\end{aligned}
$$

where $C(A,B,C;d,e)$ is the Clebsch-Gordon coefficient, $(a_{mnn'}^{LL'})_K/\rho$, the decay constants, are the eigenvalues of the Γ matrix, and $(b_{mnn'}^{LL'})_K$, the relative weights of the exponentials, are the corre-

74

sponding eigenvectors. In the limit that $G_{mnn'}^{LL'}$ can be represented by a single exponential, then

$$b_{mnn'}^{LL'} = G_{mnn'}^{LL'}(0) - G_{mnn'}^{LL'}(\infty) \tag{4.25}$$

For $L = L' = 2$ and $n = n'$. b_{mn}^{22} reduces to the $\kappa(m,n)$. the mean square of the Wigner rotation matrices. given by Freed[4.7].

4.3 Spectral Densities

The spectral densities $J_{LL'nn'}^{(AB)}(\omega)$ are given by the following sum of Fourier transformations of the correlation functions in Eq. (4.24)

$$J_{LL'm}^{(AB)}(m\omega) = \sum_{nn'} A_{MOL}^{Ln*} B_{MOL}^{L'n'} \int_0^\infty G_{mnn'}^{LL'}(t) \exp(-im\omega t) dt \tag{4.26}$$

For deuteron NMR experiments. $L = L' = 2$. $A = \sqrt{3/2}\pi q_{CD} d_{n0}^2(\theta)$. $B = \sqrt{3/2}\pi q_{CD} d_{n'0}^2(\theta)$. where θ is the angle between the molecular z_M axis and the principal z axis of the efg tensor (e.g. the direction of C-D bond). The spectral densities for a biaxial molecule in uniaxial phases are given by

$$J_m(m\omega) = \frac{3\pi^2}{2}(q_{CD})^2 \sum_{nn'} d_{n0}^2(\theta) d_{n'0}^2(\theta) \sum_{\kappa} \frac{(b_{mnn'}^{22})_\kappa (a_{mnn'}^{22})_\kappa}{(a_{mnn'}^{22})_\kappa^2 + (m\omega)^2} \tag{4.27}$$

4.4 The Ring Rotation and Internal Motions

Eq. (4.27) is for deuterons without internal degrees of freedom. When the aromatic ring is rotating freely about its para axis with a diffusion constant D_R. the spectral densities are given by

$$\begin{aligned}
J_m^{(R)}(m\omega) &= \frac{3\pi^2}{2}(q_{CD}^{(R)})^2 \sum_{nn'} \sum_p \left[d_{p0}^2(\theta_{R,Q})\right]^2 d_{n,p}^2(\theta_{M,R}) d_{n',p}^2(\theta_{M,R}) \\
&\quad \times \sum_\kappa \frac{(b_{mnn'}^{22})_\kappa \left[(a_{mnn'}^{22})_\kappa + (1-\delta_{p0})D_R\right]}{\left[(a_{mnn'}^{22})_\kappa + (1-\delta_{p0})D_R\right]^2 + (m\omega)^2}
\end{aligned} \tag{4.28}$$

75

where the strong collision limit is used for ring rotations. $\theta_{R,Q}$ is the angle between the $C - D$ bond and the para axis. and $\theta_{M,R}$. the angle between the para axis and the molecular z_M axis. usually can be set to zero.

Now the following more general spectral densities are obtained for the case with internal motions:

$$J_m^{(i)}(m\omega) = \frac{3\pi^2}{2}(q_{CD}^{(i)})^2 \sum_{nn'} \sum_{K} \sum_{l=0}^{\infty} \frac{(b_{mnn'}^{22})_K \left[(a_{mnn'}^{22})_K + c_{nn'l}\right]}{\left[(a_{mnn'}^{22})_K + c_{nn'l}\right]^2 + (m\omega)^2} \Gamma(n, n'l) \tag{1.29}$$

where $c_{nn'l}$ is related to the correlation time of internal motion and $\Gamma(n, n'l)$ is a function describing the internal motions. The ring internal motion could be free rotation. restricted motion. or π flip of ring around its para-axis. etc. For the special case that the ring is fixed on the molecular frame. i.e.. the internal motion was frozen. only one term inside $\sum_l$ survives ($\Gamma(n, n'l) = \delta_{l0}$ and $c_{nn'l} = 0$) and Eq. (4.29) goes back to Eq. (4.27).

For deuterons residing in flexible chains. the spectral density for the chain internal motions (described by a rate equation) has a form similar to Eq. (4.29) except the internal function $\Gamma(n, n'l)$ now includes the chain geometric information and eigenvectors of the rate matrix and the $c_{nn'l}$ is related to the eigenvalues of jump rate matrix. The explicit expression will be given in Chapter 6. Eq. (6.18).

4.5 Calculations

In the calculations presented here. we investigate the simplest and most important case for the potential of mean torque. that is. only the second rank contribution to the potential of mean torque is retained. Hence,

$$\frac{U(\beta, \gamma)}{kT} = a_{20}(T)P_2(\cos\beta) + a_{22}(T)[D_{02}^2(\beta, \gamma) + D_{0-2}^2(\beta, \gamma)] \tag{4.30}$$

where $a_{2-2} = a_{22}$ is assumed[4.20,4.23]. The ratio $\xi = a_{22}/a_{20}$, is a measure of the deviation of molecular symmetry from cylindrical symmetry. Then the symmetrized diffusion operator given by Eq. (4.10) can be evaluated using

$$\langle \mathcal{D}_{mn'}^{L'} | - \nabla^2 | \mathcal{D}_{mn}^L \rangle = [-L(L+1) - n^2(\eta - 1)]\delta_{L'L}\delta_{n'n}$$

$$\left\langle \mathcal{D}_{mn'}^{L'} \left| -\frac{1}{2}\nabla^2 \frac{U(\beta,\gamma)}{kT} \right| \mathcal{D}_{mn}^L \right\rangle = -\frac{\sqrt{2L+1}}{2\sqrt{2L'+1}} \sum_{Jq} a_{Jq}[J(J+1) + (\eta - 1)q^2]$$

$$\times C(L,J,L';m,0)C(L,J,L';n'-q,q)\delta_{n,n'-q} \qquad (4.31)$$

$$\left\langle \mathcal{D}_{mn'}^{L'} \left| \frac{1}{4}\left(L_-\frac{U(\beta,\gamma)}{kT} \right)\left(L_-\frac{U(\beta,\gamma)}{kT} \right) \right| \mathcal{D}_{mn}^L \right\rangle$$

$$= \frac{\sqrt{2L+1}}{4\sqrt{2L'+1}} \sum_{Jq} \sum_{J'q'} a_{Jq}a_{J'q'} \sqrt{J(J+1) - q(q+1)}\sqrt{J'(J'+1) - q'(q'+1)}$$

$$\times \sum_{J''=J-J'}^{J+J'} C(J,J',J'';0,0)C(J,J',J'';q+1,q'-1)$$

$$\times C(L,J'',L';m,0)C(L,J'',L';n'-q-q',q+q')\delta_{n,n'-q-q'} \qquad (4.32)$$

$$\left\langle \mathcal{D}_{mn'}^{L'} \left| \frac{1}{4}\eta\left(L_z\frac{U(\beta,\gamma)}{kT} \right)^2 \right| \mathcal{D}_{mn}^L \right\rangle$$

$$= \frac{\eta\sqrt{2L+1}}{4\sqrt{2L'+1}} \sum_{Jq} \sum_{J'q'} qq' a_{Jq}a_{J'q'} \sum_{J''=J-J'}^{J+J'} C(J,J',J'';0,0)C(J,J',J'';q,q')$$

$$\times C(L,J'',L';m,0)C(L,J'',L';n'-q-q',q+q')\delta_{n,n'-q-q'} \qquad (4.33)$$

$$\left\langle \mathcal{D}_{mn'}^{L'} \left| \frac{1}{2}\epsilon(L_+^2 + L_-^2) \right| \mathcal{D}_{mn}^L \right\rangle$$

$$= \frac{1}{2}\epsilon\sqrt{[L'(L'+1) - (n'-2)(n'-1)][L'(L'+1) - n'(n'-1)]}\delta_{LL'}\delta_{n,n'-2}$$

$$+ \frac{1}{2}\epsilon\sqrt{[L'(L'+1) - (n'+2)(n'+1)][L'(L'+1) - n'(n'+1)]}\delta_{LL'}\delta_{n,n'-2} \qquad (4.34)$$

$$\left\langle \mathcal{D}_{mn'}^{L'} \left| \frac{1}{4}\epsilon\left(L_+^2\frac{U(\beta,\gamma)}{kT} \right) \right| \mathcal{D}_{mn}^L \right\rangle$$

$$= \frac{\epsilon\sqrt{2L+1}}{4\sqrt{2L'+1}} \sum_{Jq} a_{Jq}\sqrt{[J(J+1) - q(q+1)][J(J+1) - (q+1)(q+2)]}$$

$$\times C(L,J,L';m,0)C(L,J,L';n'-q-2,q+2)\delta_{n,n'-q-2} \qquad (4.35)$$

77

$$\left\langle \mathcal{D}_{mn'}^{L'} \left| \frac{1}{4}\epsilon \left(L_-^2 \frac{U(\beta,\gamma)}{kT} \right) \right| \mathcal{D}_{mn}^{L} \right\rangle$$

$$= \frac{\epsilon\sqrt{2L+1}}{4\sqrt{2L'+1}} \sum_{Jq} a_{Jq} \sqrt{[J(J+1)-q(q-1)]\,[J(J+1)-(q-1)(q-2)]}$$

$$\times C(L,J,L';m,0)C(L,J,L';n'-q+2,q-2)\delta_{n,n'-q-2} \qquad (4.36)$$

$$\left\langle \mathcal{D}_{mn'}^{L'} \left| \frac{1}{8}\epsilon \left(L_- \frac{U(\beta,\gamma)}{kT} \right)^2 \right| \mathcal{D}_{mn}^{L} \right\rangle$$

$$= \frac{\epsilon\sqrt{2L+1}}{8\sqrt{2L'+1}} \sum_{Jq}\sum_{J'q'} a_{Jq}a_{J'q'} \sqrt{J(J+1)-q(q+1)}\sqrt{J'(J'+1)-q'(q'+1)}$$

$$\times \sum_{J''=J-J'}^{J+J'} C(J,J',J'';0,0)C(J,J',J'';q+1,q'+1)C(L,J'',L';m,0)$$

$$\times C(L,J'',L';n'-q-q'-2,q+q'+2)\delta_{n,n'-q-q'-2} \qquad (4.37)$$

$$\left\langle \mathcal{D}_{mn'}^{L'} \left| \frac{1}{8}\epsilon \left(L_- \frac{U(\beta,\gamma)}{kT} \right)^2 \right| \mathcal{D}_{mn}^{L} \right\rangle$$

$$= \frac{\epsilon\sqrt{2L+1}}{8\sqrt{2L'+1}} \sum_{Jq}\sum_{J'q'} a_{Jq}a_{J'q'} \sqrt{J(J+1)-q(q-1)}\sqrt{J'(J'+1)-q'(q'-1)}$$

$$\times \sum_{J''=J-J'}^{J+J'} C(J,J',J'';0,0)C(J,J',J'';q-1,q'-1)C(L,J'',L';m,0)$$

$$\times C(L,J'',L';n'-q-q'+2,q+q'-2)\delta_{n,n'-q-q'-2} \qquad (4.38)$$

In deriving Eqs. (4.31)-(4.38), the following relations have been used[4.24]:

$$\nabla^2 \mathcal{D}_{mn}^{L} = \left[L(L+1) + (\eta - 1)n^2 \right] \mathcal{D}_{mn}^{L} \qquad (4.39)$$

$$L_z \mathcal{D}_{mn}^{L} = n \mathcal{D}_{mn}^{L} \qquad (4.40)$$

$$L_{\pm} \mathcal{D}_{mn}^{L} = \sqrt{L(L+1)-n(n\pm 1)}\,\mathcal{D}_{mn\pm 1}^{L} \qquad (4.41)$$

$$L_{\pm}^2 \mathcal{D}_{mn}^{L} = \sqrt{[L(L+1)-n(n\pm 1)]\,[L(L+1)-(n\pm 1)(n\pm 2)]}\,\mathcal{D}_{mn\pm 2}^{L} \qquad (4.42)$$

Then, the matrix elements of $\hat{\Gamma}$ are given by

$$\langle \mathcal{D}_{m'n}^{L'} | \hat{\Gamma} | \mathcal{D}_{mn}^{L} \rangle = (\hat{R}^m)_{L'n'Ln}$$

$$= [-L(L+1) - n^2(\eta - 1) - K_0]\delta_{LL'}\delta_{n'n}$$

$$-\frac{1}{2}\epsilon\sqrt{[L'(L'+1) - (n'-2)(n'-1)][L'(L'+1) - n'(n'-1)]}\delta_{LL'}\delta_{n,n'-2}$$

$$-\frac{1}{2}\epsilon\sqrt{[L'(L'+1) - (n'+2)(n'+1)][L'(L'+1) - n'(n'+1)]}\delta_{LL'}\delta_{n,n'-2}$$

$$+\frac{\sqrt{2L+1}}{\sqrt{2L'+1}}C(L,2,L';m,0)[C(L,2,L';n',0)K_1\delta_{n'n}$$

$$+C(L,2,L';n'-2,2)K_2\delta_{n,n'-2} + C(L,2,L';n'+2,-2)K_2\delta_{n,n'-2}]$$

$$+\frac{\sqrt{2L+1}}{\sqrt{2L'+1}}C(L,4,L';m,0)[C(L,4,L';n',0)K_3\delta_{n'n}$$

$$+C(L,4,L';n'-2,2)K_4\delta_{n,n'-2} + C(L,4,L';n'+2,-2)K_4\delta_{n,n'-2}$$

$$+C(L,4,L';n'-4,4)K_5\delta_{n,n'-4} + C(L,4,L';n'+4,-4)K_5\delta_{n,n'-4} \qquad (4.43)$$

The following constants have been used in the above equation

$$K_0 = -\frac{1}{5}(\frac{3}{2}a_{20}^2 + a_{22}^2\sqrt{6\epsilon}a_{20}a_{22}) - \frac{2}{5}\eta a_{22}^2$$

$$K_1 = -3a_{20} - \sqrt{6\epsilon}a_{22} - \frac{1}{7}(\frac{3}{2}a_{20}^2 + a_{22}^2 + \sqrt{6\epsilon}a_{20}a_{22}) + \frac{4}{7}\eta a_{22}^2$$

$$K_2 = -(1+2\eta)a_{22} - \frac{\sqrt{6}}{2}\epsilon a_{20} + \frac{\sqrt{6}}{7}\left[\frac{\sqrt{6}}{2}a_{20}a_{22} + \frac{3}{4}\epsilon a_{20}^2 + \frac{1}{2}\epsilon a_{22}^2\right]$$

$$K_3 = \frac{12}{35}\frac{3}{2}(\frac{3}{2}a_{20}^2 + a_{22}^2 + \sqrt{6\epsilon}a_{20}a_{22}) - \frac{6}{35}\eta a_{22}^2$$

$$K_4 = \frac{6}{7}\sqrt{\frac{2}{5}}\left[\frac{\sqrt{6}}{2}a_{20}a_{22} + \frac{3}{4}\epsilon a_{20}^2 + \frac{1}{2}\epsilon a_{22}^2\right]$$

$$K_5 = 3\sqrt{\frac{2}{35}}\eta a_{22}^2$$

$$(4.44)$$

References

4.1 Debye. P. In *Polar Molecules*; Dover Publications. Inc.: New York. 1928.

4.2 Huntress. W.T.. Jr. *Adv. Magn. Reson.* **4**. 1. 1970.

4.3 Nordio. P. L.; Busolin. P. *J. Chem. Phys.* **55**. 5485. 1971.

4.4 Nordio. P. L.; Rigatti. G.; Segre. U. *J. Chem. Phys.* **56**. 2117. 1972.

4.5 Polnaszek. C. F.; Freed. J. H. *J. Chem. Phys.* **79**, 2283. 1975.

4.6 Polnaszek. C. F.; Bruno. G. V.; Freed. J. H. *J. Chem. Phys.* **58**. 3185. 1973.

4.7 Freed. J. H. *J. Chem. Phys.* **66**. 4183. 1977.

4.8 Moro. G; Nordio. P. L. *Chem. Phys. Lett.* **96**. 192. 1983.

4.9 Vold. R. R.; Vold. R. L.. *J. Chem. Phys.* **88**. 1443. 1988.

4.10 Bernassau. J. M.; Black. E. P.; Grant. D. M. *J. Chem. Phys.* **76**. 253. 1982.

4.11 Nordio. P.L.; Segre. U. *Chem. Phys.* **44**. 849. 1981.

4.12 Dozov. I.; Kirov. N.; Petroff. B. *Phys. Rev. A* **36**. 2870. 1987.

4.13 Bulthuis. J.; Plomp. B. *J. Phys. (France)* **51**. 2581. 1990.

4.14 Tarroni. R.; Zannoni. C. *J. Chem. Phys.* **95**. 4550. 1991.

4.15 Berggren. E; Tarroni. R.; Zannoni, C. *J. Chem. Phys.* **99**. 6180. 1993.

4.16 Berggren. E; C. *Mol. Phys.* **85**, 299, 1995.

80

4.17 Dickerson, W. H.; Vold, R. R.; Vold, R. L. *J. Phys. Chem.* **87**, 166, 1983.

4.18 Luyten, P.R.; Vold, R. R.; Vold, R. L. *J. Phys. Chem.* **89**, 545, 1985.

4.19 Huo, S.; Vold, R. R. *J. Phys. Chem.* **99**, 12391, 1995.

4.20 G.R. Luckhurst, In *The Molecular Physics of Liquid Crystals,* edited by G.R. Luckhurst and G.W. Gray, Academic, New York, 1979, Chap. 4, p.85.

4.21 C. Zannoni, In *The Molecular Physics of Liquid Crystals*, edited by G. R. Luckhurst and G. W. Gray (Academic, New York, 1979), Chap. 3, p.51

4.22 P.L. Nordio and U. Segre, *In The Molecular Physics of Liquid Crystals*, edited by G.R. Luckhurst and G.W. Gray, Academic, New York, 1979, Chap. 18, p.411.

4.23 F. Biscarini, C. Chiccoli, P. Pasini, F. Semeria, and C. Zannoni, *14th International Liquid Crystal Conference*, 1992.

4.24 M. E. Rose, In *Elementary Theory of Angular Momentum*, Wiley, New York, 1957.

Chapter 5

Theory: The Director Fluctuations

5.1 Introduction

Director fluctuation is a unique dynamic property of liquid crystals. and involves slow collective motions of a large number of molecules. In the quadrupolar Hamiltonian. there are fluctuating terms because of the rotational and/or collective motions of liquid crystal molecules. The autocorrelation function $G_{m_L}(t)$ may be evaluated in terms of the Wigner rotation matrix $D^2_{m_L m_M}(\Omega_{LM})$ in the fluctuating Hamiltonian

$$
G_{m_L}(t) = \sum_{m_M} \sum_{m'_M} \left[d^2_{m_M 0}(\theta) \right] \left[d^2_{m'_M 0}(\theta) \right] \left\langle \left[D^2_{m_L m_M}(\Omega_{LM}(0)) - \overline{D^2_{m_L m_M}} \right] \right.
$$
$$
\left. \times \left[D^{2*}_{m_L m'_M}(\Omega_{LM}(t)) - \overline{D^{2*}_{m_L m'_M}} \right] \right\rangle \tag{5.1}
$$

Now $\Omega_{LM} (\equiv \alpha, \beta, \gamma)$ denotes the Euler angles that transform between a molecular frame attached to the molecular core and the laboratory frame. θ is the angle between the C-D bond and the z_M axis of the molecular frame. and m_L and m_M are the projection indices for a tensor of rank two in the laboratory and molecular z axis. respectively.

82

There are several motional processes (e.g. reorientation, director fluctuations) that take place simultaneously and may cause spin relaxation in liquid crystals. Because of thermal fluctuations of the director, the orientation of director has both spatial and temporal variation. In the nematic and/or smectic A phases of the liquid crystals, a local (instantaneous) director $\hat{n}(\vec{r})$ may be introduced to represent the average direction of molecules within a neighborhood of any point in the sample. The time interval between molecular collisions is about $10^{-10} \sim 10^{-12}$s. Changes in molecular orientation due to collisions could change the local director on the NMR time scale. Thus, an additional coordinate system is needed to specify the local director $\hat{n}(\vec{r})$. The average director $\hat{n}_0$ is obtained by spatially averaging the local directors over the sample.
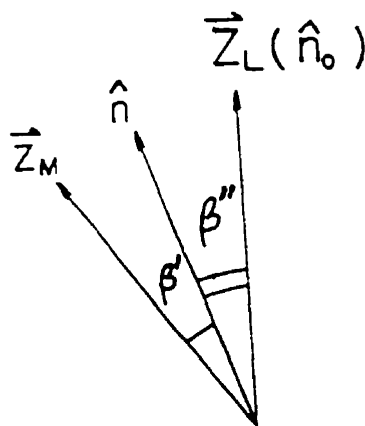
Figure 5.1 A schematic illustration of the coordinate systems used to account for director fluctuations in liquid crystals.

The Euler angles $\Omega_{LM}(t)$ in the autocorrelation function (Eq. (5.1)) denote the orientation of the principal molecular axes (x_M, y_M, z_M) in the laboratory (X_L, Y_L, Z_L) frame. The coordinate

transformation from the (x_M, y_M, z_M) frame to the (X_L, Y_L, Z_L) frame must be carried out through successive transformations [Fig. (5.1)] to account for the fast motions of a molecule and the slow collective fluctuations of the director. That is, $\Omega_{LM} \equiv (\Omega', \Omega'')$, where the Euler angles Ω' transform from the molecular frame (x_M, y_M, z_M) to the instantaneous director (x, y, z) frame. Ω'' is used to transform the (x, y, z) frame to the laboratory frame (X_L, Y_L, Z_L). Here we assume the average director $\hat{n}_0$ is parallel to the external field $\vec{B}$, which is used to define the laboratory frame.

For director fluctuations, the high frequency cut-off ω_c arises from the fact that the collective motions are only valid over the length scales which are large compared with the length of the liquid crystalline molecules, i.e., in the limit of Larmor frequency $\omega_0 \ll \omega_c$. Whereas in the cases of $\omega_0 > \omega_c$, the experiment is carried out at a frequency such that no collective motions are detected and the director fluctuations are not expected to contribute significantly to the spectral densities. (see Eq. (5.4))

In the nematic phase and perhaps high temperature smectic phases, molecules perform long range cooperative motions, which are slow compared to the rapid reorientational motions of individual molecules. The dynamics of these fluctuations depend on the viscosity coefficients and the elastic constants of the liquid crystal. In the continuum theory, the elastic constants K_1, K_2 and K_3 are the splay, twist and bend elastic constants, respectively[5.1-5.2]. Freed has included these collective effects in the spin relaxation theory by allowing the orienting potential $U(\Omega)$ to fluctuate slowly in time. It is assumed that the director shows small fluctuations about its mean position, and that the magnitude of ordering does not change. Then there are three types of motions that contribute to spectral densities: molecular reorientation, director fluctuations and a cross-term arising from

both of these motions.

5.2 First Order Contribution

Accordinging to Pincus[5.3], when director fluctuations are assumed to give small angular amplitude, director fluctuations only contribute to $J_1(\omega)$ in a first order approximation. In the 'one-constant' approximation, that is, $K_1 = K_2 = K_3 = K$ and one effective viscosity coefficient instead of five Leslie coefficients, the contribution to $J_1(\omega)$ from the director fluctuations is[5.4]

$$J_{1DF}(\omega) = \frac{3\pi^2}{2}(q_{CD})^2 \langle P_2 \rangle_0^2 A \left[d_{00}^2(\beta_{M,Q}) \right]^2 U(\omega_c/\omega)\omega^{-1/2} \qquad (5.2)$$

where the prefactor A in $s^{1/2}$ is

$$A = \frac{3kT}{4\sqrt{2}\pi K (D_t + K/\eta)^{1/2}} \qquad (5.3)$$

where D_t is the averaged translational self-diffusion constant, and the cutoff function[5.4,5.5] $U(\omega_c/\omega)$ involves a high frequency cutoff $\omega_c = 4\pi^2 K/\eta \lambda_c^2$ of the coherent modes with a cutoff wavelength λ_c typically the order of the molecular length.

$$U(x) = \frac{1}{2\pi} \left[\frac{x - \sqrt{2x} + 1}{x + \sqrt{2x} + 1} \right] + \frac{1}{\pi} \tan^{-1} \left(\sqrt{2x} - 1 \right) + \frac{1}{\pi} \tan^{-1} \left(\sqrt{2x} + 1 \right) \qquad (5.4)$$

$U(\omega_c/\omega)$ is unity at low frequency and becomes small for the Larmor frequency much larger than ω_c. η and K are the one constant approximation to the viscosities and the elastic constants of the medium, and $\langle P_2 \rangle_0$ is the nematic order parameter of the molecule relative to the local director and is related to the usual nematic order parameter $\langle P_2 \rangle$ according to[5.6]

$$\langle P_2 \rangle_0 = \frac{\langle P_2 \rangle}{1 - 3\alpha} \qquad (5.5)$$

where the parameter $\alpha = kT/\pi K' \lambda_c$ is a measure of the magnitude of director fluctuations. Furthermore, if director fluctuations are slow in comparison with molecular rotations, couplings between

85

these two motions produce[5.4,5.7] a small cross term contribution to $J_1(\omega)$. Following Freed[5.4], this negative cross term for the methine deuteron in MBBA can be shown as

$$J_{1CR}(\omega) = -\frac{3\pi^2}{2}(q_{CD})^2 A \frac{\langle P_2 \rangle^2}{(1-3\alpha)^2} \left[d_{00}^2(\beta_{M,Q})\right]^2 \frac{\sqrt{8\omega_c}}{\pi} \sum_K \beta_K \frac{(a_{100}^2)_K}{(a_{100}^2)_K^2 + \omega^2} \quad (5.6)$$

where the subscript CR is to denote the cross term and $\beta_K = (b_{100}^2)_K / (b_{100}^2)_1$ are relative weights of exponentials that describe the molecular reorientation[see Chapter 4, Eqs.(4.23-4.24)].

5.3 Second Order Contribution

Standard theories[5.1,5.8-5.9] of spin relaxation by director fluctuations in nematics are based on the notion that the mean square amplitude $\langle \beta^2 \rangle$ of the director's displacement is small such that terms of this and higher orders can be neglected. When angular excursions of the local director are not small [e.g., low K or large α], second-order and higher terms are needed and their contributions to $J_{2DF}(2\omega)$ and $J_{0DF}(0)$ become nonzero. Faber[5.10] was the first to consider these higher-order contributions. Recently, second-order contributions from director fluctuations are predicted[5.6, 5.11-5.12] in $J_0(0)$, $J_1(\omega)$ and $J_2(2\omega)$. When treating deuterons residing on the rigid part of a molecule, the spectral densities are calculated as follows:

$$\begin{aligned} J_{2DF}(\omega) &= J_{0DF}(\omega)/3 \\ &= 4(q_{CD})^2 A^2 \langle P_2 \rangle_0^2 \left[d_{00}^2(\beta_{M,Q})\right]^2 L(\omega) \end{aligned} \quad (5.7)$$

For methine deuterons in 5O.7 and MBBA, $q_{CD} = 185$ kHz, and

$$L(\omega) = \int_0^{q_c} dq \int_0^{q_c} \frac{q^2 + q'^2}{(q^2 + q'^2)^2 + (\eta/K)^2 \omega^2} dq' \quad (5.8)$$

with $q_c = (\eta/K)^{1/2} \omega_c^{1/2}$. By intergrating over a circle in q, q' space rather than a square, Vold et

86

al.[5.6] obtained from the above equation

$$L(\omega) = \frac{\pi}{8}\ln\left[1 + \left(\frac{\omega_c}{\omega}\right)^2\right]$$ (5.9)

Hence

$$J_{0DF}(\omega) = \frac{3\pi^2}{2}(q_{CD})^2 A^2 \frac{\langle P_2\rangle^2}{(1-3\alpha)^2}\left[d_{00}^2(\beta_{M,Q})\right]^2 \frac{1}{\pi}\ln\left[1+\left(\frac{\omega_c}{\omega}\right)^2\right]$$ (5.10)

$$J_{2DF}(2\omega) = \frac{3\pi^2}{2}(q_{CD})^2 A^2 \frac{\langle P_2\rangle^2}{(1-3\alpha)^2}\left[d_{00}^2(\beta_{M,Q})\right]^2 \frac{1}{3\pi}\ln\left[1+\left(\frac{\omega_c}{2\omega}\right)^2\right]$$ (5.11)

To get the zero-frequency component $J_{0DF}(0)$, one needs to introduce[5.4,5.6] a low-frequency cutoff in order to remove its divergence as $\omega \to 0$. This cutoff frequency can arise from bulk susceptibility effects. However, this procedure does not allow one to write down an analytical expression for $J_{0DF}(0)$. A less exact procedure[5.6] is to replace the lower limit in the mode expression by a finite wave number q_1 and gives

$$J_{0DF}(\omega) = \frac{3\pi^2}{2}(q_{CD})^2 A^2 \frac{\langle P_2\rangle^2}{(1-3\alpha)^2}\left[d_{00}^2(\beta_{M,Q})\right]^2 \frac{1}{\pi}\ln\left[\frac{1+(\omega_c/\omega)^2}{1+(\omega_1/\omega)^2}\right]$$ (5.12)

where ω_1 may be estimated from the magnetic coherence length ξ in the presence of the magnetic field[5.13], i.e., $\omega_1 = K/\eta\xi^2$ and[see Chapter 1]

$$\xi = \left(\frac{K}{\Delta\chi}\right)^{1/2}\frac{1}{B}$$ (5.13)

with $\Delta\chi$ being the diamagnetic susceptibility anisotropy and B the applied magnetic field. When second-order contributions are included in $J_{1DF}(\omega)$, Joghems et al.[5.12] found that it has a correction factor $(1-4\alpha)$, which reduces to 1 when α is very small. Then Eq. (5.2) becomes

$$J_{1DF}(\omega) = \frac{3\pi^2}{2}(q_{CD})^2 A\langle P_2\rangle^2\left[d_{00}^2(\beta_{M,Q})\right]^2\frac{(1-4\alpha)}{(1-3\alpha)^2}U(\omega_c/\omega)\omega^{-1/2}$$ (5.14)

and the cross term contributions are still given by Eq. (5.6).

5.4 Contributions to Flexible Chains of Molecule

For C-D bonds located in the flexible chain, the effect of director fluctuations is made smaller as a result of additional averaging within the chain from conformational changes[see Chapter 3]. It has been recognized[5.14] in earlier deuterium NMR studies that the spin-lattice relaxation rates for the chain deuterons should scale with the square of their quadrupolar splittings if the spin relaxation is caused only by director fluctuations. Indeed the quadrupolar splitting can give the segmental order parameter of C-D bond at carbon site i, which is defined by

$$S_{CD}^{(i)} = \left\langle \left\langle P_2(\cos \Theta^{(i)}) \right\rangle \right\rangle \tag{5.15}$$

where $\Theta^{(i)}$ is the angle between the ith C-D bond and the equilibrium director. $\langle\langle \ \rangle\rangle$ denotes both the conformational average and overall motional average. In uniaxial phases like the nematic and semetic A, the above equation can be expressed as[5.9]

$$\begin{aligned} S_{CD}^{(i)} &= \left\langle \left\langle P_2(\cos \beta_{M,Q}^{(i)}) P_2(\cos \theta) \right\rangle \right\rangle \\ &= \overline{d_{00}^2(\beta_{M,Q}^{(i)})} \langle P_2 \rangle \end{aligned} \tag{5.16}$$

where $\overline{d_{00}^2(\beta_{M,Q}^{(i)})}$ denotes the conformational average over the $\beta_{M,Q}^{(i)}$ angle of the particular C-D bond with respect to the molecular z_M axis, and θ is the angle between the z_M axis and the equilibrium director. The assumption was made for the last step in Eq. (5.16) that the motional modes for the internal chain motions and for the molecular reorientation are decoupled. Using this simplifying assumption in writing down the director fluctuation contributions to chain deuterons as Eqs. (5.6, 5.10-5.12, 5.14), the geometric factors must involve an additional average due to internal motions and together with $\langle P_2 \rangle$ can be replaced by the segmental order parameter (or in terms of the quadrupolar splitting) of the ith deuterons. Thus, director fluctuations contribute to the chain

deuterons according to

$$J_{0DF}^{(i)}(\omega) = \frac{3\pi^2}{2}(q_{CD}^{(i)})^2 \frac{A^2}{(1-3\alpha)^2}\left(S_{CD}^{(i)}\right)^2 \frac{1}{\pi} \ln\left[\frac{1+(\omega_c/\omega)^2}{1+(\omega_1/\omega)^2}\right] \qquad (5.17)$$

$$J_{1DF}^{(i)}(\omega) = \frac{3\pi^2}{2}(q_{CD}^{(i)})^2 \frac{A}{(1-3\alpha)^2}(1-4\alpha)\left(S_{CD}^{(i)}\right)^2 U(\omega_c/\omega)\omega^{-1/2} \qquad (5.18)$$

$$J_{2DF}^{(i)}(2\omega) = \frac{3\pi^2}{2}(q_{CD}^{(i)})^2 \frac{A^2}{(1-3\alpha)^2}\left(S_{CD}^{(i)}\right)^2 \frac{1}{3\pi} \ln\left[1+\left(\frac{\omega_c}{2\omega}\right)^2\right] \qquad (5.19)$$

$$J_{1CR}^{(i)}(\omega) = -\frac{3\pi^2}{2}(q_{CD}^{(i)})^2 \frac{A}{(1-3\alpha)^2}\left(S_{CD}^{(i)}\right)^2 \frac{\sqrt{8\omega_c}}{\pi}\sum_K J_K \frac{(a_{100}^2)_K}{(a_{100}^2)_K^2 + \omega^2} \qquad (5.20)$$

where $q_{CD}^{(i)} = 165$ kHz for methylene deuterons.

5.5 Conclusion

The first order contribution of the director fluctuation to spectral density is proportional to the prefactor A and the second order contribution is proportional to A^2. Since A is a small number, the value $J_{2DF}^{(i)}(2\omega)$ is indeed very small because of its second order nature and can be neglected in the megahertz region. But the second contribution to $J_{0DF}^{(i)}(0)$ is non-trival due to the small low-frequency cutoff ω_1. Finally, the calculated spectral densities for the ith deuterons are obtained from

$$J_1^{(i)}(\omega) = J_{1R}^{(i)}(\omega) + J_{1DF}^{(i)}(\omega) + J_{1CR}^{(i)}(\omega) \qquad (5.21)$$

$$J_2^{(i)}(2\omega) = J_{2R}^{(i)}(2\omega) + J_{2DF}^{(i)}(2\omega) \simeq J_{2R}^{(i)}(2\omega) \qquad (5.22)$$

$$J_0^{(i)}(0) = J_{0R}^{(i)}(0) + J_{0DF}^{(i)}(0) \qquad (5.23)$$

where the subscript R is used to denote molecular rotation.

It is noted that in all equations for director fluctuations, the contributions to J_0, J_1 and J_2 are all related to the high frequency cutoff ω_c. The ω_c value depends on molecular properties and perhaps

also on the detailed molecular structure. Thus. it is expected to change from sample to sample. When the Larmor frequency $\omega_0 \ll \omega_c$. like the case in 5O.7 (see Chapter 7). the cutoff function of Eq. (5.4) approaches unity and the differences in ω_c of different samples become immaterial in $J_1(\omega)$. As the cutoff frequency drops below the Larmor frequency. like the case of MBBA (see Chapter 8). the cutoff function approaches zero and the negative cross term can in fact cancel the $J_{1DF}^{(i)}(\omega)$. The total director fluctuation contribution to $J_1^{(i)}(\omega)$ may even be negative. Thus. it may be difficult to study director fluctuations in the megahertz regime using only the spectral densities $J_1^{(i)}(\omega)$ and $J_2^{(i)}(2\omega)$ [see Eqs. (5.21-5.22)]. The zero-frequency component $J_0^{(i)}(0)$ becomes a unique and useful tool in study director fluctuations in this case.

References

5.1 R.Y. Dong. In *Nuclear Magnetic Resonance of Liquid Crystals* second edition. Spring-Verlag. N.Y., 1997.

5.2 P.G. de Gennes. In *The Physics of Liquid Crystals* Oxford University Press. 1974.

5.3 P. Pincus. *Solid State Commun.* **7**, 415, 1969.

5.4 J.H. Freed. *J. Chem. Phys.* **66**, 4183, 1977.

5.5 J.W. Doane, C.E. Tarr and M.A. Nickerson. *Phys. Rev. Lett.* **33**, 620, 1974.

5.6 R.L. Vold, R.R. Vold, M.J. Warner, *J. Chem. Soc. Faraday Trans.* 2 **84**, 997, 1988.

5.7 P. Ukleja, J. Pirs and J.W. Doane. *Phys. Rev. A* **14**, 414, 1976.

5.8 R.L Vold, R.R. Vold. In *The Molecular Dynamics of Liquid Crystals*. G.R. Luckhurst, C.A. Veracini. Eds; Kumer Academic: Dordrecht, 1994.

5.9 C.G. Wade, *Annu. Rev. Phys. Chem.* **28**, 47, 1977.

5.10 T.E. Faber, *Proc. R. Soc. London Ser. A* **353**, 277, 1977.

5.11 G. van der Zwan, L. Plomp *Liq. Crys.* **4**, 133, 1989.

5.12 E.A. Joghems, G. van der Zwan *J. Phys. II* **6**, 845, 1996.

5.13 P.G. de Gennes. In *Proceeding of the 2nd international Liquid Conference*. G.H. Brown Ed., Gorden & Breach: New York, 1969; p531.

5.14 R.Y. Dong, J. Lewis, E. Tomchuk, E. Bock *J. Chem. Phys.* **69**, 5314, 1978.

Chapter 6

Theory: The Flexible Chain Dynamics

6.1 Introduction

Liquid crystals are organic molecules whose structures usually consist of a rigid core with flexible pendant chains. It is known that molecular flexibility is crucial in determining the physical properties of liquid crystals. The theoretical treatment of dynamical processes of flexible molecules in an anisotropic medium is not an easy task[6.1-6.3]. This often requires a certain number of simplifying assumptions which may only be justified by comparison between the model predictions and experiments. When modelling internal rotations about each carbon-carbon bond in the pendant chains, the configuration transitions of the chain may be superimposed on the rotational diffusion of the whole molecule. This implies that the molecular core is 'massive' such that its motion is independent of configuration transitions in the chain. In modelling quadrupolar splittings in liquid crystals, the rotational isomeric state (RIS) model[6.4. see also Chapter 3] has been used to generate all configurations in the chain and anisotropic interactions with the neighbours are described by a mean-field potential. This model has been extended[6.1-6.2] to the time domain in order to describe spin relaxation in flexible nematogens. It involves a master equation which describes transitions

among all allowed configurations in the pendant chains. To simplify numerical computations, a decoupled model was developed[6.1] in which the overall motion is described by a single average rotational diffusion tensor. It assumes that in a molecule with N distinct conformations, rotation diffusion tensors for different rotamers do not differ appreciably and that an 'average' molecular diffusion tensor may be used to solve the rotational diffusion equation[6.5-6.6]. Transitions among configurations are described by elementary jump modes[6.7-6.8]: one-bond(k_1), two-bond(k_2) and three-bond(k_3) motions. A one-bond rotation involves rotation of the last bond in the chain defined as $\{\cdots, l, m, n\} \to \{\cdots, l, m, n'\}$, where $\{\ \}$ denotes the C-C bond orientations in the carbon-carbon backbone of a pendant chain. A two-bond rotation is defined as rotation of the penultimate bond only $\{\cdots, l, m, n\} \to \{\cdots, l, m', n'\}$, i.e., it represents motion of the last two $C - C$ bonds in the chain as a pair, with no rotation about the penultimate carbon[6.9]. In the case of a trans bond, i.e., $l = n$, then $n = n'$. A three-bond rotation is a kink motion in the chain, i.e., the interchanging of two alternate bonds, defined as $\{\cdots, i, j, k, \cdots\} \to \{\cdots, k, j, i, \cdots\}$, is also called the crankshaft transition[Fig. 6.1].

6.2 Superimposed Rotations Model

In writing the auto-correlation functions that describe both internal and external motions of a flexible mesogen, the Euler angles Ω_{LQ} are used to specify the orientation of the principal axes of a spin tensor (e.g. efg) with respect to the external magnetic field. Suppose that in a local (α) frame, the orientation ($\Omega_{\alpha Q}$) of a $C_\alpha -^2 H$ bond is time independent. A molecule-fixed (M) frame is chosen to coincide with the principal axis system of the rotational diffusion tensor of the molecule. The Euler angles $\Omega_{M\alpha}$ that transform between the local frame and the molecular frame are time-dependent due to the internal motions. The angles Ω_{LM} depend on time because of reorientation

of the whole molecule. By successive coordinate transformations, the following is obtained:

$$D^2_{m_L 0}\left[\Omega_{LQ}\left(t\right)\right] = \sum_{m_M}\sum_{m_\alpha} D^2_{m_L m_M}\left[\Omega_{LM}\left(t\right)\right] D^2_{m_M m_\alpha}\left[\Omega_{M\alpha}\left(t\right)\right] D^2_{m_\alpha 0}\left[\Omega_{\alpha Q}\right] \qquad (6.1)$$

where $\Omega_{\alpha Q}$ is time independent.

(a)

(b)

(c)
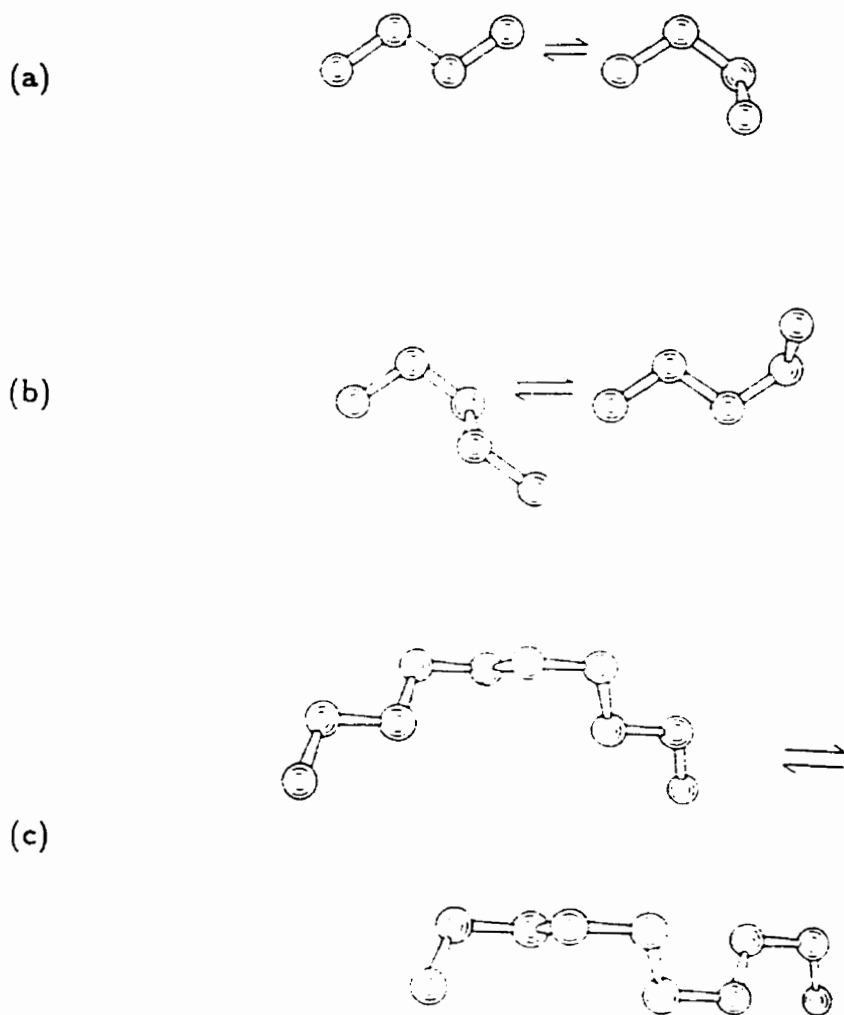
Figure 6.1 The illustration of jump motions of (a) k_1 (b) k_2 and (c) k_3

The auto-correlation function is

$$G_{m_L}(t) = \left\langle D^2_{m_L 0} \left[\Omega_{LQ}(0)\right] D^{2*}_{m_L 0} \left[\Omega_{LQ}(t)\right] \right\rangle - \overline{D^2_{m_L 0} \left[\Omega_{LQ}(0)\right] D^{2*}_{m_L 0} \left[\Omega_{LQ}(t)\right]} \qquad (6.2)$$

where the second term is to ensure that the auto-correlation functions tend to zero as $t \to \infty[6.10]$.
Now Eq. (6.2) can be rewritten using Eq. (6.1) as

$$G_{m_L}(t) = \sum_{m_\alpha} \sum_{m'_\alpha} D^2_{m_\alpha 0}(\Omega_{\alpha Q}) D^{2*}_{m'_\alpha 0}(\Omega_{\alpha Q}) G_{m_L m_\alpha m'_\alpha}(t) \qquad (6.3)$$

where

$$\begin{aligned}
G_{m_L m_\alpha m'_\alpha}(t) &= \sum_{m_M} \sum_{m'_M} \left\langle D^2_{m_L m_M} \left[\Omega_{LM}(0)\right] D^{2*}_{m_L m'_M} \left[\Omega_{LM}(t)\right] \right\rangle \\
&\quad \times \left\langle D^2_{m_M m_\alpha} \left[\Omega_{M\alpha}(0)\right] D^{2*}_{m'_M m'_\alpha} \left[\Omega_{M\alpha}(t)\right] \right\rangle \\
&\quad - \overline{D^2_{m_L m_M}(\Omega_{LM}) D^{2*}_{m_L m'_M}(\Omega_{LM}) D^2_{m_M m_\alpha}(\Omega_{M\alpha}) D^{2*}_{m'_M m'_\alpha}(\Omega_{M\alpha})} \qquad (6.4)
\end{aligned}$$

because of the usual assumption of decoupling between internal and external motions such that the two motional parts can be averaged separately. When the correlation functions of internal motions can be written as

$$G_{m_M m'_M m_\alpha m'_\alpha}(t) = \left\langle D^2_{m_M m_\alpha} \left[\Omega_{M\alpha}(0)\right] D^{2*}_{m'_M m'_\alpha} \left[\Omega_{M\alpha}(t)\right] \right\rangle - \overline{D^2_{m_M m_\alpha}(\Omega_{M\alpha}) D^{2*}_{m'_M m'_\alpha}(\Omega_{M\alpha})} \qquad (6.5)$$

then

$$\begin{aligned}
G_{m_L m_\alpha m'_\alpha}(t) &= \sum_{m_M} \sum_{m'_M} [G_{m_L m_M m'_M}(t) G_{m_M m'_M m_\alpha m'_\alpha}(t) + G_{m_M m'_M m_\alpha m'_\alpha}(t) \overline{D^2_{m_L m_M} D^{2*}_{m_L m'_M}} \\
&\quad + G_{m_L m_M m'_M}(t) \overline{D^2_{m_M m_\alpha} D^{2*}_{m'_M m'_\alpha}}] \qquad (6.6)
\end{aligned}$$

where the correlation functions $G_{m_L m_M m'_M}(t)$ describe the overall motions of molecules, and are given for the TZ model by Eq.(4.24). The complexity here is that the the correlation functions are not

simply given by a linear combination of products of the correlation functions for each motion. The correlation functions in the above equation include terms that are products of correlation functions for one motion and averaged Wigner matrix components for the other motion. These extra terms are zero for the case of relaxation in normal liquids since the average of Wigner matrix elements are identical to zero. Unlike the random isotropic motions in normal liquids, these terms become non-zero in mesophases because some restricted (preferred) motional degrees of freedom would produce non-zero averages of Wigner matrices. However, Eq. (6.6) may be simplified in certain specific cases. In the superimposed rotations model[6.3], it is assumed that internal rotations about different $C-C$ bonds are independent, and that rod-like molecules reorienting in uniaxial mesophases with each of their internal motions involve cylindrically symmetric rotation about a single axis, then $m_\alpha = m'_\alpha$ and

$$\overline{D^2_{m_L m_M}} = \delta_{m_L 0} \delta_{m_M 0} \langle P_2 \rangle$$

$$\overline{D^2_{m_M m_\alpha}} = 0 \tag{6.7}$$

Therefore, Eq. (6.2) can be written as [6.10]

$$G_{m_L}(t) = \sum_{m_M} \sum_{m'_M} \sum_{m_\alpha} \left[d^2_{m_\alpha 0}(\beta_{\alpha.Q}) \right]^2 G_{m_L m_M m'_M}(t) G_{m_M m'_M m_\alpha}(t)$$

$$+ \delta_{m_L 0} \langle P_2 \rangle^2 \sum_{m_\alpha} \left[d^2_{m_\alpha 0}(\beta_{\alpha.Q}) \right]^2 G_{00 m_\alpha}(t) \tag{6.8}$$

The second term in the above expression represents a cross-term between the internal motions and overall motions, but is zero except when $m_L = 0$, i.e., it is only required in calculating $J_0(0)$, or the spin-spin relaxation time. Otherwise, in calculating $J_1(\omega)$ and $J_2(2\omega)$, or the spin-lattice relaxation times, the overall correlation functions are given by the linear combinations of the products of the

96

correlation functions for each motion. When treating the internal motions further down the chain. additional coordinate frames are needed to carry out successive transformations from a local α frame to the molecular fixed frame. (see Chapter 3).

6.3 Decoupled Model for Correlated Internal Motions

To evaluate the correlation functions in Eq. (6.3), it is necessary to find the conditional probability $P_{il_0}[\Omega_{LM}, t|\Omega_{LM}(0), 0]$ that at time t, the molecule has configuration i and orientation Ω_{LM} given at $t = 0$, the molecule has configuration l and $\Omega_{LM}(0)$. Using the assumption of decoupling internal and external motions, it can be expressed as the product of configuration and orientation conditional probability:

$$P_{il_0}[\Omega_{LM}, t|\Omega_{LM}(0), 0] = p(i, t|l, 0)p[\Omega_{LM}, t|\Omega_{LM}(0), 0] \tag{6.9}$$

Now using the above conditional probability to express the ensemble average in Eq. (6.3),

$$G_{m_L}(t) = \sum_{i,l} \int \int d\Omega_{LM} d\Omega_{LM}(0) \left(D^2_{m_L 0}[\Omega_{LQ}(0)] D^{2*}_{m_L 0}[\Omega_{LQ}(t)] - \overline{D^2_{m_L 0} D^{2*}_{m_L 0}} \right)$$
$$\times p_{eq}(l)p_{il_0}[\Omega_{LM}, t|\Omega_{LM}(0), 0] \tag{6.10}$$

where $p_{eq}(l)$ is the probability of occurrence of configuration l at equilibrium. This can be calculated, for example, using the additive potential method [see Chapter 3]. The orientation conditional probability $p[\Omega_{LM}, t|\Omega_{LM}(0), 0]$ was used to evaluate $G^2_{m_L m_M m'_M}(t)$ in Chapter 4, and $p(i, t|l, 0) \equiv p_{il_0}(t)$ is required to evaluate internal correlation functions. To evaluate $G_{m_L}(t)$, one needs to transform the electric-field-gradient tensor through successive coordinates to allow for internal motions and reorientation of the molecule. Instead of using many local coordinate systems, it is more convenient to define a coordinate system (N) in which the chain may have N distinct configurations. The N frame is attached rigidly on a molecule-fixed (M) frame with an orientation specified by the

97

time-independent Euler angles Ω_{MN}. In each configuration, a $C - D$ bond has a known orientation. Its motion due to conformational transitions is responsible for spin relaxation. Transitions between different configurations take place by means of one-bond, two-bond, or three-bond motion[6.7,6.8] in the chain[see section 6.1]. These bond motions involve jump rate constants k_1, k_2, and k_3, respectively. Transitions among configurations are described by a master equation[6.11].

$$\frac{\partial p_{il_0}(t)}{\partial t} = \sum_{j=1}^{N} R_{ij} p_{jl_0}(t) \tag{6.11}$$

where R_{ij} is the rate constant for transition from configuration j to configuration i. R_{ij} is related to the elementary jump rate constant r_{ij} which depends on the type of bond motion in the transition. r_{ij} is zero if transition cannot occur via one of the three types of bond motion. The diagonal matrix elements R_{ii} are the negative of sum of all jump rates that deplete configuration i.

$$R_{ii} = -\sum_{j \neq i} R_{ji} \tag{6.12}$$

Moreover, R_{ij} satisfy the detailed-balance principle.

$$R_{ij} p_{eq}(j) = R_{ji} p_{eq}(i) \tag{6.13}$$

To construct the R matrix, it is required that $r_{ij} = r_{ji}$ and $R_{ij} = p_{eq}(i) r_{ij}$. The master equation can be solved[6.9] as an eigenvalue problem. This is achieved by symmetrizing R and then diagonalizing to give N real and negative eigenvalues λ_n and eigenvectors $\vec{x}^{(n)}$. One of these eigenvalues ($n = 1$) is zero, and the corresponding eigenvector $\vec{x}^{(1)}$ is given by the equilibrium distribution of configurations:

$$x_l^{(1)} = [p_{eq}(l)]^{1/2} \tag{6.14}$$

The conditional probability $p_{il_0}(t)$ is given by

$$p_{il_0}(t) = x_i^{(1)} \left(x_l^{(1)} \right)^{-1} \sum_{n=1}^{N} x_i^{(n)} x_l^{(n)} \exp(-|\lambda_n| t) \tag{6.15}$$

98

Now. applying the N frame coordinate system described above. and using the decomposition theorem for the Wigner matrix components. Eq. (6.1) can be rewritten as

$$D^2_{m_L 0} [\Omega_{LQ}(t)] = \sum_{m_M} \sum_{m_N} D^2_{m_L m_M} [\Omega_{LM}(t)] D^2_{m_M m_N} [\Omega_{MN}] D^2_{m_N 0} [\Omega_{NQ}(t)] \tag{6.16}$$

where the Euler angle Ω_{NQ} give the orientation of $C-D$ bond in the N frame. Both Ω_{LM} and Ω_{NQ} are time dependent because of molecular reorientation and internal motion. respectively. Following the procedure of section 6.2. the decoupled model gives

$$
\begin{aligned}
G_{m_L}(t) &= \sum_{m_M} \sum_{m'_M} \sum_{m_N} \sum_{m'_N} D^2_{m_M m_N}(\Omega_{MN}) D^2_{m'_M m'_N}(\Omega_{MN}) g_{m_L m_M m'_M} \\
&\quad \times \left\langle D^2_{m_N 0} [\Omega_{NQ}(0)] D^{2*}_{m'_N 0} [\Omega_{NQ}(t)] \right\rangle \\
&\quad + \delta_{m_L 0} \langle P_2 \rangle^2 \sum_{m_N} \sum_{m'_N} \left\langle D^2_{m_N 0} [\Omega_{NQ}(0)] D^{2*}_{m'_N 0} [\Omega_{NQ}(t)] \right\rangle \tag{6.17}
\end{aligned}
$$

The internal correlation functions are given by

$$
\begin{aligned}
\left\langle D^2_{m_N 0} [\Omega_{NQ}(0)] D^{2*}_{m'_N 0} [\Omega_{NQ}(t)] \right\rangle &= \sum_{l,l'} \exp(-im_N \alpha^l_{NQ}) d^2_{m_N 0}(\beta^l_{NQ}) p_{eq}(l) \\
&\quad \times \exp(-im'_N \alpha^l_{NQ}) d^2_{m'_N 0}(\beta^l_{NQ}) p_{il_0}(t) \\
&= \sum_{k=1}^{N} \exp(-|\lambda_k|t) \left[\sum_{l=1}^{N} x^{(1)}_l x^{(k)}_l \exp(-im_N \alpha^l_{NQ}) d^2_{m_N 0}(\beta^l_{NQ}) \right] \\
&\quad \times \left[\sum_{l'=1}^{N} x^{(1)}_{l'} x^{(k)}_{l'} \exp(-im'_N \alpha^{l'}_{NQ}) d^2_{m'_N 0}(\beta^{l'}_{NQ}) \right] \tag{6.18}
\end{aligned}
$$

where β^l_{NQ} and α^l_{NQ} are polar angles of a $C-D$ bond in the rotamer of configuration l in the N frame. and Eq. (6.15) was substituted in the last step.

When applying the TZ model to treat chain deuterons of an asymmetric rotor and letting $\Omega_{MN} = 0$ for simplicity, i.e., the N frame is coincident with the M frame. the spectral densities of C_i deuterons

can be obtained as

$$
\begin{aligned}
J_{m_L}^{(i)}(m_L\omega) &= \frac{3\pi^2}{2}\left(q_{CD}^{(i)}\right)^2 \sum_{m_M}\sum_{m_M'}\sum_{k=1}^{N}\left[\sum_{l=1}^{N} x_l^{(1)} x_l^{(k)} \exp(-im_M\alpha_{MQ}^{(i)l})d_{m_M0}^2(\beta_{MQ}^{(i)l})\right] \\
&\times \left[\sum_{l'=1}^{N} x_{l'}^{(1)} x_{l'}^{(k)} \exp(-im_M'\alpha_{MQ}^{(i)l'})d_{m_M'0}^2(\beta_{MQ}^{(i)l'})\right] \\
&\times \sum_K \frac{\left(b_{m_Lm_Mm_M'}^{22}\right)_K\left[\left(a_{m_Lm_Mm_M'}^{22}\right)_K + |\lambda_k|\right]}{\left[\left(a_{m_Lm_Mm_M'}^{22}\right)_K + |\lambda_k|\right]^2 + (m_L\omega)^2} \\
&+ \frac{3\pi^2}{2}\left(q_{CD}^{(i)}\right)^2 \delta_{m_L0}\langle P_2\rangle^2 \sum_{k=1}^{N}\left|\sum_{l=1}^{N} x_l^{(1)} x_l^{(k)} d_{00}^2(\beta_{MQ}^{(i)l})\right|^2 \frac{|\lambda_k|}{(m_L\omega)^2 + |\lambda_k|^2} \quad (6.19)
\end{aligned}
$$

where a and b are defined in section 4.2. Eq. (4.24). The last term of Eq. (6.19) is only needed in calculating the zero frequency spectral densities $J_0^{(i)}(0)$ for the chain deuterons.

References

6.1 R.Y. Dong, *Phys. Rev. A* **43**, 4310, 1991.

6.2 A. Ferrarini, G.J. Moro, P.L. Nordio, *Liq. Cryst.* **8**, 593, 1990.

6.3 P.A. Beckmann, J.W. Emsley, G.R. Luckhurst, D.L. Turner, *Mol. Phys.* **59**, 97, 1986.

6.4 P.J. Flory, In *Statistical Mechanics of Chain Molecules*, inter-science, New York, 1969.

6.5 P.L Nordio, P. Busolin, *J. Chem. Phys.* **55**, 5485, 1971.

6.6 P.L. Nordio, G. Rigatti, U. Segre, *J. Chem. Phys.* **56**, 2117, 1972.

6.7 B. Valeur, J.P. Jarry, F. Geny, L. Monnerie, *J. Polym. Sci.* **13**, 667, 1975.

6.8 B. Valeur, L. Monnerie, J.P. Jarry, *J. Polym. Sci.* **13**, 675, 1975.

6.9 R.Y. Dong, G.M. Richard, *Chem. Phys. Lett.* **200**, 541, 1992.

6.10 J.P. Caniparoli, A. Grassi, C. Chachaty, *Mol. Phys.* **63**, 419, 1988.

6.11 R.J. Wittebort, A. Szabo, *J. Chem. Phys.* **69**, 1722, 1978.

Chapter 7

Rotational Dynamics of 5O.7

7.1 Introduction

There are two deuterated 5O.7 samples. The $5O.7\text{-}d_1$ is deuterated at the methine site and $5O.7\text{-}d_4$ is deuterated at the aniline ring. Their experimental data were analyzed[7.1] previously at each temperature based on either the third rate model or Nordio model, which uses cylindrically symmetric diffusion tensor. In particular, Nordio model didn't seem to work well. The motivation of re-analyzing these data is to see if a non-cylindrically symmetric diffusion tensor (implemented by TZ model) would be more appropriate for molecular motions, i.e., does the asymmetry parameter of diffusion tensor ϵ defined in Eq. (4.8) play a role in the melecular dynamics? The earlier treatments with $\epsilon = 0$ were inadequate. The spectral densities at two Larmor frequencies, shown in Fig. 7.1, are essentially those reported before[7.1]. Since the two samples have slightly different clearing points, we scale the temperatures to give a common T_c of 77.6°C. The transition temperatures for $N - S_A$, $S_A - S_C$, and $S_C - S_B$ are 64, 55, and 52°C, respectively. At first, the data were satisfactorily analyzed[7.1] using the third rate model in which the molecules were treated as cylindrical rotors plus first order director fluctuations in J_1. The third rate model is one way of addressing the

102
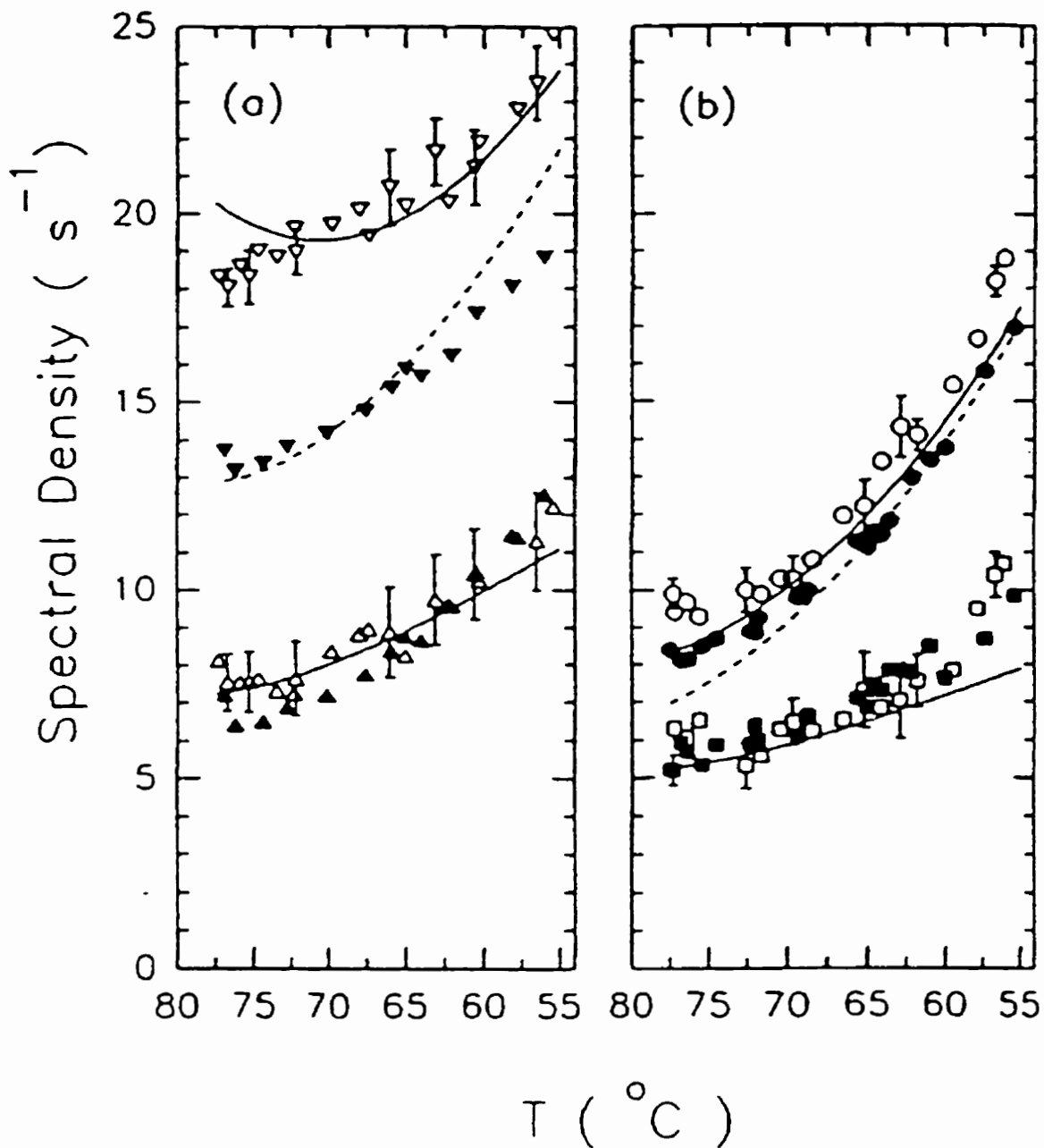
Figure 7.1. Plots of experimental spectral densities versus temperature in the nematic and smectic A phases of 5O.7-d_1 (a) where $\triangledown$ and $\triangle$ denote $J_1(\omega)$ and $J_2(2\omega)$, respectively, and of 5O.7-d_4 (b) where $\bigcirc$ and $\square$ denote $J_1(\omega)$ and $J_2(2\omega)$, respectively. Open symbols denote data at 15.3 MHz, while closed symbols at 46 MHz. Solid and dashed curves are theoretical spectral densities for 15.3 MHz and 46MHz, respectively.

103

inadequacy of the Nordio model. Here. we reexamine the 50.7 data in the N and S_A phases[7.2] using an extension to the Nordio model proposed by Tarroni and Zannoni[see Chapter 4]. For $\langle P_2 \rangle < 0.75$ in Table 7.1. it is sufficient to solve the rotational diffusion equation (4.11) using a Wigner basis set up to rank 14.

7.2 Analysis

To calculate the spectral densities for the methine and ring deuterons. Eqs. (4.24). (4.27) were used to account for the molecular orientation. and Eqs. (5.2) and (5.6) were used to calculate director fluctuations and the cross term in the first order approximation. Thus the calculated spectral densities for the ith deuteron(s) were obtained from

$$J_1^{(i)calc}(\omega) = J_{1R}^{(i)}(\omega) + J_{1DF}^{(i)}(\omega) + J_{1CR}^{(i)}(\omega)$$

$$J_2^{(i)calc}(2\omega) = J_{2R}^{(i)}(2\omega) \tag{7.1}$$

The spectral density data at different temperatures in the nematic and S_A phases were handled in the same fitting procedure. This is called the global target approach[7.3,7.4]. A minimization routine[7.5] (AMOEBA) was used to minimize the sum squared error F.

$$F = \sum_k \sum_\omega \sum_i \sum_m \left[J_m^{(i)calc}(m\omega) - J_m^{(i)exp}(m\omega) \right]_k^2 \tag{7.2}$$

where the sum over k was for nine different temperatures. $m = 1$ or 2, and the sum over ω was for two Larmor frequencies. The fitting quality factor Q is given by the percentage mean-squared deviation.

$$Q = \frac{\sum_k \sum_\omega \sum_i \sum_m \left[J_m^{(i)calc}(m\omega) - J_m^{(i)exp}(m\omega) \right]_k^2}{\sum_k \sum_\omega \sum_i \sum_m \left[J_m^{(i)exp}(m\omega) \right]_k^2} \times 100 \tag{7.3}$$

Smoothed lines of data were used to obtain experimental values of the spectral densities at nine different temperatures. First, the individual target analysis (i.e., minimization at a single temperature) must be performed before the global procedure in order to get some ideas on temperature relations of the model parameters. The global target analysis takes advantage of the fact that target parameters of the model vary smoothly with temperature. This was found particularly useful when the parameters of the model were highly correlated and/or affected by large statistical errors.

From the individual target approach, it was found that the rotational diffusion constants obey simple Arrhenius-type relations, giving

$$D_z = D_z^0 \exp\left[-E_a^t/RT\right] \tag{7.4}$$

$$D_y = D_y^0 \exp\left[-E_a^-/RT\right] \tag{7.5}$$

$$D_x = D_x^0 \exp\left[-E_a^-/RT\right] \tag{7.6}$$

$$D_R = D_R^0 \exp\left[-E_a^R/RT\right] \tag{7.7}$$

where a common activation energy E_a^- is assumed for D_x and D_y in a first approximation. In Eqs. (7.4)-(7.7), the global parameters are pre-exponentials D_z^0, D_y^0, D_x^0, and D_R^0, and their corresponding activation energies E_a^t, E_a^-, and E_a^R. When such a relation does not exist for a target parameter like the prefactor A of the director fluctuations, it is still possible to introduce an interpolating relation linking its value at different temperatures, e.g.,

$$A = A_0 + A_1(T - T_{\min}) + A_2(T - T_{\min})^2 \tag{7.8}$$

where the temperature $T_{\min}$ is taken at the $S_C - S_B$ phase transition, and A_0, A_1, and A_2 are global parameters for A. Since the high frequency cutoff is related to the viscosities and the elastic constants of the medium(see section 5.2), it could vary with temperature. In order not to increase

the number of global parameters further, the high frequency cutoff is assumed to vary linearly with temperature from 145 MHz at 348.15K to 85 MHz at 328.15K. This choice appears to be good in minimizing F.

7.3 Results

In the earlier work of 5O.7, the spectral densities were interpretted using the 'third-rate' model[7.1]. In contrast with the Nordio model, the rotational diffusion tensor may be diagonized in the laboratory frame with its Z_L axis along the director[7.6]. The α-motion represents diffusive precession of the long molecular axis about the director(D_α). The β-motion refers to the tumbling motion, i.e., the diffusive motion towards or away the director($D_\beta \equiv D_-$). In addition, the rotational motion about a molecular z_M axis(D_γ) is the so-called γ-motion[7.7]. These three motions give rise to the 'third-rate' model.

In the present study, we used nine temperatures with 72 spectral densities to derive ten global parameters for a given $\xi (= a_{22}/a_{20})$ value[see Eq. (4.30)]. For convenience, the diffusion pre-exponentials were not used as global parameters. Rather Eqs. (7.4-7.7) were rewritten in terms of the activation energies and the rotational diffusion constants D_x', D_y', D_z', and D_R' at 348.15K, giving the set of global parameters used in the minimization. Initial rotational diffusion values at the chosen temperature (348.15K) were first obtained by an "individual" target analysis. In the initial global target analysis, the Nordio model was first used (i.e., ξ is set to zero and $D_x = D_y$) together with first order director fluctuations and the small cross term. A global minimization of F produced a Q value of 0.37%. The fits between calculated and experimental spectral densities were poor in comparison with those using the third rate model[7.1], especially in the low temperature region.

Therefore. ξ was varied between -0.2 to +0.2 and assumed to be independent of the temperature. This assumption is necessary since there is no information from the side chains to determine $S_{xx} - S_{yy}$ as the chain deuterated sample is not available in the present study. As a result. it is found that a best Q value (0.25%) occurs at $\xi = -0.093$.

Table 7.1. Order parameters. effective potential coefficients of the biaxial potential. and the prefactor A[(defined in Eq. (5.3)] for $5O.7$ used in the calculation. $\langle D_{04}^4 \rangle$ is not listed bacuse of its very small (positive) values. The prefactor A values are based on $\alpha = 0.085$.

$T(K)$	a_{20}	a_{22}	$\langle P_2 \rangle$	$\langle P_4 \rangle$	$\langle D_{02}^2 \rangle$	$\langle D_{02}^4 \rangle$	$A(s^{1/2})$
328.15	-4.473	0.416	0.746	0.407	-0.0045	-0.0073	1.14×10^{-6}
333.15	-3.790	0.352	0.693	0.338	-0.0055	-0.0071	1.81×10^{-6}
338.15	-2.878	0.268	0.588	0.232	-0.0069	-0.0062	3.42×10^{-6}
343.15	-2.369	0.220	0.507	0.169	-0.0077	-0.0052	6.06×10^{-6}
348.15	-1.795	0.167	0.397	0.103	-0.0080	-0.0037	1.27×10^{-5}

For uniaxial media. the orienting potential is expressed in Eq. (4.27). in which the second rank coefficients a_{20} and a_{22} can be determined from a knowledge of order parameters $S_{zz}(\langle P_2 \rangle)$ and $S_{xx} - S_{yy}$ based on the maximum entropy principle[7.8]. By applying Eq. (3.23). the experimental doublet splitting of the methine deuteron ($\Delta \nu$) may be used to determine a_{20} and the order parameter $\langle P_2 \rangle$ of the molecular core for a given ξ. In this equation. $\theta = \theta_{bz}$ is the angle between the C-D bond and the molecular z_M axis, and the molecular x_M axis is chosen to lie on the plane which contains $C = N$ and $C - D$ bonds such that $\theta_{bx} = 90° - \theta$ and $\theta_{by} = 0$. Table 7.1 summarizes the derived

order parameters and the effective coefficients of the biaxial potential at several temperatures. It is noted that $\langle P_2 \rangle$ is about 0.3 near T_c, lower than the typical value of 0.43 deduced from the simple Maier-Saupe theory[7.9-7.10]. From the global minimization, the calculated spectral densities at 15.3 MHz are shown as solid curves, while those at 46 MHz as dashed curves in Fig. 7.1. The fits between the calculated and experimental spectral density data are quite acceptable in view of many assumptions used in our model. It is also noted that systematic deviations do exist, especially at low temperatures and near T_c. We summarized the model parameters by plotting the rotational diffusion constants in Fig. 7.2 and by listing the prefactor A ($\alpha = 0.09$ is assumed) for director fluctuations in Table 7.1. The present analysis seems to indicate that the relaxation data of 5O.7 could be better reproduced by the rotational diffusion of a 5O.7 molecule as an asymmetric rotor, since the Q value was improved by about 50%.

The activation energies and pre-exponentials are summarized in Table 7.2. The error limit for a particular global parameter was estimated by varying the one under consideration while keeping all other global parameters identical to those for the minimum F, to give an approximate doubling in the F value. Thus these activation energies are fairly well defined. The activation energy for the tumbling motion (E_a^-) is found larger than that for the spinning motion ($E_a^{\shortmid}$), indicating that rotations about the molecular z_M axis is easier than the rotation of this axis as expected for a rod-like molecule like 5O.7. It is noted from Fig. 7.2 that the behaviours of D_z and D_R are similar and D_R is slightly smaller than D_z. Normally one should expect the internal ring rotation to be faster. But these two diffusion constants are correlated making D_R less accurate. For the calculated pre-exponentials, although both D_z^0 and D_R^0 are well defined, the uncertainty in D_x^0 (or D_y^0) is still large, i.e., D_x^0 lies between 1.0×10^{14} and 1.4×10^{16} with an increase of 50% in F value. This indicates
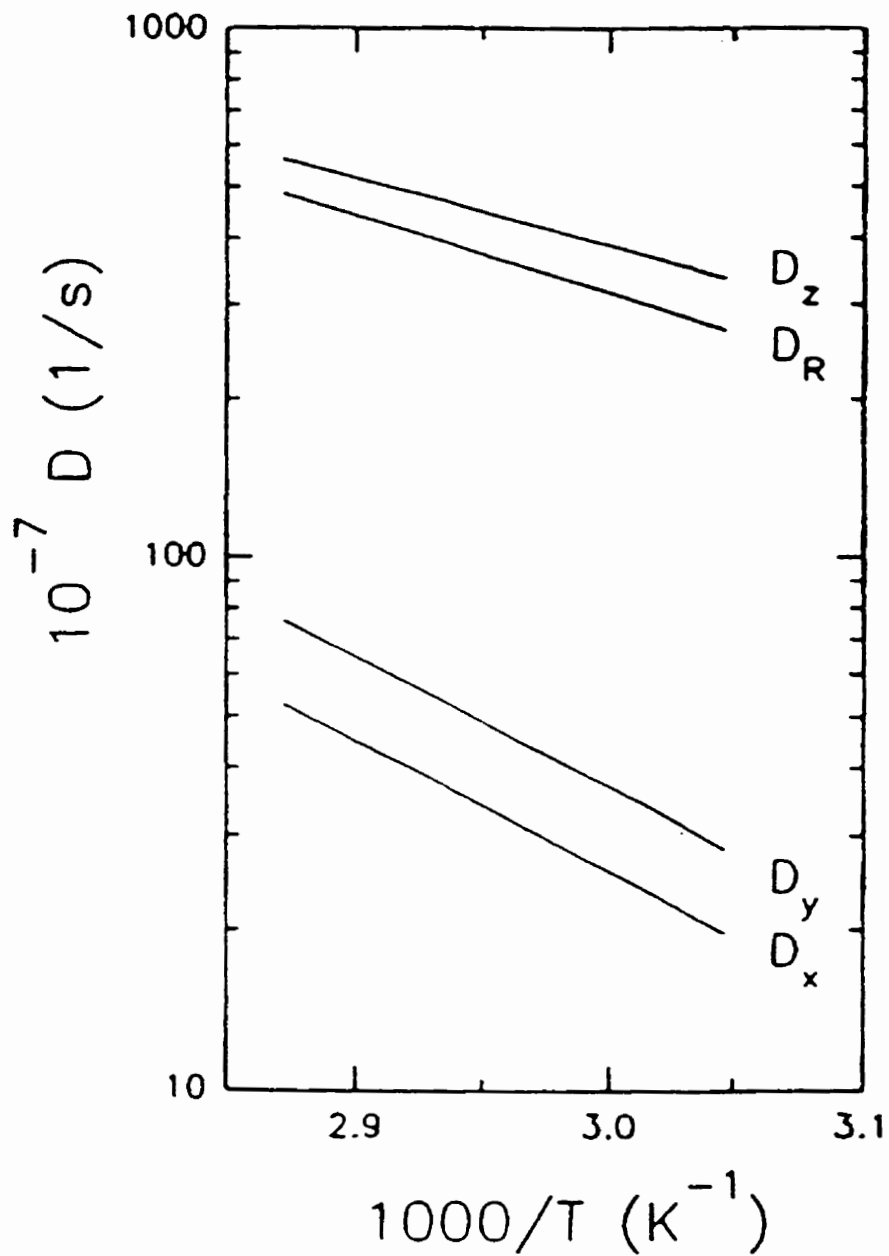
Figure 7.2. Plots of derived rotational diffusion constants D_x, D_y, D_z, and D_R, versus the reciprocal temperature

109

a very shallow minimum in F with respect to D_z^0 and is related to a common problem in relaxation calculations for liquid crystals, viz. a large uncertainty[7.11-7.12] in the magnitude of D_- value seems to exist. We will encounter this situation in other samples(6OCB and HAT6, etc.). It is for this reason that we have not used the pre-exponentials as target parameters.

Finally, the contribution to the experimental spectral density from director fluctuations, $J_{1DF}^{(0)}(\omega)$ and $J_{1DF}^{(R)}(\omega)$ for methine and ring deuterons versus temperature is plotted in Fig. 7.3. As seen from this figure, the contribution depends on the atomic site, the frequency and the temperature. These spectral densities $J_{1DF}^{(i)}(\omega)$ decrease with decreasing temperature. Using typical values of $K = 5 \times 10^{-12} N$ and $\eta = 6.5 \times 10^{-2} Pa$ s gives prefactor $A = 1.8 \times 10^{-5} s^{1/2}$ at 338.15K. Thus the derived A values in Table 7.1 are more or less in agreement with the theory. Its temperature behavior is consistent with the material constants in MBBA[see Chapter 8]. That the high-frequency cutoff decreases from 153 MHz near T_c to 85 MHz in the S_A phase is also reasonable[7.13].

Table 7.2. The pre-exponentials (in units of s^{-1}) and activation energies (in units of kJ/mol) derived from the analysis of spectral densities of the 5O.7 samples. The arrows denote lower($\downarrow$) and upper($\uparrow$) error limits.

	E_a^-	$E_a^\parallel$	E_a^R	D_r^0	D_y^0	D_z^0	D_R^0
	47±1	24.8±0.2	28.3±0.7	5.6×10^{15}	7.8×10^{15}	3.0×10^{13}	8.5×10^{13}
$\downarrow$				1.0×10^{14} (*)		2.78×10^{13}	6.5×10^{13}
$\uparrow$				1.4×10^{16} (*)		3.2×10^{13}	1.1×10^{14}

(*) The value reflects a 50% increase in F.
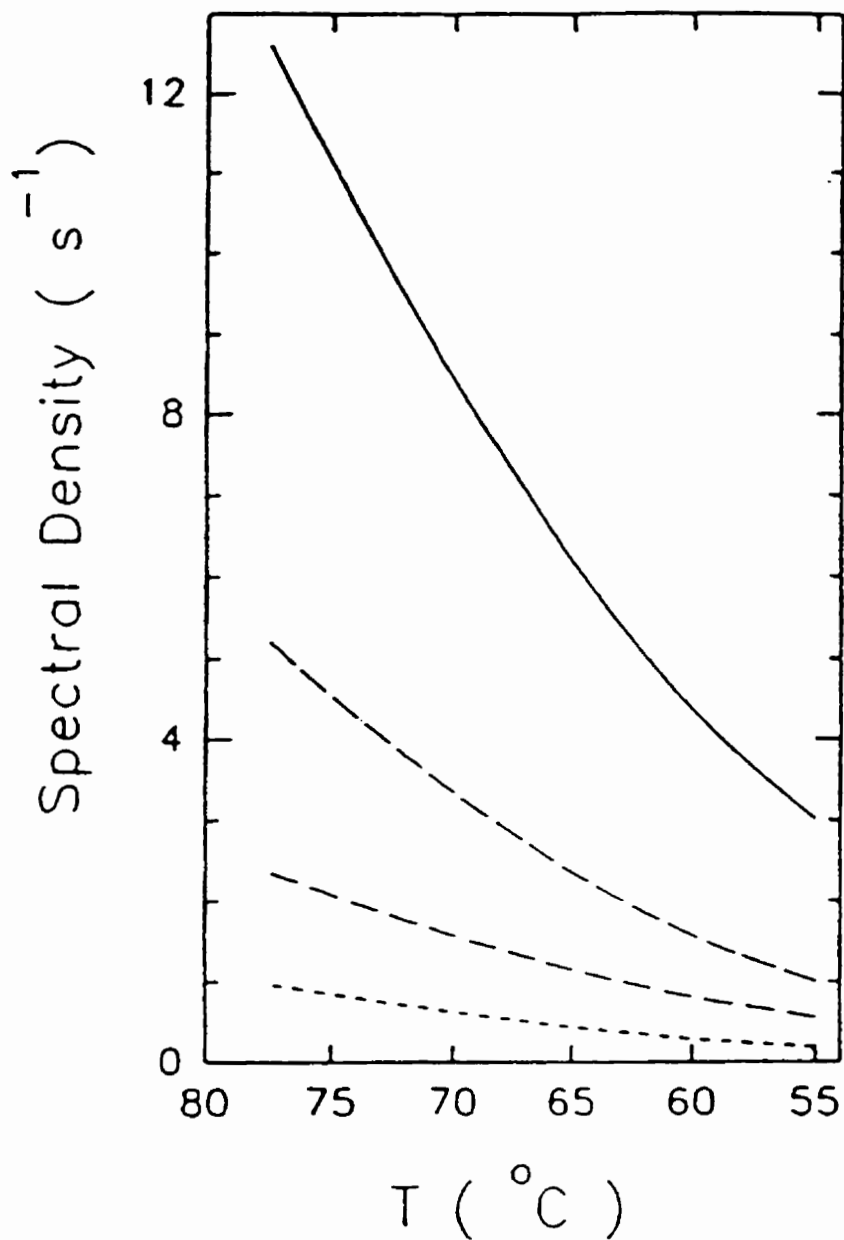
Figure 7.3. Plots of derived spectral densities due to director fluctuations $J_{1DF}(\omega)$ of 5O.7-d$_1$ (solid and dash-dotted curves for 15.3 and 46 MHz, respectively) and of 5O.7-d$_4$ (dashed and short-dashed curves for 15.3 and 46 MHz, respectively).

References

7.1 X. Shen, *M.Sc. Thesis*, the University of Manitoba, 1994; R.Y. Dong, X. Shen, *Phys. Rev. E* **49**, 538, 1994.

7.2 R.Y. Dong, X. Shen, *J. Chem. Phys.* **105**, 2016, 1996.

7.3 A. Arciono, F. Bertinelli, R. Tarroni, C. Zannoni, *Chem. Phys.* 1990, 143, 259.

7.4 R.Y. Dong, *Mol. Phys.* **88**, 979, 1996.

7.5 W.H. Press, B.P. Flannery, S.A. Teukolsky, W.T. Vetterling, *Numerical Recipes*, Cambridge University Press, Combridge, 1986.

7.6 C.F. Polnaszek, G.V. Bruno, J.H. Freed, *J. Chem. Phys.* **58**, 3185, 1973; C.F. Polnaszek, J.H. Freed, *J. Phys. Chem.* **79**, 2283, 1975.

7.7 R.R. Vold, R.L. Vold, *J. Chem. Phys.* **88**, 1443, 1988.

7.8 C. Zannono, in *The Molecular Dynamics of Liquid Crystals*, edited by G.R. Luckhurst and C.A. Veracini, Kumer Academic, Dordrecht, 1994.

7.9 W. Maier, A. Saupe, Z. Naturforsch, *Teil A*, **14**, 882, 1959; **15**, 287, 1960.

7.10 E.B. Priestly, P.J. Wojtowicz, P. Sheng, *Introduction to Liquid Crystals*, Plenum, New York, 1974.

7.11 V. Rutar, M. Vilfan, R. Blinc, E. Bock, *Mol. Phys.* **35**, 721, 1978.

7.12 R.Y. Dong, G.M. Richards, *J. Chem. Soc. Faraday Trans.* **88**, 1885, 1992.

7.13 S.R. Goren, C. Korn, S.B. Marks, *Chem. Phys. Lett.* **45**, 283, 1997.

Chapter 8

The Analysis of Director Fluctuations and Reorientation of MBBA

8.1 Introduction

It is well known that director fluctuations contribute a frequency term in the spectral density $J_1(\omega)$ and have zero contributions in $J_2(2\omega)$ and $J_0(\omega)$ when using the small angle (θ) approximation. where θ is the angle between the instantaneous director and its equilibrium orientation[8.1]. However. angular excursions of the local director can have large amplitudes and high order terms of θ can now contribute to $J_1(\omega)$. $J_2(2\omega)$ and $J_0(\omega)$. Second-order director fluctuations ($\propto \theta^2$) have been considered by Vold et al.[8.2] and van der Zwan et al.[8.3]. The frequency dependence in J_2 is calculated to be generally small. whereas J_0 is predicted to be quite large as $\omega \to 0$[8.2].

Although director fluctuations normally give small contributions in the megahertz region. there are at least two liquid crystals 5O.7[see Chapter 7] and 4O.8[8.4.8.5] in which director fluctuations have been used to account for part of $J_1(\omega)$. For these two liquid crystals. the high-frequency cutoffs

appear to be of the order of 10^2 MHz, while for MBBA (or IO.4), there is no detectable contribution from director fluctuations to the deuteron spin-lattice relaxation in the MHz regime[8.6]. The same conclusion was made by Vilfan et al.[8.7] based on their proton NMR study. Recent published data[8.8] show, however, that there is a substantial contribution from director fluctuations to $J_0(0)$. It is believed that a possible explanation of the different behaviours among the studied liquid crystals of nO.m series may be due to their high-frequency cutoffs, since the prefactors A for these liquid crystals are expected to be comparable. The possible origin of different cutoff frequencies may be the different viscoelastic constants or different temperature ranges, since MBBA has a much lower T_c in comparing with 5O.7 and 4O.8. The motivation is to explore if the high frequency cutoff is low for MBBA by looking for zero frequency director fluctuatnion contributions.

8.2 Analysis

The data analysis involves both the deuteron spin-spin[8.8] and spin-lattice relaxation[8.6] in the nematic phase of MBBA using the director fluctuations up to second-order contributions as well as rotational diffusion model of Tarroni and Zannoni (Chapter 4). Eqs. (4.24) and (6.19) were used to calculate the molecular rotations of methine deuteron and methylene deuterons of the chain, respectively. The second order director fluctuation contributions are accounted for by Eqs. (5.14), (5.6) and (5.10-5.11) for the methine deuteron and Eqs. (5.17-5.20) for deuterons on the flexible chain. Finally, the calculated spectral densities for the ith deuterons are obtained from:

$$J_1^{(i)}(\omega) = J_{1R}^{(i)}(\omega) + J_{1DF}^{(i)}(\omega) + J_{1CR}^{(i)}(\omega)$$

$$J_2^{(i)}(2\omega) = J_{2R}^{(i)}(2\omega) + J_{2DF}^{(i)}(2\omega)$$

$$J_0^{(i)}(0) = J_{0R}^{(i)}(0) + J_{0DF}^{(i)}(0) \qquad (8.1)$$

where $i = 0, 1, 2$, and 3, with $i = 0$ denoting the methine site.

The experiments consist of measurements of the spin-spin relaxation rate[8.8] $1/T_2$ at 46 MHz, and measurements of the Zeeman and quadrupolar spin-lattice relaxation rates[8.6] $1/T_{1Z}$ and $1/T_{1Q}$ at 15.3 and 46 MHz. From the spin relaxation theory for deuteron (I=1), these are related to the spectral densities $J_m(m\omega)$ by[8.9-8.11]

$$T_2^{(i)-1} = \frac{3}{2}J_0^{(i)}(0) + \frac{3}{2}J_1^{(i)}(\omega) + J_2^{(i)}(2\omega)$$

$$T_{1Z}^{(i)-1} = J_1^{(i)}(\omega) + 4J_2^{(i)}(2\omega)$$

$$T_{1Q}^{(i)-1} = 3J_1^{(i)}(\omega) \qquad (8.2)$$

where ω is the Larmor frequency.

8.3 Results and Discussion

The spectral densities $J_m^{(i)}(m\omega)$ at two different Larmor frequencies are reproduced in Figures 8.1 and 8.2[8.6, 8.8]. The analysis of quadrupolar splittings[8.6] using the internal energies $E_{tg} = 2550$ J/mol and $E_{gg} = 6000$ J/mol gave the model parameters $(X_a, \lambda_c = X_c/X_a, <P_2>$ and $S_{xx} - S_{yy})$ needed in the analysis. In particular, the order parameter tensor of the average conformer allows us to adopt a biaxial orienting potential (specified by a_{20}, a_{22}) for solving the rotational diffusion equation. A global target approach was also used to analyze the spectral densities of methine C_0 and methylene C_i (i=1, 2, 3) deuterons at six different temperatures. Smoothed lines of data were used to obtain the $J_0^{(i)exp}(0)$, $J_1^{(i)exp}(\omega)$ and $J_2^{(i)exp}(2\omega)$ values at these temperatures. The optimization routine (AMOEBA) is used to minimize the sum squared percent error F.

$$F = \sum_k \sum_\omega \sum_i \sum_m \left[\frac{J_m^{(i)calc}(m\omega) - J_m^{(i)exp}(m\omega)}{J_m^{(i)exp}(m\omega)} \times 100 \right]_k^2 \qquad (8.3)$$

115
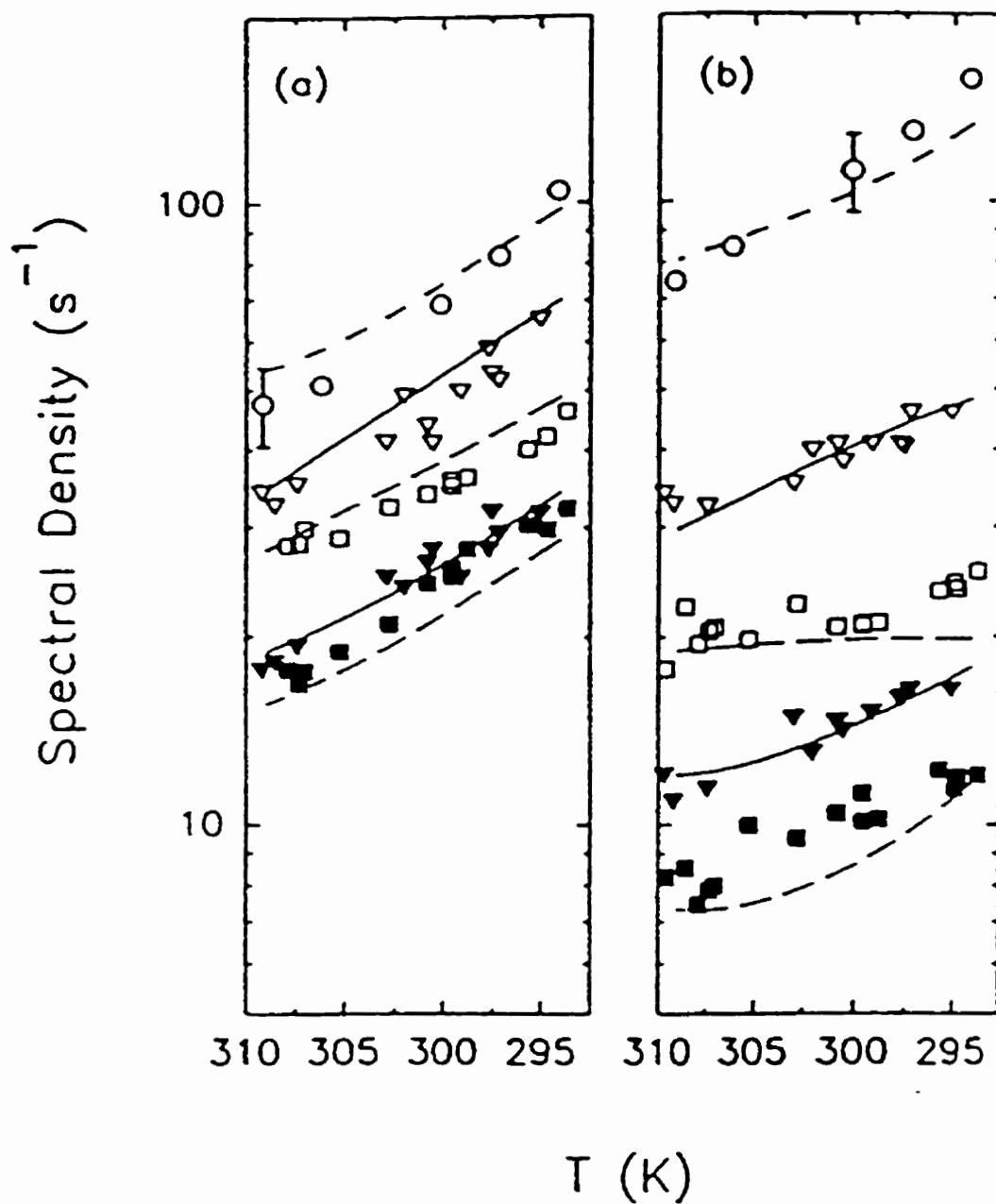
Figure 8.1. Plots of experimental and calculated spectral densities of MBBA by using $\omega_c = 10$ MHz. The circles denote the spectral densities $J_0(0)$, the open symbols denote $J_1(\omega_0)$, while the closed symbols denote $J_2(2\omega_0)$. The triangles represent the data at 15.3 MHz, while the squares represent data at 46 MHz. Figures 8.1(a) and 8.1(b) are for C_0, and C_1, respectively.
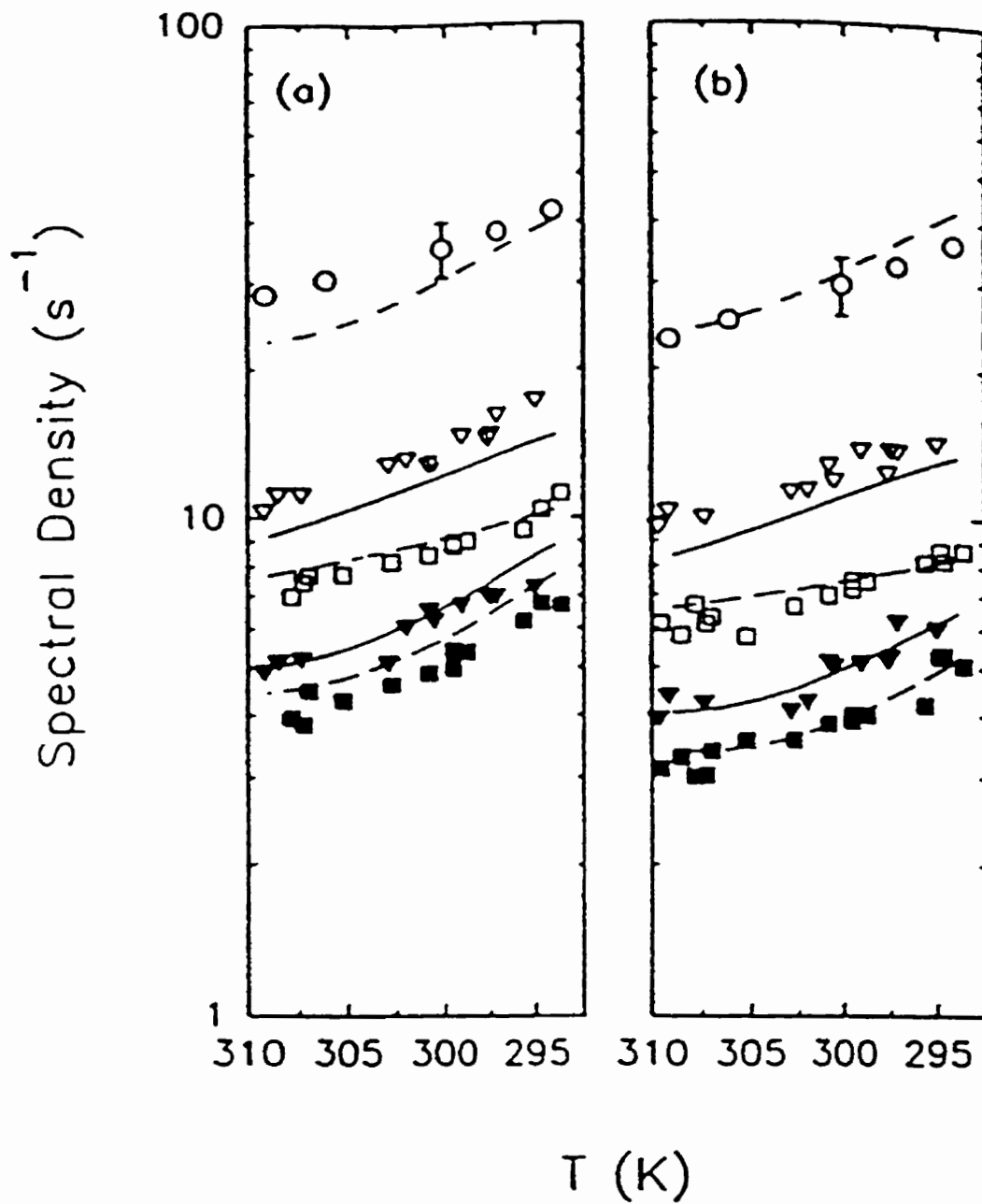
Figure 8.2. Plots of experimental and calculated spectral densities of MBBA by using $\omega_c = 10$ MHz. The legends are same as those in Figure 8.1. Figures 8.2(a), and 8.2(b) are for C_2, and C_3, respectively.

where the sum k is over six different temperatures, the sum over ω for two Larmor frequencies, and $m = 0$, 1 or 2. In comparison with Eq. (7.2), the definition of F here is slightly different. The reason is that the spectral densities of penultimate site C_3 deuterons in the chain are much smaller than those of methine deuteron. In order to equally weight the data of different sites, the sum of relative deviations rather than absolute deviations are adopted. The fitting quality Q is still given by the percentage mean squared deviation.

$$
Q = \frac{\sum_k \sum_\omega \sum_i \sum_m \left[J_m^{(i)calc}(m\omega) - J_m^{(i)exp}(m\omega) \right]_k^2}{\sum_k \sum_\omega \sum_i \sum_m \left[J_m^{(i)exp}(m\omega) \right]_k^2} \times 100\% \tag{8.4}
$$

It is believed that the motional biaxiality for the MBBA molecule is very small. Therefore, $D_x = D_y$ is set in our minimization. From the individual target analysis, it is clear that the diffusion constants and the jump constants k_1 and k_3 all obey simple Arrhenius-type relations, giving:

$$
D_x = D_x^0 \exp(-E_a^{D_x}/RT) \tag{8.5}
$$

$$
D_z = D_z^0 \exp(-E_a^{D_z}/RT) \tag{8.6}
$$

$$
k_1 = k_1^0 \exp(-E_a^{k_1}/RT) \tag{8.7}
$$

$$
k_3 = k_3^0 \exp(-E_a^{k_3}/RT) \tag{8.8}
$$

where the global parameters are the pre-exponentials D_x^0, D_z^0, k_1^0 and k_3^0, and their corresponding activation energies $E_a^{D_x}$, $E_a^{D_z}$, $E_a^{k_1}$, and $E_a^{k_3}$. When such a relation does not exist for a target parameter like k_2 and the prefactor A of director fluctuations, the following interpolating relations are used for k_2 and $A_{DF}(= A < P_2 >^2)$:

$$
k_2 = k_2' - k_2''(T - T_{max}) \tag{8.9}
$$

$$
A_{DF} = A_{DF}' - A_{DF}''(T - T_{max}) \tag{8.10}
$$

where the temperature T_{max} is the highest temperature used in the global analysis, and the global parameters k'_2, k''_2, A'_{DF} and A''_{DF} are optimized. The above equations are based on weak temperature dependences for k_2 and A_{DF}. Thus there are twelve global parameters (two from each of Eqs. (8.5)-(8.10)) for the global fit.

We analyze the deuteron data at four carbon sites (C_0, C_1, C_2, C_3). At each site, there are two experimental J_1 and two experimental J_2 values from the two Larmor frequencies, but only one $J_0(0)$ value due to the zero frequency component being independent of the Larmor frequency. So we have a total of 120 spectral densities from six temperatures to derive twelve global parameters for a given ω_c value. For convenience, the diffusion and jump rate pre-exponentials were not used as global parameters. Rather Eqs. (8.5)-(8.8) were rewritten in terms of the activation energies and the diffusion and jump constants D'_x, D'_z, k'_1, k'_3 at 309 K (T_{max}), giving the set of global parameters used in our minimization. Initial values at the chosen temperature (309 K) were first obtained by an individual target analysis.

Table 8.1: Comparisons of activation energies E_a (in kJ/mol) and fitting results using different high-frequency cutoffs for MBBA.

ω_c(MHz)	$E_a^{k_1}$	$E_a^{k_3}$	$E_a^{D_x}$	$E_a^{D_z}$	F	Q
3	103	80.0	49.9	45.0	10600	0.95%
10	102 ± 2	78 ± 2	50.0 ± 0.8	44.3 ± 0.6	9600	0.97%
13	100	77.2	49.2	44.0	9000	0.97%
20	95.9	75.1	47.8	43.4	7900	0.99%

It is assumed for simplicity that ω_c is constant in the nematic phase of MBBA. The assumption is probably good for the temperature range studied here. Several high-frequency cutoff values, between 3 MHz and 20 MHz, were tested (Table 8.1); these fits between the calculated and experimental spectral density data are in general acceptable, since Q values are all less than 1%. The derived activation energies vary slightly with ω_c. At $\omega_c = 3$ MHz, a better Q value of 0.95% was obtained, whereas at $\omega_c = 20$ MHz, a better F value of 7900 was achieved. Thus, it is reasonable to estimate the ω_c value for MBBA to be around 3 MHz - 10 MHz. It is noted that the $E_a^{D_r}$ is a little larger than $E_a^{D_z}$, indicating the spinning motion of the MBBA molecule is less hindered than the tumbling motion. This was not achieved when a global target analysis was carried out[8.12] using only the $J_1(\omega)$ and $J_2(2\omega)$ data. Without loss of generality, the $\omega_c = 10$ MHz is taken in the following discussion. From the global minimization, the calculated site dependences of the spectral densities and director fluctuation contributions are listed in Table 8.2 for one temperature. Director fluctuations mainly have effects on the zero frequency spectral densities. They account for 35% of the methine $J_0(0)$, and over 50% for the methylene (C_1-C_3) $J_0^{(i)}(0)$. Their total first-order contributions ($J_{1DF}^{(i)}$ plus negative $J_{1CR}^{(i)}$) to $J_1^{(i)}(\omega)$ are small but negative; the biggest effects occur at the chain deuterons, where the director fluctuation contributions amount to about 10% of $J_1^{(i)}(\omega)$. The second-order contributions of $J_{2DF}^{(i)}$ to $J_2^{(i)}(2\omega)$ are indeed very small and less than 1%. Indeed the observed frequency dependences in $J_2^{(i)}(2\omega)$ are mainly due to "slow" molecular rotations. From this table, it is found that the J_{0DF} for the methine deuteron is smaller than that of C_1 and larger than those of C_2 and C_3. This result may be inferred from Eqs. (5.13) and (5.16)-(5.17). The director fluctuation contributions to the zero frequency components are scaled by the factors of $[d_{00}^2(\beta_{M,Q})]^2$ and $[\overline{d_{00}^2(\beta_{M,Q}^{(i)})}]^2$, for methine deuteron and chain deuterons, respectively. For C_2 and

120

C_3, there are more conformational averaging of $\overline{d_{00}^2(\beta_{M,Q}^{(i)})}$ over the $\beta_{M,Q}^{(i)}$ angles, making the overall contributions to C_2 and C_3 progressively smaller. The model parameters (3 ks, 2 Ds and A) for $\omega_c = 10$ MHz at each chosen temperature are summarized in Table 8.3. The activation energies (Table 8.1) and the pre-exponentials ($k_1^0 = 1.75 \times 10^{29}$ s^{-1}, $k_3^0 = 4.3 \times 10^{25}$ s^{-1}, $D_r^0 = 1.74 \times 10^{16}$ s^{-1}, and $D_z^0 = 1.13 \times 10^{17}$ s^{-1}) are used to plot the theoretical spectral density curves in Figures 8.1 and 8.2. The $J_2^{(i)}$ values at 46 MHz show deviations between calculated and experimental values at C_0 to C_2. Although there are some systematic deviations between experimental and calculated spectral densities, the overall fits are quite satisfactory. It is interesting to note that a comparison of the rate and diffusion constants with those reported before[8.12] shows reasonable agreements. In Table 8.4, the prefactor A values for the different samples of n0.m series are listed. It is noted that the prefactor A obtained for MBBA is slightly larger than that of 50.7 and 40.8[8.5], yet there is negligible contribution from director fluctuations to J_1 of MBBA at the same Larmor frequencies. This is of course due to the lower high-frequency cutoff in MBBA. Using typical values of $K = 5 \times 10^{-12}$ N and $\eta = 6.5 \times 10^{-2}$ Pa·s, $A = 1.6 \times 10^{-5}$ s$^{1/2}$ is calculated from Eq. (5.3) at 300 K. Thus, the derived A values appear to agree with the theory. The calculated cross-term $J_{1CR}^{(i)}$ has absolute values slightly larger than $J_{1DF}^{(i)}$ contrary to the prediction that the cross-term should be "small". Therefore, the controversy[8.13-8.15] with the cross-term remains to be explored with proper theoretical models. As seen in Table 8.4, the temperature dependence of A in MBBA differs from those of 50.7 and 40.8. It is not clear at present why the differences exist. The error limit for a particular global parameter was estimated by varying the one under consideration while keeping all other global parameters identical to those for the minimum F, to give an approximate doubling in the F value. Thus the error bar for D_r^0 is given by $1.25 - 2.54 \times 10^{16}$ s^{-1}, while that of D_z^0 is

$0.88 - 1.53 \times 10^{17}$ s^{-1}. Similarly, k_1^0 lies between 0.85×10^{29} s^{-1} and 5.2×10^{29} s^{-1} and k_3^0 from 1.8 $\times 10^{25}$ s^{-1} to 4.3 $\times 10^{26}$ s^{-1}. Finally, the error bars for the derived activation energies are indicated in Table 8.1 for $\omega_c = 10$ MHz. These activation energies are fairly well-defined by the global target analysis.

Table 8.2: Calculated spectral densities for C_0-C_3 deuterons due to director fluctuations and molecular reorientation in the global minimization with a high-frequency cutoff $\omega_c = 10$ MHz. The numbers (in s^{-1}) within brackets are for 46 MHz, while those without brackets are for 15.3 MHz, and the temperature is 300 K.

C_i	$J_0(0)$	$J_{0DF}(0)$	$J_1(\omega)$	$J_{1DF}(\omega)$	$J_{1CR}(\omega)$	$J_2(2\omega)$	$J_{2DF}(2\omega)$
C_0	74.59	26.16	53.17	2.46	-4.17	26.2	0.04
	(74.59)	(26.16)	(38.54)	(0.3)	(-2.0)	(21.75)	(0.00)
C_1	102.7	58.29	40.38	5.47	-9.29	14.34	0.09
	(102.7)	(58.29)	(19.75)	(0.68)	(-4.5)	(8.60)	(0.01)
C_2	30.42	18.43	12.21	1.73	-2.94	6.63	0.03
	(30.42)	(18.43)	(9.12)	(0.21)	(-1.4)	(5.72)	(0.00)
C_3	31.62	20.11	11.1	1.89	-3.21	4.97	0.03
	(31.62)	(20.11)	(7.48)	(0.23)	(-1.5)	(3.93)	(0.00)

Table 8.3: Motional parameters derived from a global analysis of spectral densities using $\omega_c = 10$ MHz.

T(K)	$k_1(\times 10^{11}\mathrm{s}^{-1})$	$k_2(\times 10^{10}\mathrm{s}^{-1})$	$k_3(\times 10^{12}\mathrm{s}^{-1})$	$D_x(\times 10^7\mathrm{s}^{-1})$	$D_z(\times 10^9\mathrm{s}^{-1})$	$A(\times 10^{-5}\mathrm{s}^{1/2})$
309	10.5	1.51	2.58	6.24	3.66	1.9±0.4
306	7.12	1.65	1.92	5.16	3.09	1.76
303	4.79	1.80	1.41	4.24	2.60	1.70
300	3.20	1.94	1.04	3.48	2.18	1.71
297	2.12	2.09	0.76	2.84	1.82	1.76
294	1.39	2.24	0.55	2.31	1.52	1.78

Table 8.4: Comparisons of A values in 10.4, 50.7 and 40.8 at different reduced temperature $T_{red}(=T/T_c)$.

T_{red}	10.4	T_{red}	50.7	T_{red}	40.8[ref. 8.5]
0.988	1.93×10^{-5}	0.993	1.27×10^{-5}	0.995	9.72×10^{-6}
0.979	1.76×10^{-5}	0.979	6.06×10^{-6}	0.981	5.27×10^{-6}
0.969	1.70×10^{-5}	0.964	3.42×10^{-6}	0.966	3.85×10^{-6}
0.96	1.71×10^{-5}	0.95	1.81×10^{-6}	0.952	2.98×10^{-6}
0.95	1.76×10^{-5}	0.936	1.14×10^{-6}	0.938	2.54×10^{-6}
0.94	1.78×10^{-5}			0.924	2.38×10^{-6}
	$T_C = 312.6$ K		$T_C = 350.6$ K		$T_C = 351.8$ K

8.4 Brief Summary

The zero-frequency spectral densities $J_0(0)$ data in the nematic phase of MBBA was quantitatively interpreted using a model that include director fluctuations and the rotational diffusion model of Tarroni and Zannoni (in the limit of $D_x = D_y$). The T_1 and T_2 data support the idea that MBBA has a relatively low value for the high-frequency cutoff. The contribution to $J_0(0)$ from director fluctuations has mainly a second-order component, whereas the first-order contribution to $J_1(\omega)$ is suppressed in the megahertz region (Larmor frequencies are 15.3 MHz and 46 MHz) due to the high-frequency cutoff, which is estimated to be around 3-10 MHz for MBBA. It is found that director fluctuations have larger effects on $J_0^{(i)}(0)$ (35% − 50%) than on $J_1^{(i)}(\omega)$ (< 10%). The derived A values are quite reasonable, ranging between 1.7×10^{-5} s$^{1/2}$ and 1.9×10^{-5} s$^{1/2}$. The fits to the available experimental spectral densities between 293 and 310 K in MBBA are on the whole very satisfactory with an overall quality Q factor of about 1%.

References

8.1 P. Pincus. *Solid State Commun.* 1969, 7, 415; T. Lubensky. *Phys. Rev.* 1970, 2, 2497.

8.2 R.L. Vold, R.R. Vold, M. Warner, *J. Chem. Soc., Faraday Trans. 2* 1988, 84, 997.

8.3 G. van der Zwan, L. Plomp, *Liq. Cryst.* 1989, 4, 133.

8.4 T.M. Barbara, R.R. Vold, R.L. Vold, M.E. Neubert, *J. Chem. Phys.* 1985, 82, 1612.

8.5 R.Y. Dong, *J. Phys. Chem.* 1996, 100, 15663.

8.6 R.Y. Dong, L. Friesen, G.M. Richards, *Mol. Phys.* 1994, 81, 1017.

8.7 M. Vilfan, R. Blinc, J.W. Doane, *Solid State Commun.* 1972, 11, 1073.

8.8 R.Y. Dong, *Chem. Phys. Lett.* 1996, 251, 387.

8.9 J.P. Jacobsen, H.K. Bildsoe, K. Schaumburg, *J. Magn. Reson.* 1976, 23, 153

8.10 S.B. Ahmad, K.J. Packer, J.M. Ramsden, *Mol. Phys.* 1977, 33, 857.

8.11 R.R. Vold, R.L. Vold, *J. Chem. Phys.* 1977, 66, 4018.

8.12 R.Y. Dong, *Mol. Phys.* 1996, 88, 979.

8.13 P. Ukleja, J. Pirs, J.W. Doane, *Phys. Rev. A* 1976, 14, 414.

8.14 J.H. Freed, *J. Chem. Phys.* 1977, 66, 4183.

8.15 B.J. Gertner, K. Lindenberg, *J. Chem. Phys.* 1991, 94, 5143.

Chapter 9

Orientational Ordering and Dynamics of 6OCB and 6OCB/8OCB Mixture: A Comparative Study

9.1 Introduction

Deuteron longitudinal (T_{1Z}) and quadrupolar (T_{1Q}) spin-lattice relaxation times and quadrupolar splittings were measured in the nematic phase of 6OCB[9.1] and over all the stable mesophases in a mixture of perdeuterated 4-n-hexyloxy-4'-cyanobiphenyl (6OCB) and 4-n-octyloxy-4'-cyanobiphenyl (8OCB) at 15.1 MHz and 46 MHz, and the results were compared with each other. The 6OCB/8OCB mixture has 28 wt. % of 6OCB and shows a nematic, smectic A and reentrant-nematic (RN) phases. The motivations are to test the decoupled model of Dong in longer side chains in rod-like molecules and in different phases. and to carry out data analyses for both samples in exactly the same manner such that the dynamic behaviours of pure 6OCB sample in its nematic phase may be compared with

those of 6OCB/8OCB mixture in high temperature nematic phase as well as in low temperature smectic A phase and reentrant-nematic phase. The additive potential method[see Chapter 3] is employed to construct the potential of mean torque using the quadrupolar splittings in these samples. A decoupled model is used to describe correlated internal motions of the end chain[see Chapter 6], which are assumed to be independent of the molecular reorientation. The latter motion is treated using the small-step rotational diffusion model of Tarroni and Zannoni[see Chapter 4], while the former motion is described using a master rate equation. In comparing the NMR results of the pure 6OCB sample and of the 6OCB/8OCB mixture, both the dynamic and static behaviours appear to be similar, and there are no dramatic changes upon entering the RN phase of 6OCB/8OCB, supporting the belief that the effects driving the reentrancy in this mixture are very subtle. The tumbling motion of 6OCB molecules, however, shows quite different behaviours in the two studied samples. Both 6OCB and 8OCB tend to form "loose" dimers, i.e., the packing of dimers is not tight. It is anticipated that the degree of dimerization may be inferred from the tumbling motion of 6OCB molecules and their internal chain dynamics.

The perdeuterated 6OCB-d_{21} sample was that used[9.2] in a previous study and was also used to make a 6OCB/8OCB mixture. For the composition ranging between approximately 25 and 31 wt. % 6OCB, this binary system exhibits a reentrant-nematic (RN) phase at atmospheric pressure[9.3], i.e. one observes a transition from the smectic A phase to a nematic phase on either heating or cooling the system. A phase diagram of 6OCB/8OCB is shown in Fig. 9.1. The 6OCB-d_{21} exhibits a nematic phase with a clearing temperature (T_C) of 75°C. Our binary sample consisting of 28% 6OCB-d_{21} and 72% protonated 8OCB by weight was prepared by weighing sufficient quantities of the components so that the final concentration was accurate to within 0.3%. The binary mixture

has a clearing temperature 79°C, N-S_A at 43°C and S_A-RN at 32.5°C. The 6OCB molecule is schematically shown in Fig. 1.4 and the peak assignment[9.4] of a representative spectrum for the 6OCB-d_{21} and/or 6OCB-d_{21}/8OCB samples is shown in Fig. 9.2.
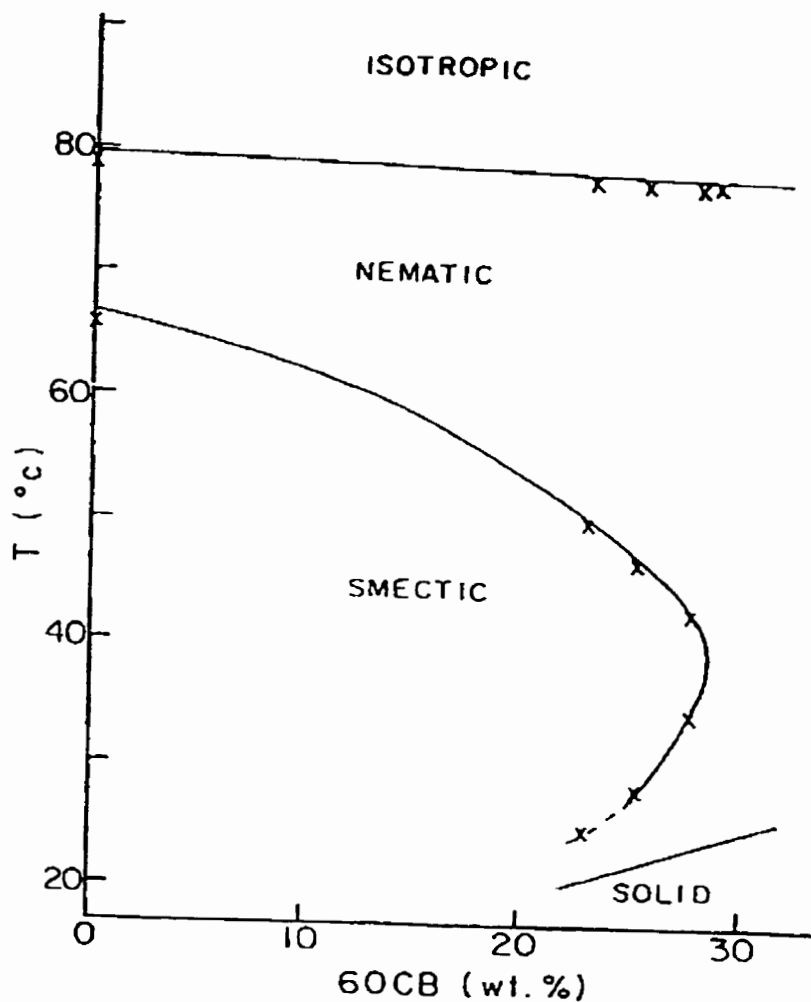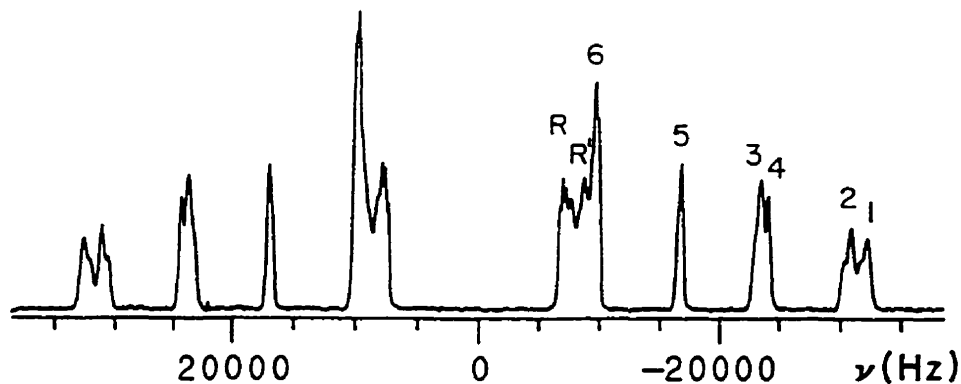

Figure 9.1 A phase diagram of 6OCB/8OCB mixture.

128

Figure 9.2 A typical deuteron NMR spectrum (at T~ 315 K) of 6OCB-d_{21} or 6OCB-d_{21}/8OCB

mixture showing the peak assignment.

Both 6OCB and 8OCB molecules possess a stong terminal electric dipole. These molecules tend

to form pairs of partially overlapping antiparallel molecules in order to minimize electrostatic in-

teractions. One can speak of "loose" dimers. The smectic A phase of 8OCB has a layer spacing

$d \simeq 1.4l$ where l is the molecular length. This type of smectic A phase with partial bilayers is

sometime labeled as A_d. Various theoretical models have been proposed by including competing

interactions to account for the occurrence of reentrant phenomena in liquid crystals[9.5-9.10]. In

particular, interpretation of experimental data has been based[9.5-9.6] on the simultaneous presence

of monomers and dimers. Recently a molecular field theory[9.10] has been made to link the occur-

rence of reentrant phases to the mole fraction x_d of dimers in a mixture of dimerizing molecules.

It is interesting to note that this molecular field theory predicts a decreasing x_d with decreasing

temperature. In the present study, 243 conformations were used to describe the internal chain mo-

tion by fixing the O-C_1 bond on the ring plane as proposed by some authors[9.11]. The decoupled model is used to predict spectral densities of motion in the nematic phase of a 6OCB sample and in the nematic, smectic A and RN phases of a 6OCB/8OCB mixture.

9.2 Analysis

In this section we outline the procedures and formulae which are given in previous chapters for discussing the measured quadrupolar splittings and spectral densities of motion. The geometry used to describe the carbon-carbon backbone of an alkyloxy chain is adopted as: $\angle C'CH=107.5°$, $\angle HCH=113.6°$ and $\angle CCC=113.5°$. The dihedral angles for rotation of a C-C bond in the chain are $\phi = 0, \pm 112°$ for the three RISs. These correspond to the trans (t) and two symmetric gauche ($g^\pm$) states. The gauche states have higher internal energy in comparison to that of the trans state by an amount E_{tg}. When the chain contains a g^-g^- or a g^-g^- linkage, an additional internal energy $E_{g^\pm g^\mp}$ is added because these linkages bring parts of the chain near to one another, the so-called "pentane effect". The E_{tg} values reported for gaseous alkanes lie between 2.1 and 3.2 kJ/mol, while the $E_{g^\pm g^\mp}$ value is about three times larger[9.12]. The values $E_{tg} = 2150$ J/mol and $E_{g^\pm g^\mp} = 6500$ J/mol were set. Due to the presence of the oxygen as well as the $\angle COC$ is larger than the $\angle CCC$[9.14-9.15], the energies for trans-gauche(COCC) and gauche-gauche(COCCC) linkages could be different from those of trans-gauche(CCCC) and gauche-gauche(CCCCC). Thus larger values of E'_{tg}(for COCC) $= 3300$ J/mol and $E'_{g^\pm g^\mp} = 10000$ J/mol were used.

The C_{ar}-O bond may be taken to be along the biphenyl para axis. It is known that the $\angle COC$ which specifies the direction of the chain relative to the molecular core plays an important role in the observed variations of segmental order and spin relaxation profiles. The molecular core, which

includes the first C_{ar}-O bond in the chain is assumed to be a rigid subunit and has cylindrical symmetry with an interaction parameter X_a. As an approximation, the bond interaction parameter of the O-C_1 bond is identical to those of C-C bonds. i.e. $X_{cc} = X_{oc}$. According to the model prediction[9.13], the ratio $\lambda_c = X_{cc}/X_a$ should be independent of temperature. The rotational minima about the O-C_1 bond of the hexyloxy chain were also taken to be 0, $\pm 112°$, while $\angle COC = 126.4°$ was adopted[9.14-9.15].

By modeling the segmental order profile, the interaction parameters X_a and X_{cc} are determined and their tensors are given by Eqs. (3.42)-(3.43). Furthermore, principal elements of the order parameter tensor ($< P_2 >$, $S_{xx} - S_{yy}$) for an 'average' conformer may be obtained[9.16][see Chapter 3]. Using the TZ model(in the limit of $D_r = D_y$) to describe the reorientation of molecules[Chapter 4], the internal motions of aromatic ring deuterons and methylene deuterons were described by Eq. (4.28) and (6.19). respectively.

9.3 Results

Figure 9.3 shows the segmental order parameters $S_{CD}^{(i)}$ versus the temperature for both 6OCB and 6OCB/8OCB mixture. These segmental order parameters for the two samples show similar temperature behaviours. An optimization routine (AMOEBA) was used to minimize the sum squared error f in fitting the splittings

$$f = \sum_i \left(\left| S_{CD}^{(i)} \right| - \left| S_{CD}^{(i)calc} \right| \right)^2 \tag{9.1}$$

where $S_{CD}^{(i)calc}$ is obtained from Eq. (3.27) with Eqs. (3.36)-(3.41) and the sum over i includes C_1 to C_5 and aromatic deuterons (see section 3.4.1). The f values at different temperatures for 6OCB
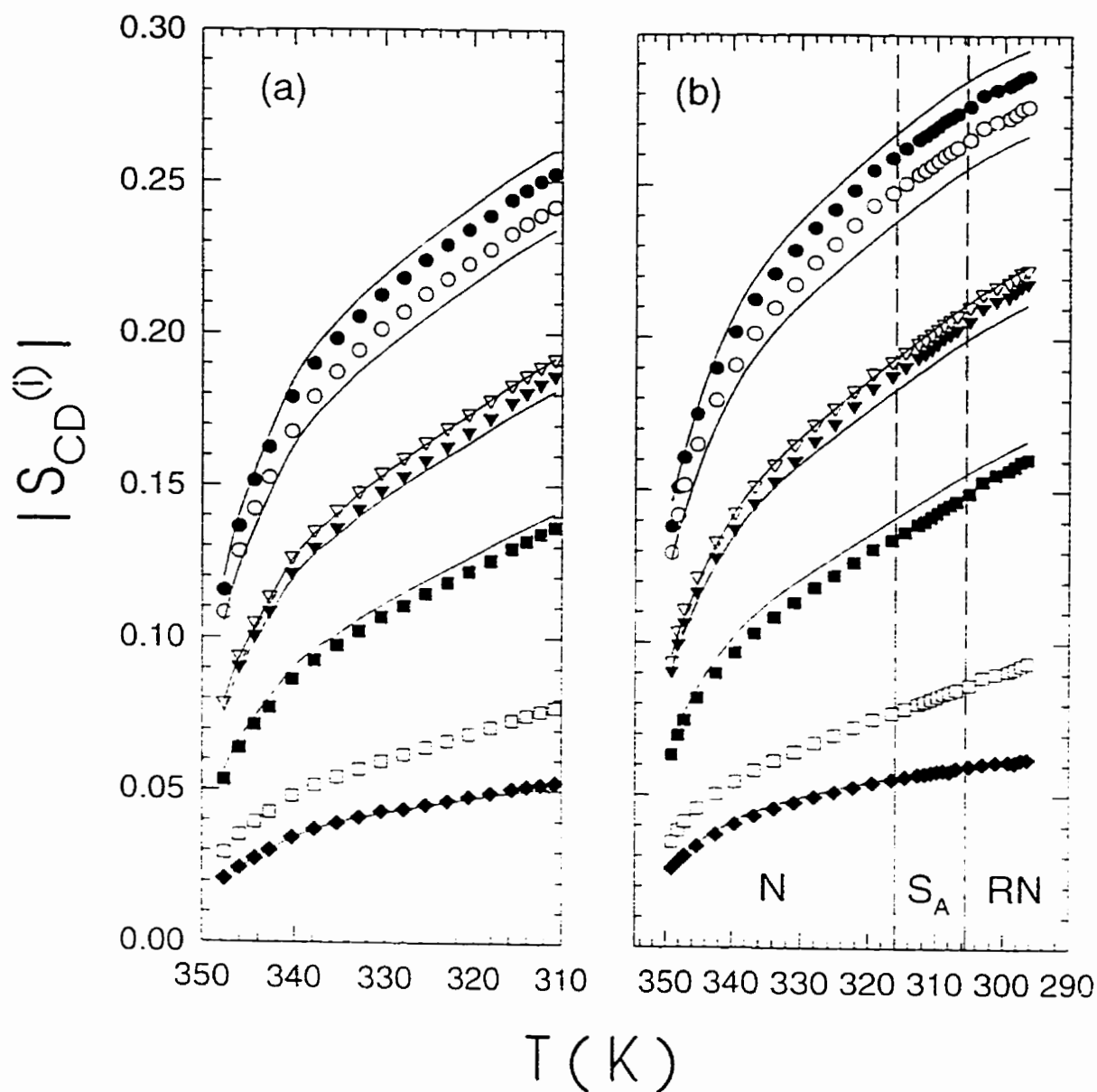
Figure 9.3 Plots of segmental order parameters as a function of temperature in (a) 6OCB and (b) 6OCB/8OCB mixture. The solid diamond denotes the aromatic sites. The solid circle, triangle, and square denote C_1, C_3, and C_5, while the corresponding open symbols denote C_2, C_4, and C_6. The solid curves are the theoretical calculations for C_1 to C_5 and C_R starting from the top. Note that the experimental splittings of C_3 and C_4 are reversed from those predicted by the theory.

Table 9.1. Model parameters derived from the analysis of quadrupolar splittings of 6OCB. The interaction parameter X_a is in kJ/mol; λ_c. a_{20} and a_{22} are dimensionless second rank coefficients.

T(K)	X_a	λ_c	$< P_2 >$	$< S_{xx}\text{-}S_{yy} >$	a_{20}	a_{22}	$10^4 f$
340.3	4.45	0.225	0.491	0.0310	-2.28	-0.347	1.4
337.8	4.73	0.224	0.519	0.0308	-2.44	-0.377	1.7
335.4	4.93	0.221	0.540	0.0304	-2.57	-0.401	2.2
332.9	5.07	0.222	0.556	0.0305	-2.67	-0.426	2.0
328.0	5.31	0.223	0.584	0.0304	-2.86	-0.472	2.2
323.1	5.52	0.223	0.607	0.0300	-3.03	-0.515	2.4
320.6	5.61	0.223	0.618	0.0299	-3.11	-0.537	2.5
315.7	5.78	0.223	0.638	0.0296	-3.28	-0.584	2.7
310.8	5.92	0.224	0.655	0.0293	-3.42	-0.629	2.9

Table 9.2. Model parameters derived from the analysis of quadrupolar splittings of the 6OCB/8OCB mixture. Symbols are same as in Table 9.1.

T(K)	X_a	λ_c	$<P_2>$	$<S_{xx}\text{-}S_{yy}>$	a_{20}	a_{22}	$10^4 f$
342.4	4.90	0.216	0.526	0.0298	-2.48	-0.373	1.9
336.7	5.51	0.213	0.582	0.0287	-2.84	-0.443	2.3
330.9	5.93	0.208	0.620	0.0277	-3.13	-0.503	2.6
325.2	6.26	0.205	0.650	0.0268	-3.38	-0.561	2.9
319.4	6.62	0.201	0.678	0.0257	-3.65	-0.624	3.2
316.5	6.69	0.200	0.686	0.0254	-3.73	-0.645	3.2
312.7	6.82	0.200	0.698	0.0250	-3.86	-0.680	3.4
309.8	6.89	0.200	0.705	0.0248	-3.95	-0.708	3.4
306.9	6.95	0.200	0.712	0.0246	-4.03	-0.736	3.5
303.1	7.07	0.204	0.722	0.0246	-4.15	-0.784	3.6
299.3	6.98	0.204	0.725	0.0248	-4.19	-0.807	3.6
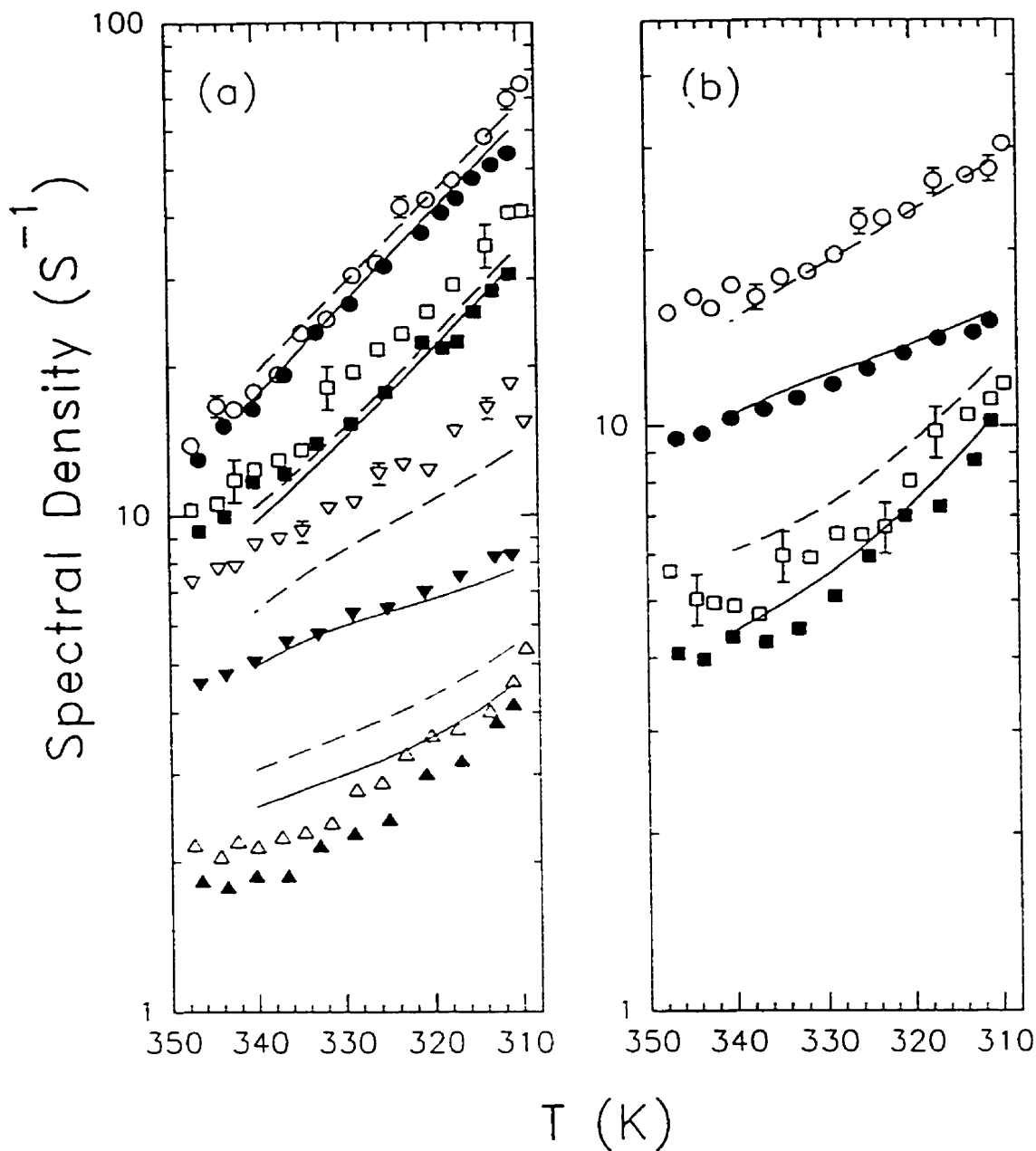
Figure 9.4 Plots of spectral densities vs temperature in 6OCB. Open symbols denote 15.1 MHz data. while solid symbols denote 46 MHz data. (a) circle and square denote $J_1^{(R)}(\omega)$ and $J_2^{(R)}(2\omega)$. while down triangle and up triangle denote $J_1^{(4)}(\omega)$ and $J_2^{(4)}(2\omega)$, respectively: (b) circle and square denote $J_1^{(2)}(\omega)$ and $J_2^{(2)}(2\omega)$:
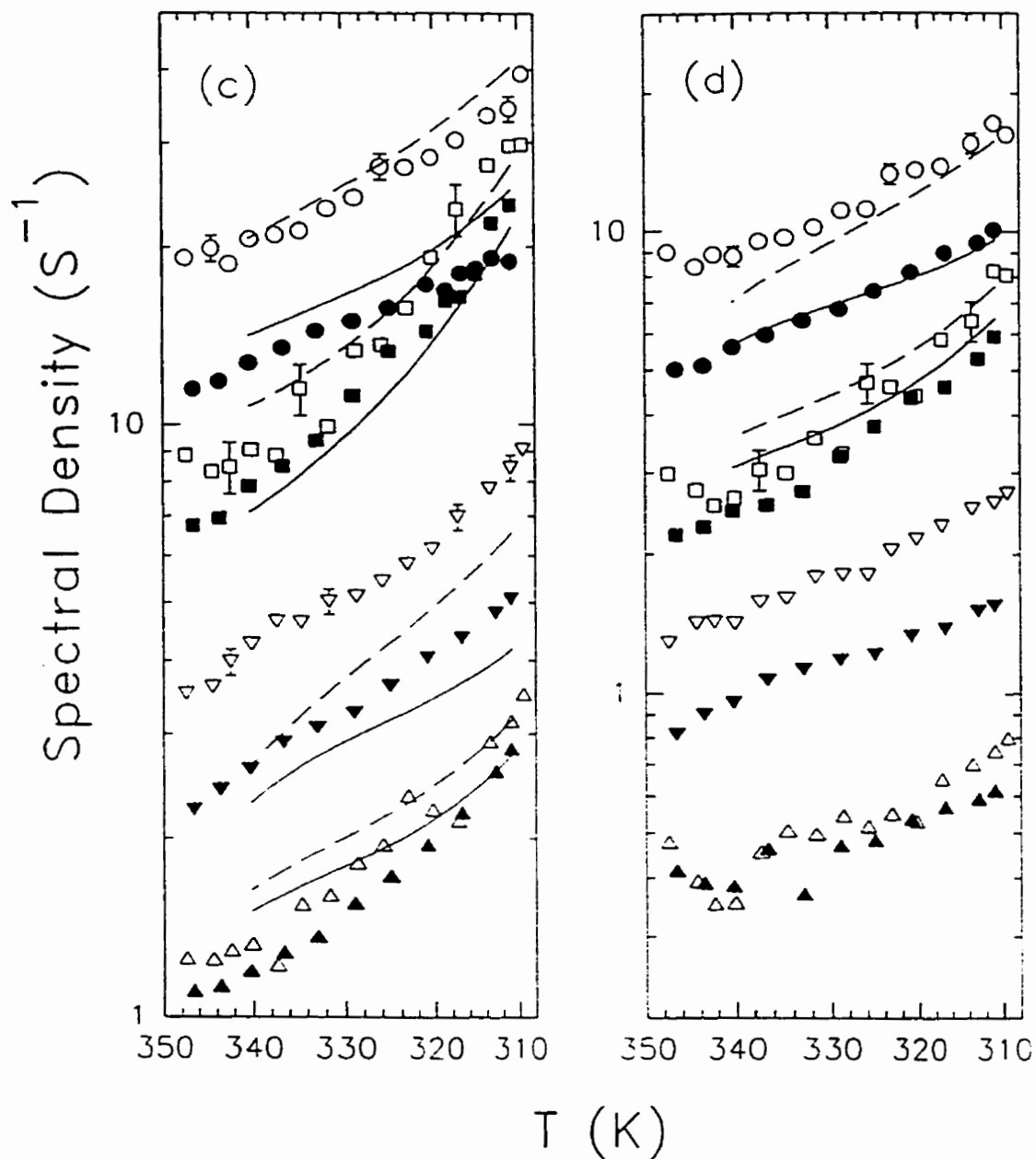
Figure 9.4 (c) circle and square denote $J_1^{(1)}(\omega)$ and $J_2^{(1)}(2\omega)$. while down triangle and up triangle denote $J_1^{(5)}(\omega)$ and $J_2^{(5)}(2\omega)$. respectively: (d) circle and square denote $J_1^{(3)}(\omega)$ and $J_2^{(3)}(2\omega)$. while down triangle and up triangle denote $J_1^{(6)}(\omega)$ and $J_2^{(6)}(2\omega)$. respectively. Dashed and solid curves are calculated spectral densities for 15.1 and 46 MHz. respectively.
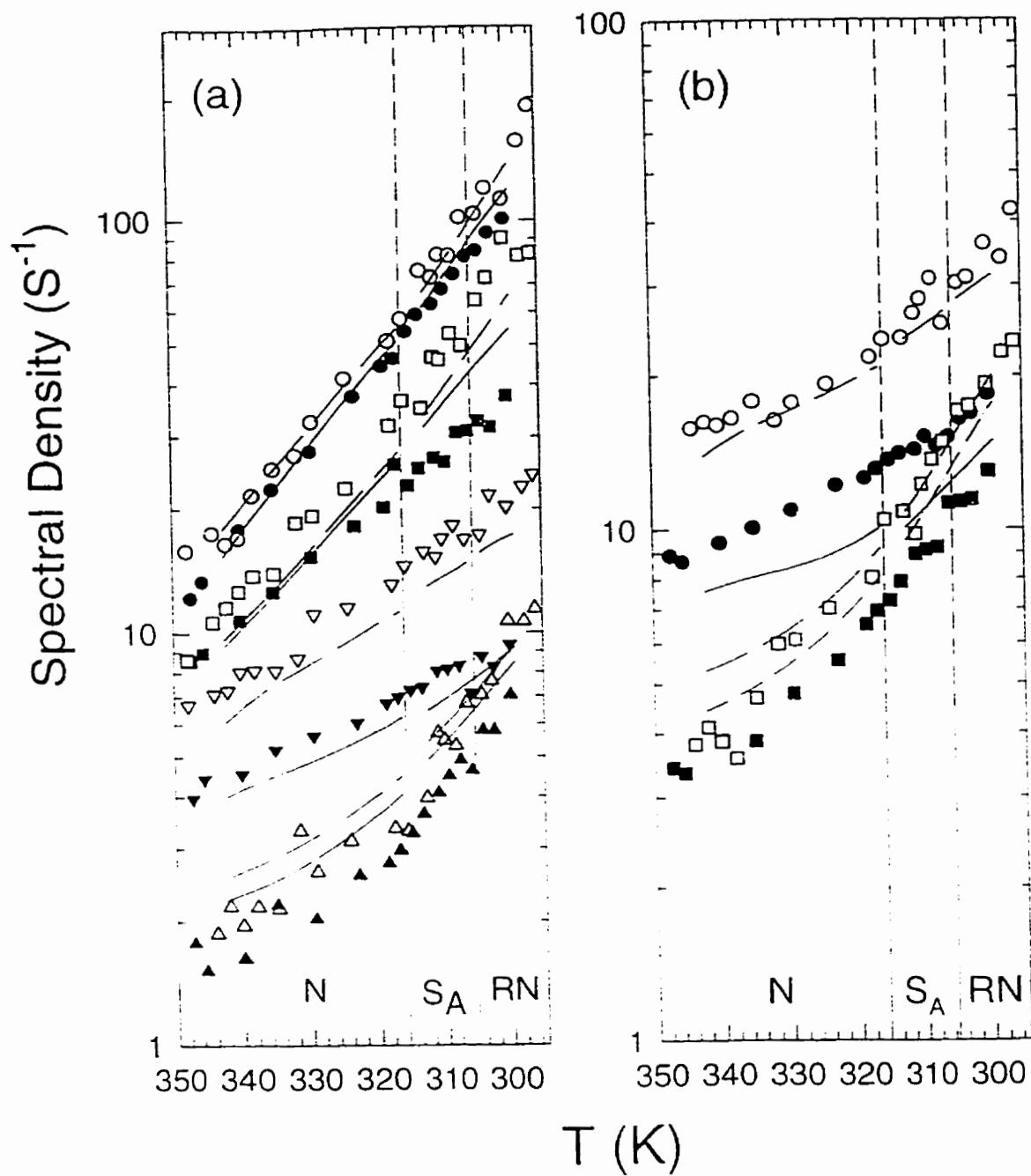
Figure 9.5 Plots of spectral densities vs temperature in 6OCB/8OCB mixture. The legends are the same as in Figure 9.4 except for clarity the dash-dot curves are used instead of solid curves to denote the calculated J_2 for C_1 and C_2. (a) and (b)
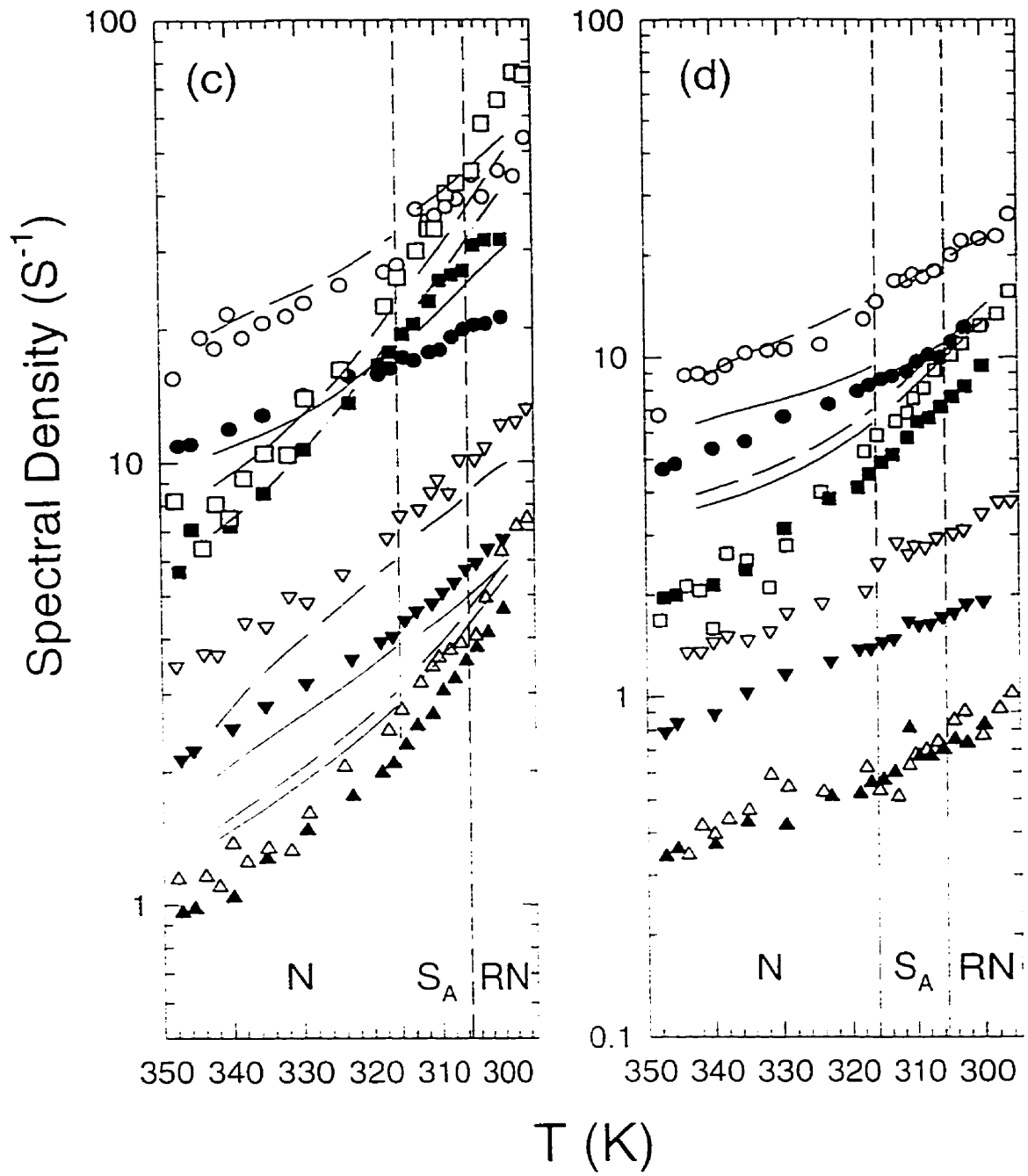
Figure 9.5 (c) and (d)

(Table 9.1) and for 6OCB/8OCB (Table 9.2) are of the order of 10^{-4}. The calculated segmental order parameters are indicated in Fig. 9.3 as solid lines. As observed in the figure, the experimental observation[9.4] of $\Delta\nu_3 < \Delta\nu_4$ cannot be reproduced by the AP method. The previous reports of mean field calculations[9.15, 9.17] for 6OCB, which give the best agreement when the splittings are assumed to decrease sequentially towards the end of the chain, are also inconsistent with the experimental observation of $\Delta\nu_3 < \Delta\nu_4$. Some of the derived parameters X_a, $X_{cc} < P_2 >$, and $(S_{xx} - S_{yy})$ are summarized in Tables 9.1 and 9.2. The a_{20} and a_{22} (also shown in these tables) are determined from the order parameter tensor of an average conformer. These specify the orientational potential used in solving the rotational diffusion equation. Despite the relatively poor fits of the segmental order parameters, the derived orientational potential is found to be rather good in describing the rotational motion of 6OCB molecules.

The spectral densities for 6OCB versus the temperature are given in Fig. 9.4, while those for the 6OCB/8OCB mixture are summarized in Fig. 9.5. It is believed that the motional biaxiality is very small for the 6OCB molecule in both these samples. Therefore, $D_x = D_y = D_-$ is chosen here. Also, we analyze the spectral densities of ring C_R and methylene C_i (i=1-5) deuterons using a global target approach. From individual target analyses (i.e. analyze the relaxation data at each temperature) of 6OCB sample, it was found that the rotational diffusion constants and jump constant k_2 obeyed simple Arrhenius-type relations, giving

$$D_- = D_-^0 \exp[-E_a^{D_-}/RT] \tag{9.2}$$

$$D_{\|} = D_{\|}^0 \exp[-E_a^{D_{\|}}/RT] \tag{9.3}$$

$$D_R = D_R^0 \exp[-E_a^{D_R}/RT] \tag{9.4}$$

$$k_2 = k_2^0 \exp[-E_a^{k_2}/RT] \qquad (9.5)$$

where the pre-exponentials D_-^0, $D_\parallel^0$, D_R^0, and k_2^0, and their corresponding activation energies $E_a^{D_-}$, $E_a^{D_\parallel}$, $E_a^{D_R}$, and $E_a^{k_2}$ were global parameters. For convenience, the diffusion and jump rate pre-exponentials were not used as global parameters. Rather Eqs. (9.2)-(9.5) were rewritten in terms of the activation energies and the diffusion and jump constants D_-', $D_\parallel'$, D_R', k_2' at T_{max}. The T_{max} for the 6OCB sample was set at the highest temperature of 340.3 K used in the global analysis. When the Arrhenius-type relation did not exist for a target parameter, it was still possible to introduce an interpolating relation linking its value at different temperatures. For the 6OCB sample, the temperature dependence of k_1 and k_3 were modeled as

$$k_1 = k_1' + k_1''(T - T_{\mathrm{max}}) + k_1'''(T - T_{\mathrm{max}})^2 \qquad (9.6)$$

$$k_3 = k_3' - k_3''(T - T_{\mathrm{max}}) \qquad (9.7)$$

with k_1', k_1'', k_1''', k_3', k_3'' being the global parameters.

In the 6OCB/8OCB mixture, the target parameters may not vary smoothly across all studied phases. In particular, we found that dynamic behaviours in the high temperature nematic phase differ from those in the smectic A and RN phases. Over the narrow temperature ranges of the smectic A and RN phases, their dynamical behaviours seemed quite similar. Thus, we used two global target routines for the two temperature regions. From individual target analyses, it was found that the rotational diffusion constants and jump constant k_2 still obeyed simple Arrhenius-type relations as described in Eqs. (9.2)-(9.5). The T_{max} was set at 342.4 K for the high temperature nematic phase and 312.7 K for the low temperature region of S_A/RN phases. For the S_A and RN phases of the 6OCB/8OCB sample, the temperature dependence of k_1 and k_3 were modeled the

same way as Eqs. (9.6)-(9.7), whereas for the high temperature nematic phase of the 6OCB/8OCB mixture, it was found that k_1 still obeyed the Arrhenius-type relation and we used

$$k_1 = k_1^0 \exp[-E_a^{k_1}/RT] \tag{9.8}$$

$$k_3 = k_3' + k_3''(T - T_{\max}) + k_3'''(T - T_{\max})^2 \tag{9.9}$$

where the global parameters k_1^0, $E_a^{k_1}$, k_3', k_3'' and k_3''' were optimized. Also, Eq. (9.8) was rewritten in terms of $E_a^{k_1}$ and the jump constant k_1' at $T_{\max} = 342.4$ K.

In each global target routine, the diffusion constants D_-', $D_\|'$, and D_R' as well as the jump constants k_1', k_2', and k_3' at $T_{\max}$ were first estimated from an individual target analysis. Again AMOEBA was used to minimize the sum squared percent error F.

9.4 Discussion

The fitting quality factor Q is defined by:

$$Q = \frac{\sum_k \sum_\omega \sum_i \sum_m \left[J_m^{(i)calc}(m\omega) - J_m^{(i)exp}(m\omega) \right]_k^2}{\sum_k \sum_\omega \sum_i \sum_m \left[J_m^{(i)exp}(m\omega) \right]_k^2} \times 100\% \tag{9.10}$$

where sum over i covers six carbon sites (C_R, C_1-C_5). At each site, there are two J_1 and two J_2 values from the two Larmor frequencies. For the 6OCB sample, we have all together 216 spectral densities from nine chosen temperatures; for the 6OCB/8OCB mixture, we have 144 spectral densities from six chosen temperatures in the nematic phase and 120 spectral densities from five chosen temperatures in the S_A and RN phases. These spectral densities are used to derive 13 global parameters in each global target routine, which occur in Eqs. (9.2)-(9.5) plus either Eqs. (9.6), (9.7) or Eqs. (9.8), (9.9). A global minimization required typically 30 hours C.P.U. time in a Digital

141

Alpha 255 workstation. The rotational diffusion constants are summarized in Fig. 9.6 and the jump rate constants in Fig. 9.7.

It is noted that the rotational diffusion constant D_- is smaller than $D_|$ in our samples. In the 6OCB sample. the D_- value is of the order of 10^7 s^{-1}. whereas in the mixture the D_- is an order of magnitude smaller and independent of temperature at $\sim 2 \times 10^6$ s^{-1} except there is a minor jump at the N-S$_A$ phase transition. Despite the spectral densities in the nematic phases of the two systems are almost identical (Figures 9.4 and 9.5). it was found that the two sets of model parameters could not be interchanged to produce good fits or comparable Q values. This is a bit surprising. and seems to point to the importance of having reliable spectral density data. The larger motional anisotropy $(D_|/D_-)$ could be explained if molecules in the mixture appear to pack closer than in the pure 6OCB sample. As a consequence. molecular tumbling is more hindered in the mixture and now occurs in a time scale of a few microseconds. This low molecular tumbling has recently been observed[9.18] in a liquid crystal. though in a more ordered S_B phase. Now the values of $D_|$ and D_R are more or less comparable in these samples (see Fig. 9.6). It is interesting to note that $D_|$ varies almost smoothly across the two temperature regions in the mixture. By comparing the activation energies and pre-exponentials of $D_|$ in both the nematic phases of 6OCB and 6OCB/8OCB samples. they are equal to each other indicating the spinning motion of a 6OCB molecule cannot distinguish whether the local environment is composed of 6OCB or 8OCB molecules. The disruption of D_-. D_R. and jump rates across the N-S$_A$ phase transition in the mixture must be taken with cautions. since the target parameters may be sensitive to the manner of fitting our experimental data as well as to their experimental uncertainties. For instance, the temperature behaviours of k_1 and k_2 in the 6OCB sample can be switched without seriously increasing the Q values. Now the jump constant
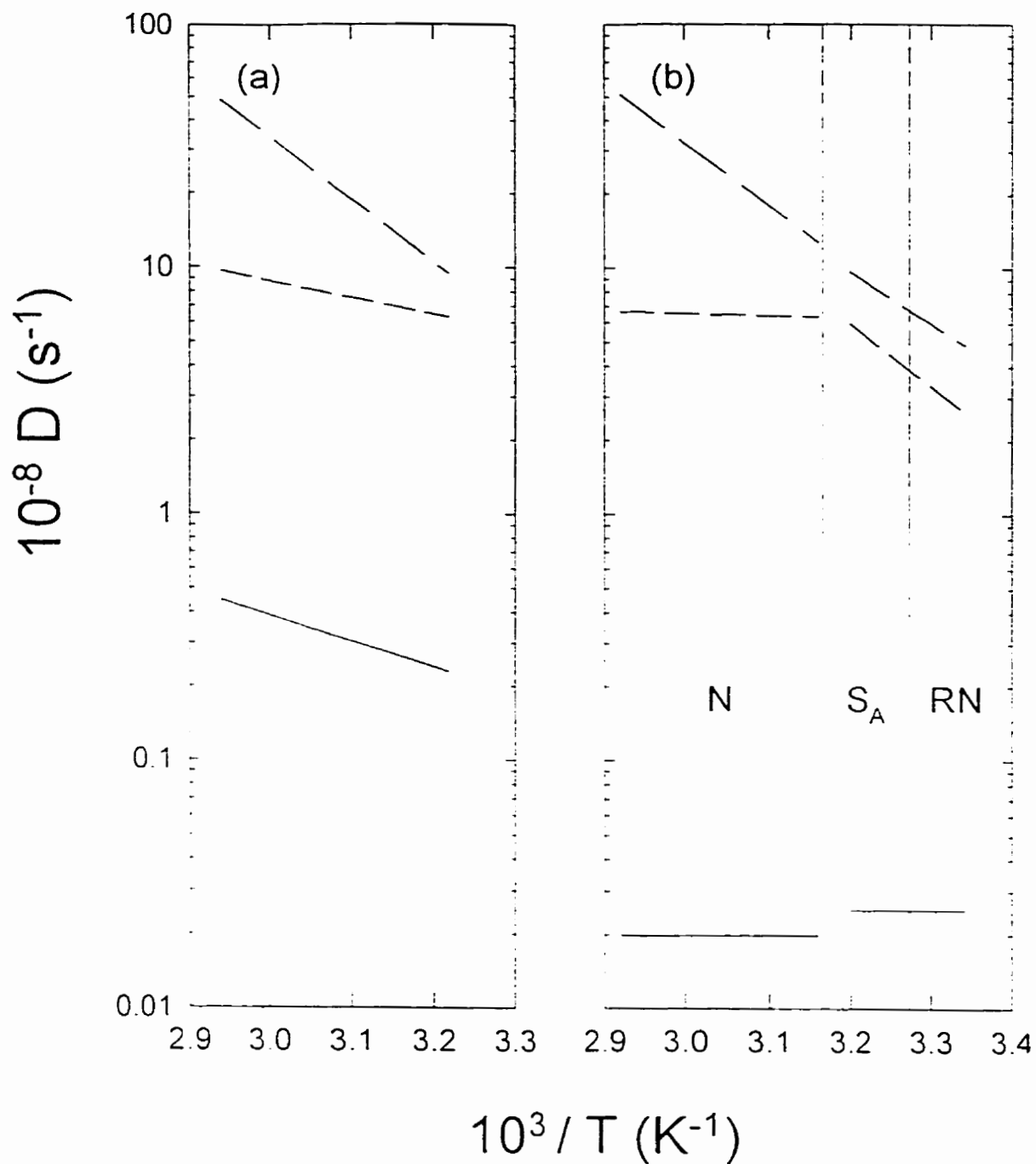
Figure 9.6 Plots of rotational diffusion constants as a function of the reciprocal temperature in (a) 6OCB and (b) 6OCB/8OCB mixture. Solid, long-dashed and dashed lines denote $D_\perp$, $D_\parallel$ and D_R, respectively.
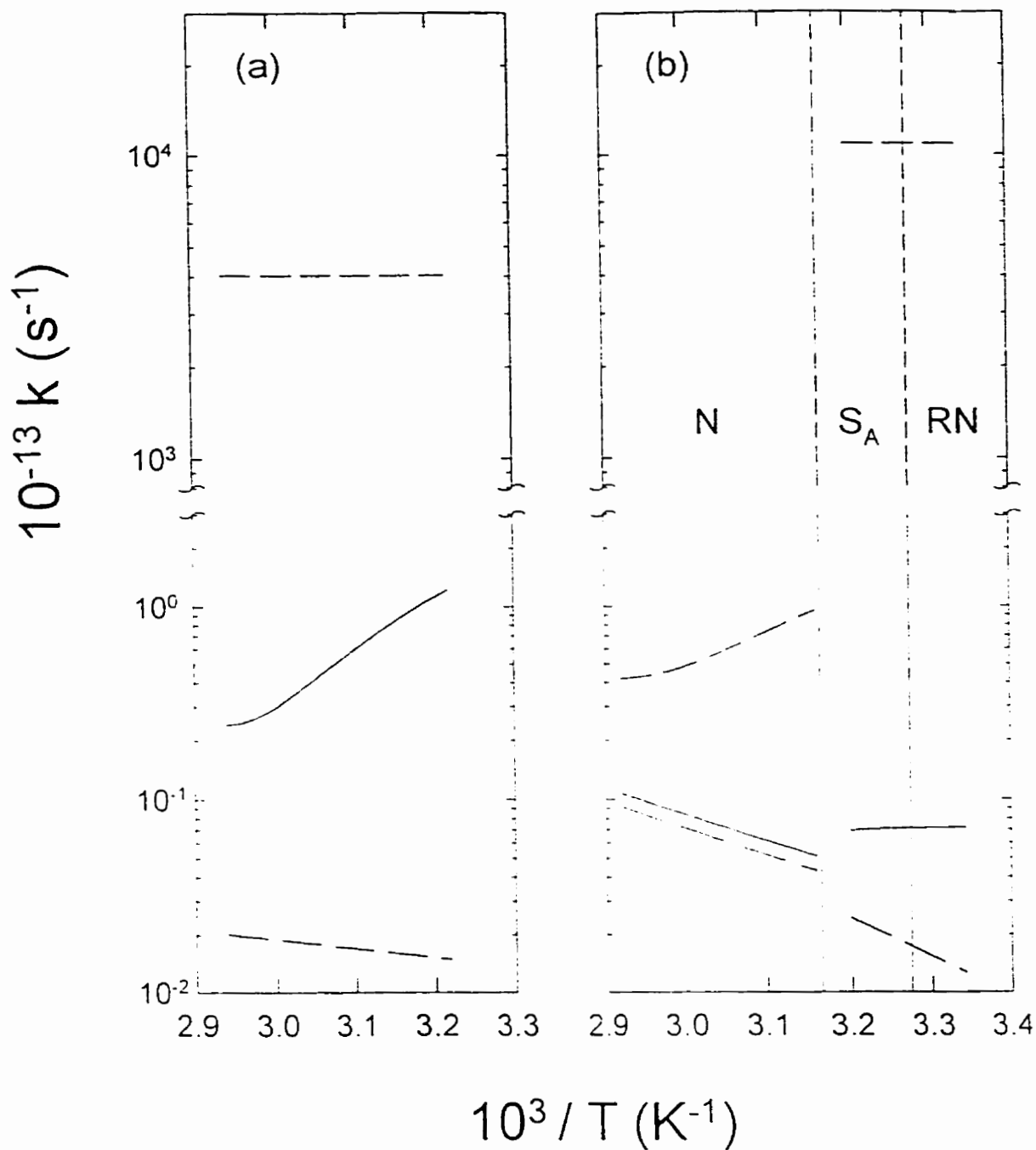
Figure 9.7 Plots of jump rate constants as a function of the reciprocal temperature in (a) 6OCB and (b) 6OCB/8OCB mixture. Solid. long-dashed and dashed lines denote k_1. k_2 and k_3. respectively.

k_3 (the so called crank-shaft motion inside the chain) is independent of the temperature in the 6OCB sample ($k'_3 = 4.0 \times 10^{16}$ s^{-1}) and in the S$_A$/RN region (1.1×10^{17} s^{-1}) of the 6OCB/8OCB mixture, while it has much lower values but increases slightly upon decreasing temperature (see Fig. 9.7(b)) within the high temperature nematic phase of the mixture. Given the k_3 value for the 6OCB sample being comparable to that in the S$_A$/RN region of the mixture, and the k_3 value being much smaller in its high temperature nematic phase, the observations are qualitatively consistent with the argument[9.10] that the dimer structure in the 6OCB/8OCB mixture becomes less frustrated and is progressively "loose" upon decreasing the temperature. In the high temperature nematic phase of the mixture, the three-bond motion is restricted due to the "close" dimer structure, while in the RN phase k_3 behaves like that in the nematic phase of pure 6OCB. In estimating the error limits for k_3, it was found that while any larger k'_3 value does not affect the fits in the 6OCB sample and in the low temperature phases of the mixture, its lower limit is 1.0×10^{13} s^{-1} for the 6OCB sample and is 1.3×10^{12} s^{-1} in the S$_A$/RN region of the mixture. In the nematic phase of the mixture, k'_3 is equal to 4.2×10^{12} s^{-1}. Its error limits (at T_{max}) are 8.0×10^{13} s^{-1} and 1.6×10^{12} s^{-1}. In Table 9.3, the activation energies and pre-exponentials in Eqs. (9.2)-(9.5) and (9.8), and their corresponding error limits, are presented. The error limit for a particular global parameter was estimated by varying the one under consideration while keeping all other global parameters identical to those for the minimum F, to give an approximate doubling in the F value. Finally, the calculated spectral densities for 6OCB (Q=0.9%), for 6OCB/8OCB mixture (Q=0.9% in nematic phase and Q=2.0% in the S$_A$/RN region) are indicated by curves in Figures 9.4 and 9.5. By comparing the fitted results in Fig. 9.4 to the earlier analysis of 6OCB[9.1], the Q value is better because of the improved geometry. Although all the Q values are acceptable, there exist some systematic deviations between the calculated and experimental spectral densities at some carbon

Table 9.3. The pre-exponentials (in s^{-1}) and activation energies (in kJ/mol) derived from the analysis of spectral densities of the 6OCB and 6OCB/8OCB samples. The arrows for k_2^0 and k_1^0 denote upper and lower error limits.

	Pure 6OCB	6OCB/8OCB(N)	6OCB/8OCB(S_A/RN)
k_2^0	4.8×10^{12}	1.0×10^{16}	7.2×10^{17}
$k_2^0 \uparrow$	1.5×10^{13}	1.6×10^{17}	4.2×10^{18}
$k_2^0 \downarrow$	1.8×10^{12}	5.0×10^{15}	2.3×10^{17}
k_1^0	/	9.6×10^{15}	/
$k_1^0 \uparrow$	/	7.8×10^{17}	/
$k_1^0 \downarrow$	/	5.2×10^{15}	/
D_-^0	$(5 \pm 2) \times 10^{10}$	/	/
$D_\|^0$	$(1.5 \pm 0.3) \times 10^{17}$	$(1.3 \pm 0.3) \times 10^{17}$	$(5 \pm 1) \times 10^{15}$
D_R^0	$(9 \pm 3) \times 10^{10}$	$(1.1 \pm 0.4) \times 10^9$	$(7 \pm 4) \times 10^{16}$
$E_a^{k_2}$	9 ± 3	27 ± 8	39 ± 5
$E_a^{k_1}$	/	26 ± 7	/
E_a^{D-}	20 ± 1	/	/
$E_a^{D_\|}$	48.8 ± 0.5	48.5 ± 0.5	40.1 ± 0.6
$E_a^{D_R}$	12.7 ± 0.9	1.5 ± 1.5	48 ± 2

146

sites (e.g. C_5 in Fig. 9.4 and C_2 in Fig. 9.5). As indicated by the Q value, the fits are relatively poor in the S_A and RN phases of the 6OCB/8OCB mixture. However, the observed $J_2/J_1 > 1$ for C_1 deuterons at 46 MHz is qualitatively reproduced by the model, yet the predicted $J_2/J_1 > 1$ for C_2 at this frequency is not observed. These discrepancies are understandable given the many assumptions and limitations of the models used in the present study. The calculated spectral densities are by and large continuous across the N-S_A phase transition in the mixture in qualitative agreement with the experiment(Fig. 9.5), despite two separate global target routines were used in the fits.

9.5 Summary

A consistent interpretation of both the quadrupolar splittings and the spin-lattice relaxation data measured in the 6OCB and 6OCB/8OCB samples have been given. From modeling the splittings using the AP method, the orienting potential needed to describe the reorientational dynamics of 6OCB molecules in these samples is obtained. It is clear that the tumbling motion of a 6OCB molecule is much slower than its spinning motion in both samples, and in comparison with the 6OCB sample, it is strongly hindered in the 6OCB/8OCB mixture. When the value of D_- becomes small, the fitting tends to be less sensitive to its value. This may be the reason why it shows no temperature dependence in the mixture. The decoupled model provides a simple description of correlated internal bond rotations in the chain. The jump rate k_3 in the S_A/RN region of the mixture is close to that in the nematic phase of pure 6OCB, which may indicate that the dimer structure of 6OCB/8OCB mixture is "loose" in the low temperature phases, i.e. similar to the "loose" dimer or monomer structure in the pure 6OCB sample. But some other parameters are, at least, not too much in favor of this point, e.g., the small value of D_- in S_A/RN region.

Finally. it is pointed out that our relaxation data in the pure 6OCB sample could not be fitted better by including director fluctuations. One possible explanation is that the high cutoff frequency for director fluctuations is lower or comparable to the Larmor frequencies used for our sample[Chapter 8]. The inclusion of director fluctuations in the RN phase may improve the Q value. but this requires more adjustable parameters. In conclusion. despite many simplifying assumptions used in the decoupled model. the quality of fits to the available spectral densities is more than satisfactory over the studied temperatures of both systems. and the degree of molecular packing in different phase structures may be qualitatively inferred from some of the derived model parameters. The present study further demonstrates the usefulness of the TZ model (or Nordio's model) in describing the overall motion of liquid crystal molecules.

References

9.1 R. Y. Dong, X. Shen, and G. M. Richards. *Phys. Rev. E.* **52**. 1753 (1995).

9.2 R. Y. Dong, G. Ravindranath. *Liq. Cryst.*. **17**. 47 (1994); R. Y. Dong, G. W. O'Bannon. *Mol. Cryst. Liq. Cryst.*. **209**. 139 (1991).

9.3 P. E. Cladis. *Mol. Cryst. Liq. Cryst.*. **67**. 177 (1981).

9.4 J. W. Emsley, E. K. Foord, P. J. F. Gandy, and D. L. Turner. *Liq. Cryst.*, **17**. 303 (1994).

9.5 P. E. Cladis, R. K. Bogardus, and D. Aadsen. *Phys. Rev. A.* **18**. 2292 (1978).

9.6 D. Guillon and A. Skoulios. *J. Phys.*, **45**. 607 (1984).

9.7 L. Longa and W. H. de Jeu. *Phys. Rev. A.* **28**. 2380 (1983).

9.8 N. V. Madhusudana and J. Rajan. *Liq. cryst.*. **7**. 31 (1990).

9.9 J. O. Indekeu and A. N. Berker. *J. Phys.*, **49**. 353 (1988).

9.10 A. Ferrarini, G. R. Luckhurst, P. L. Nordio, and E. Spolaore. *Mol. Phys.*. **89**. 1087 (1996).

9.11 J. W. Emsley, G. Celebre, G. De Luca, M. Longeri, and F. Lucchesini, *Liq. Cryst.*. **16**. 1037 (1994).

9.12 P. J. Flory. *Statistical Mechanics of Chain Molecules* (Wiley, New York, 1969).

9.13 J. W. Emsley, G. R. Luckhurst, and C. P. Stockley, *Proc. R. Soc.* London. Ser. A **381**. 117 (1982).

9.14 C. J. R. Counsell. Ph.D. thesis. Southampton (1983).

9.15 C. J. R. Counsell, J. W. Emsley, G. R. Luckhurst, H. S. Sachdev, Mol. Phys. 63, 33 (1988).

9.16 R. Y. Dong, *Nuclear Magnetic Resonance of Liquid Crystals*, second edition (Springer-Verlag, N.Y., 1997).

9.17 D. J. Photinos, E. T. Samulski, and H. Toriumi, *J. Chem. Phys.*, **94**, 2758 (1991).

9.18 C. A. Veracini, private communication.

Chapter 10

Orientational Ordering and Dynamics in the Columnar Phase of a Discotic Liquid Crystal-HAT6

10.1 Introduction

The novel charge transport properties of the columnar phases[10.1] formed by disc-like molecules such as the hexakis(alkyloxy)triphenylenes (HATn) are potentially exploitable in applications ranging from sensing devices to high-resolution xerography[10.2]. These disc-like molecules are stacked, with only short-range positional order, into columns which are arranged on a two-dimensional lattice, typically hexagonal (Figure 1.5). HATn molecules have been studied using proton and deuteron NMR by Luz and coworkers[10.3-10.6] more than 10 years ago. Nordio model[10.7] was used to explain[10.8] the spectral densities of aromatic deuterons in HAT6, and some rotational diffusion constants for the HAT6 molecule were derived. The quadrupolar splittings of the chain

deuterons were modeled[10.9] using the additive potential (AP) method. This earlier attempt for

the homologous series HATn unfortunately contained numerical errors and the good fits were for-

tuitous. Also an interpretation of spectral densities from the chain deuterons[10.6] has not been

attempted. In the present study, there are two deuterated HAT6 samples, one is ring deuterated

and the other is chain deuterated. The motivations are to investigate the dynamics of these discotic

liquid crystal samples and to test Dong's decoupled model, for the first time, in flexible disk-like

molecules. The discotic-isotropic transition temperature T_c of samples was determined by means

of NMR signals. The chain-deuterated sample exhibited a $T_c = 99.4°$ C, while the ring-deuterated

sample a $T_c = 100.4°$ C. When comparing the NMR data of these samples, we scaled the tempera-

tures to give a common T_c of 99.9°C. The HAT6 molecule is schematically shown in Figure 1.5. and

the peak assignments for the chain-deuterated sample are shown on the representative spectrum in

Figure 10.1 with the peak labels denote the carbon sites (6 refers to the methyl deuterons).
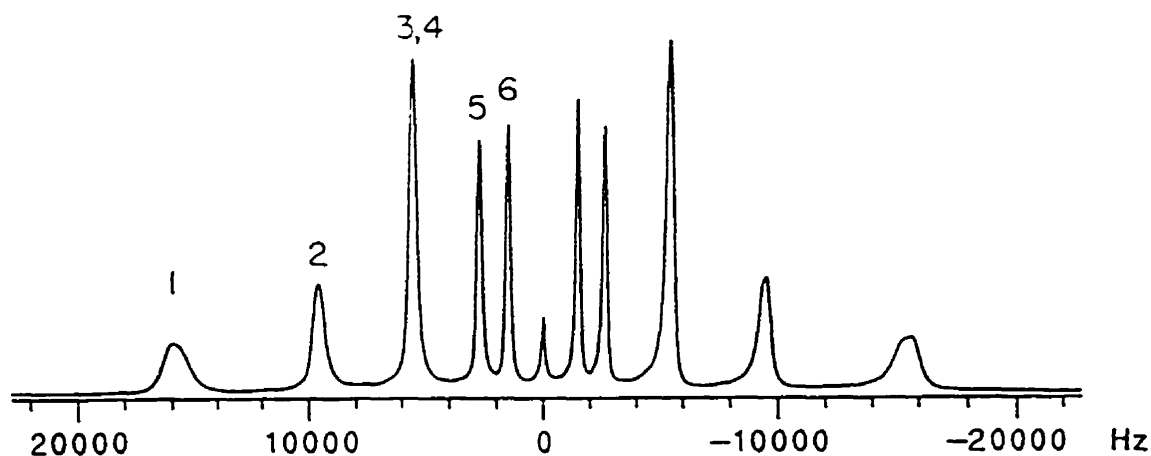
Figure 10.1 A typical deuteron NMR spectrum of chain-deuterated HAT6.

We measured the quadrupolar splittings and the spin-lattice relaxation times T_{1Q} and T_{1Z} of the methylene and ring deuterons at two different Larmor frequencies as a function of temperature in the columnar phase of HAT6 samples. The additive potential method is used to model the quadrupolar splittings, from which the potential of mean torque is parameterized, and the order parameter tensor for an 'average' conformer is determined. The small-step rotational diffusion model is used to find the rotational diffusion constants $D_{\parallel}$ and $D_{\perp}$ for an 'average' conformer is determined. The small-step rotational diffusion model is used to find the rotational diffusion constants $D_{\parallel}$ and $D_{\perp}$ for the spinning and tumbling motions of the molecular core. It is found that $D_{\perp}$ is slightly larger than $D_{\parallel}$ in contrast with the findings in calamitic liquid crystals. The decoupled model[10.10] for correlated internal rotations in the end chains is used for the first time in a discotic liquid crystal.

10.2 Analysis

Using the method described in Chapter 3, the quadrupolar splittings are used to obtain the order parameters $< P_2 >$ and $< S_{xx} - S_{yy} >$ for an 'average' conformer. These in turn determine at each temperature the orienting potential (a_{20}, a_{22})[see Chapter 4] needed for solving the rotational diffusion equation[10.11]. The decoupled model is used to deal with the dynamics of internal bond rotations[see Chapter 6]. A realistic geometry is used for HAT6 to generate all possible conformations in one of the chains using the Flory model[10.12]. Since the O-C$_1$ bond is taken[10.5] to be on the plane of the aromatic core, there are 243 conformations in the chain. The transition rate matrix **R**, which describes conformational changes in the chain, is a 243×243 matrix and contains jump constants[10.11] k_1, k_2 and k_3 for the one-, two- and three-bond motions in the chain[see Chapter 6]. A global target approach is used to analyze all the spectral density data at different temperatures and frequencies in the same fitting procedure, since this has been found to give reliable target model parameters in calamitic liquid crystals.[see Chapters 8-9]

Since HAT6 has $\triangle_\chi < 0$. the columnar axes (directors) are aligned perpendicular to the magnetic field. The measured T_{1Z} and T_{1Q} with the director at $90°$ with the field direction are

$$T_{1Q}^{-1} = 3J_1(\omega. 90°)$$

$$T_{1Z}^{-1} = J_1(\omega. 90°) + 4J_2(2\omega. 90°) \tag{10.1}$$

which give $J_1(\omega. 90°)$ and $J_2(2\omega. 90°)$. These can be calculated in terms of $J_m(m\omega. 0°) \equiv J_m(m\omega)(m = 0. 1. 2)$ as follows[10.13]:

$$J_1^{(i)calc}(\omega. 90°) = \frac{1}{2} \left[J_1^{(i)}(\omega) + J_2^{(i)}(\omega) \right] \tag{10.2}$$

$$J_2^{(i)calc}(2\omega. 90°) = \frac{3}{8} J_0^{(i)}(2\omega) + \frac{1}{2} J_1^{(i)}(2\omega) + \frac{5}{4} J_2^{(i)}(2\omega) \tag{10.3}$$

Substituting Eqs. (4.23) and (6.18) into the above equations, the measured spectral densities in our experiments can be calculated. As seen in Figure 10.1. the doublet splittings from C_3 and C_1 sites are not resolved. Thus the spin-lattice relaxation times at these sites can not be measured separately.

10.3 Results and Discussion

Figure 10.2 shows the experimental $S_{CD}^{(i)}$ versus the temperature. The temperature dependences of the measured relaxation rates T_{1Z}^{-1} and T_{1Q}^{-1} are summarized in Figures 10.3 and 10.4. The relaxation rates measured at 46 MHz are similar to those reported in the literature[10.6]. except our values for the aromatic deuterons are slightly lower and the values for the C_1 deuterons show slightly different temperature behaviours. In fitting the segmental order profiles of the alkyloxy chain. the $O - C$ bond is taken to be identical to $C - C$ bond. The COC angle[10.14-10.15] is set at $126.4°$. and the different internal energies $E'_{tg}(COCC)$ and $E'_{g=g\pm}(COCCC)$ are used due to the presence of the oxygen and the larger COC angle. We had inputted various values of E_{tg}. E'_{tg}. $E_{g=g\pm}$. and $E'_{g=g\pm}$
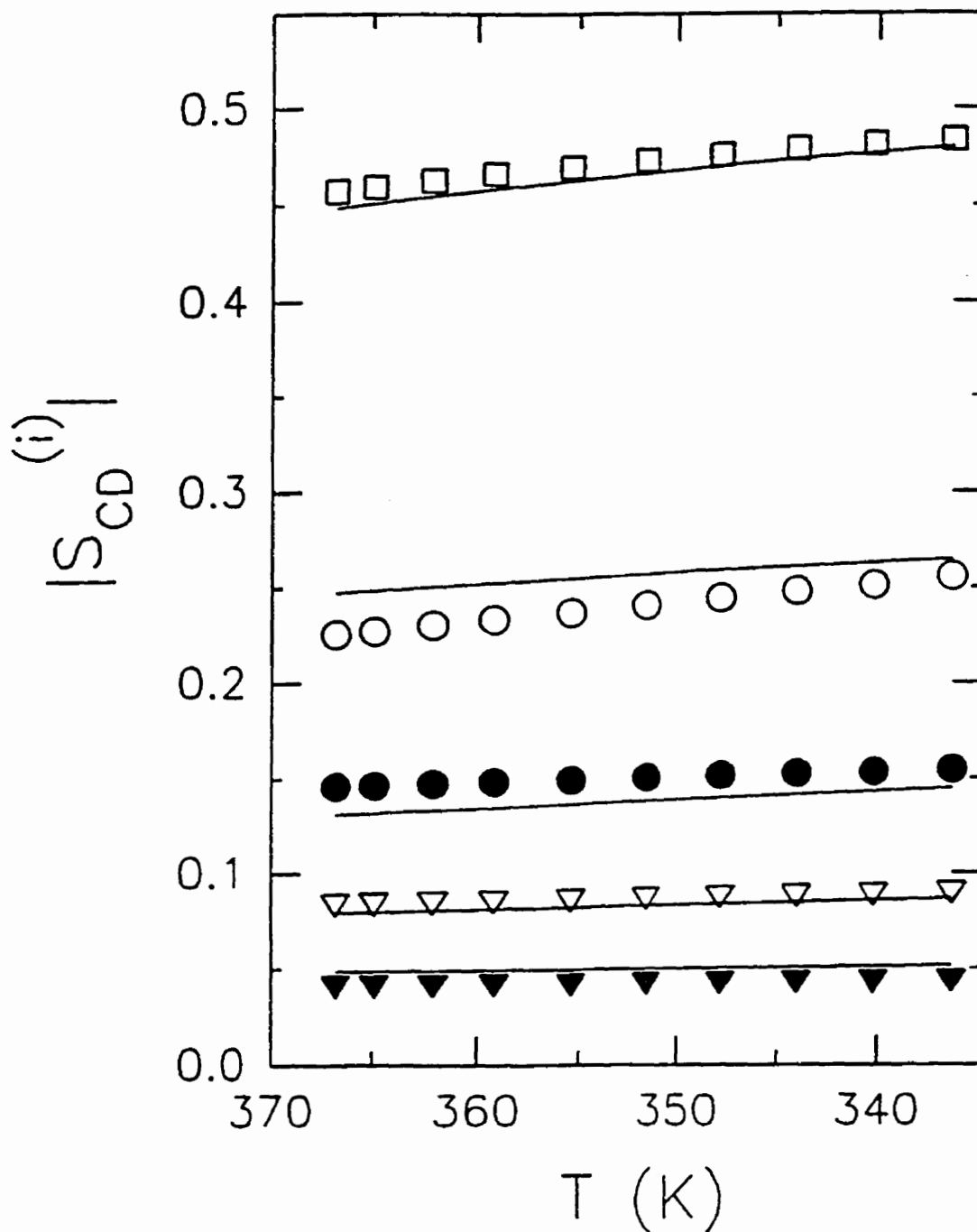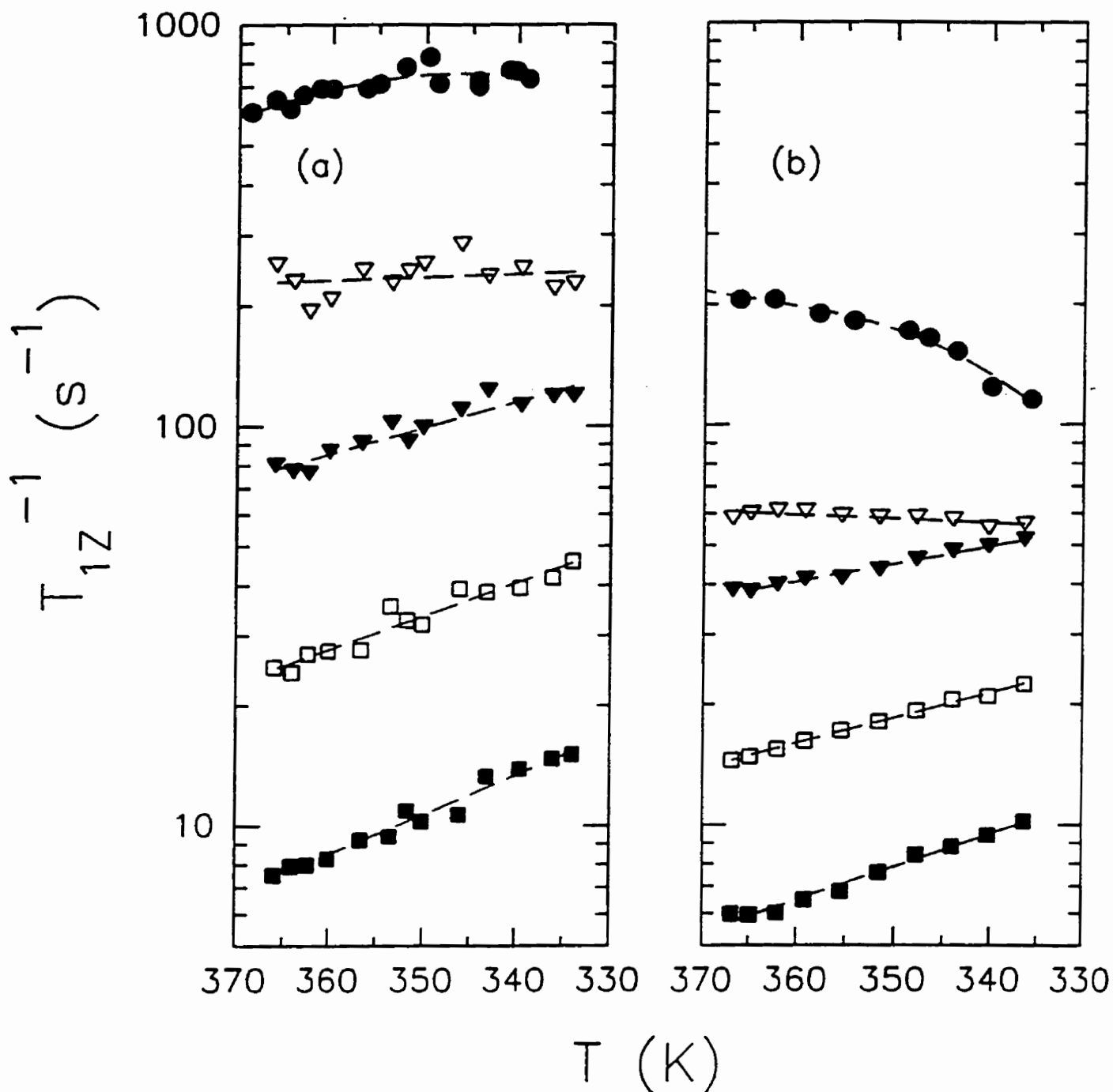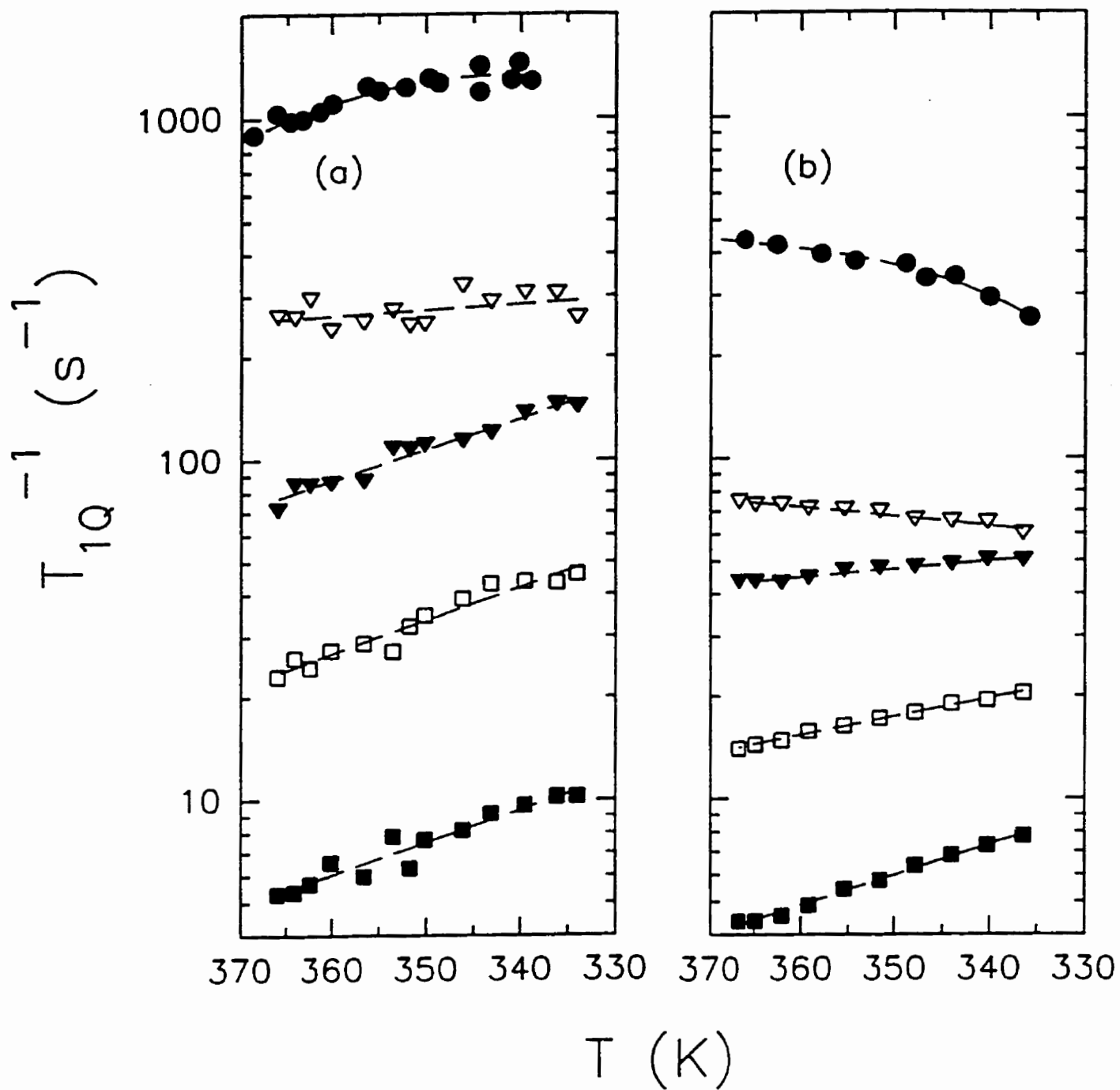
Figure 10.2 Plots of segmental order parameters as a function of temperature in the columnar phase of HAT6. $\square$ denotes the aromatic sites, open and closed $\bigcirc$s denote C_1 and C_2, respectively, while open and closed $\triangledown$s denote C_{3-4} and C_5, respectively. The solid curves are the theorectical predictions using the additive potential method.

Figure 10.3 Plot of experimental Zeeman spin-lattice relaxation rates versus the temperature in the columnar phase of HAT6. Figure (a) and (b) are for data at 15.1 and 46 MHz, respectively. Circle denotes the aromatic sites, open and closed ∇s denote C_1 and C_2, respectively, while open and closed $\square$s denote C_{3-4} and C_5, respectively. The dashed lines are drawn to aid the eyes.

Figure 10.4 Plot of experimental quadrupolar spin-lattice relaxation rates versus the temperature in the columnar phase of HAT6. Figure (a) and (b) are for data at 15.1 and 46 MHz, respectively. ○ denotes the aromatic sites, open and closed ▽s denote C_1 and C_2, respectively, while open and closed □s denote C_{3-4} and C_5, respectively. The dashed lines are drawn to aid the eyes.

and found that the calculated $\Delta \nu_3$ and $\Delta \nu_4$ were different and the best results were obtained by using $E_{tg} = 3.7$ kJ/mol. $E'_{tg} = 1.9$ kJ/mol. and $E_{g\pm g\mp} = E'_{g\pm g\mp} = 10$ kJ/mol. It is not clear at the present time why E'_{tg} is smaller than E_{tg} for HAT6. To model the splitting profiles. we used Eq. (3.33) and Eqs. (3.36)-(3.41) to evaluate $\Delta \nu_i$ and $S_{CD}^{(i)}$ [Eqs.(3.26) and (3.27)]. In these discotic samples. the interaction tensors for the disk-shaped core and rodlike $C - C$ segment are expressed by Eq. (3.50) and Eq. (3.51). respectively. The total interaction tensor for each conformer is obtained by Eqs. (3.52) and (3.53). The optimization routine (AMOEBA) was used to minimize the sum squared error f in fitting the splittings

$$ f = \sum_i (|S_{CD}^{(i)}| - |S_{CD}^{(i),calc}|)^2 \tag{10.4} $$

where the sum over i includes C_1 to C_5 and aromatic deuterons(see section 3.4.2). The f values are of the order of 10^{-3} (see Table 10.1). The calculated segmental order parameters are indicated in Figure 10.2 as solid lines. Note that $\Delta \nu_3$ and $\Delta \nu_4$ were averaged for comparison with the experimental values. We summarize in Table 10.1 some of the derived parameters X_a. X_{cc}. $< P_2 >$. $< S_{xx} - S_{yy} >$. a_{20} and a_{22}. As seen in Table 10.1. $< S_{xx} - S_{yy} >$ is vanishingly small indicating that the HAT6 molecule is essentially a uniaxial molecule.

From the results of Figures 10.3-10.4 and Eq. (10.1). the spectral densities of the aromatic and aliphatic deuterons could be determined. These are summarized in Figures 10.5 and 10.6. To show the site dependence of spectral densities, we plot them in Figure 10.7 for two different temperatures. The $J_1(\omega, 90°)$ and $J_2(2\omega. 90°)$ are in general largest at the aromatic site ($i = 0$) and decrease monotonically along the chain to the methyl group. At 336.4 K and 46 MHz. $J_2(2\omega. 90°)$ of C_0 is slightly less than that of C_1. We model the spectral densities by using Eqs. (4.27). (6.19) and (10.1-

158

10.3). In particular, we take advantage of the fact that the target parameters of the model vary smoothly with temperature by simultaneously analyzing data at all temperatures. From individual target analyses (i.e. analyze the data at each temperature), we found that the rotational diffusion constants and the jump constant k_2 obey simple Arrhenius-type relations, giving

Table 10.1: Model parameters derived from the analysis of quadrupolar splittings at different temperatures in the columnar phase of HAT6. The interaction parameters X_a and X_{cc} are in units of kJ/mol. a_{20}, a_{22} are dimensionless second rank coefficients in the orienting potential which is used in the rotational diffusion equation.

T(K)	X_a	X_{cc}	$< P_2 >$	$< S_{xx} - S_{yy} >$	a_{20}	$10^2 a_{22}$	$10^3 f$
364.9	17.3	0.145	0.848	0.00101	-7.0	-10.5	1.5
362.1	17.9	0.136	0.855	0.00087	-7.3	-10.0	1.5
359.2	18.5	0.124	0.862	0.00073	-7.6	-9.3	1.4
355.4	19.4	0.111	0.869	0.00059	-8.1	-8.4	1.4
351.6	20.4	0.098	0.878	0.00046	-8.6	-7.5	1.3
347.8	21.2	0.085	0.884	0.00037	-9.0	-6.6	1.3
344.0	22.2	0.072	0.890	0.00028	-9.5	-5.7	1.2
340.2	23.1	0.058	0.896	0.00021	-10.0	-4.7	1.2
336.4	24.1	0.050	0.902	0.00016	-10.6	-4.1	1.1
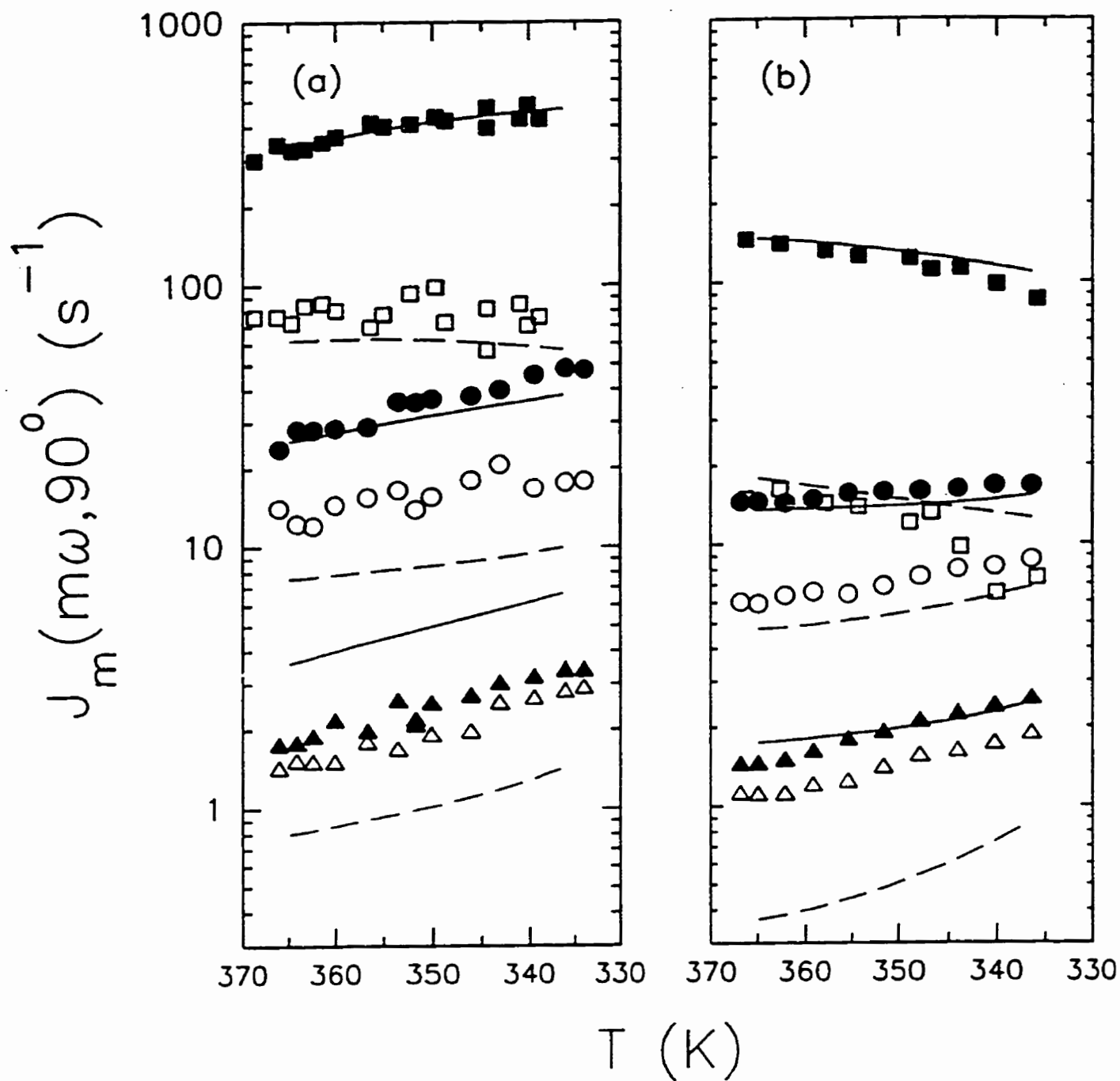
Figure 10.5 Plots of experimental (symbols) and calculated (lines) spectral densities of HAT6. Figure (a) and (b) are for data obtained at 15.1 and 46 MHz. The open symbols denote $J_1(\omega_0, 90°)$, while the closed symbols denote $J_2(2\omega_0, 90°)$. The $\triangledown$s represent data for C_5, while the $\square$s and $\bigcirc$s represent data at the aromatic sites and C_2, respectively.
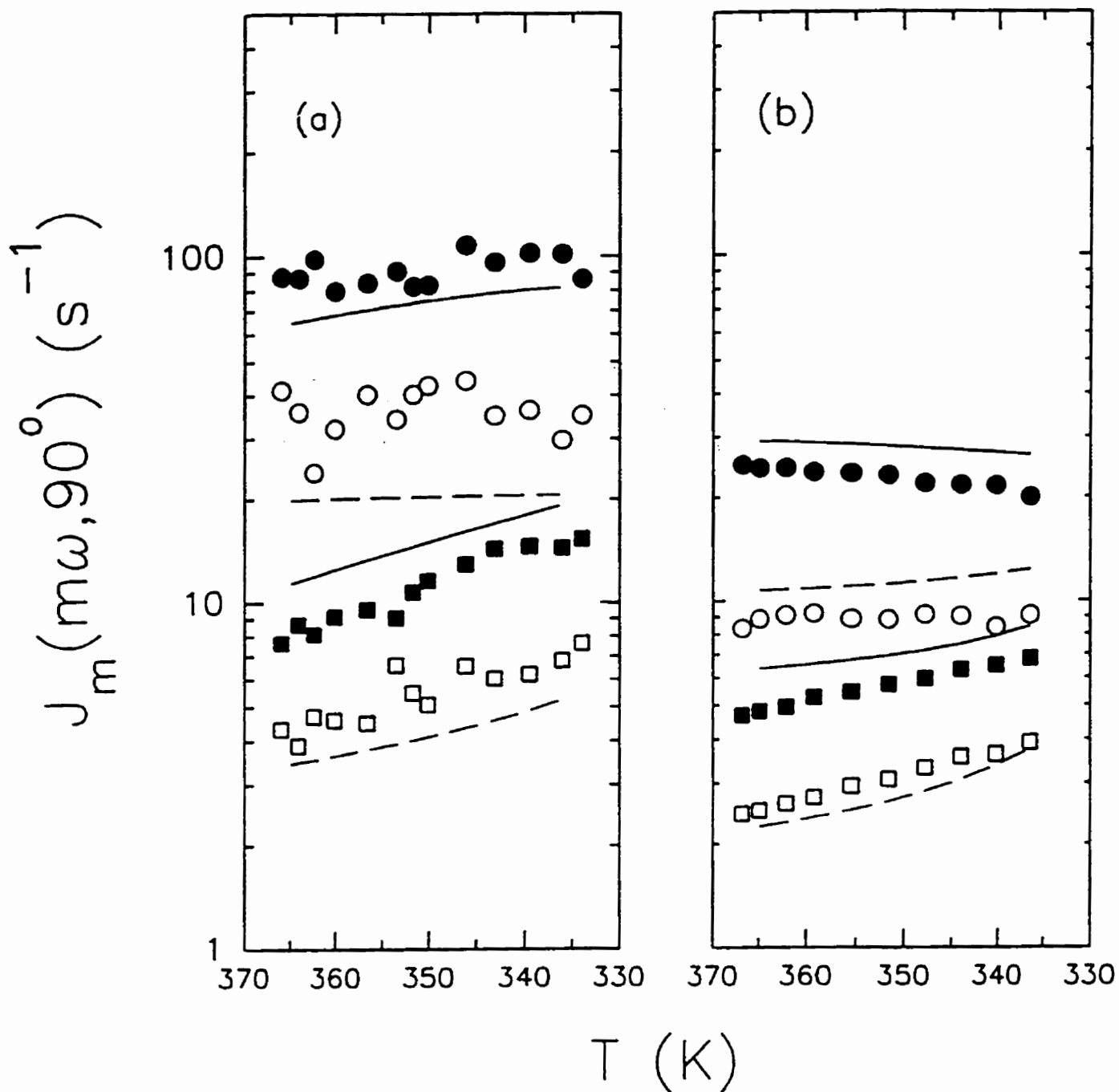
Figure 10.6 Plots of experimental (symbols) and calculated (lines) spectral densities of HAT6. Figure (a) and (b) are for data obtained at 15.1 and 46 MHz. The open symbols denote $J_1(\omega_0, 90°)$, while the closed symbols denote $J_2(2\omega_0, 90°)$. The $\bigcirc$s represent data for C_1, while the $\square$s represent data at C_{3-4}.
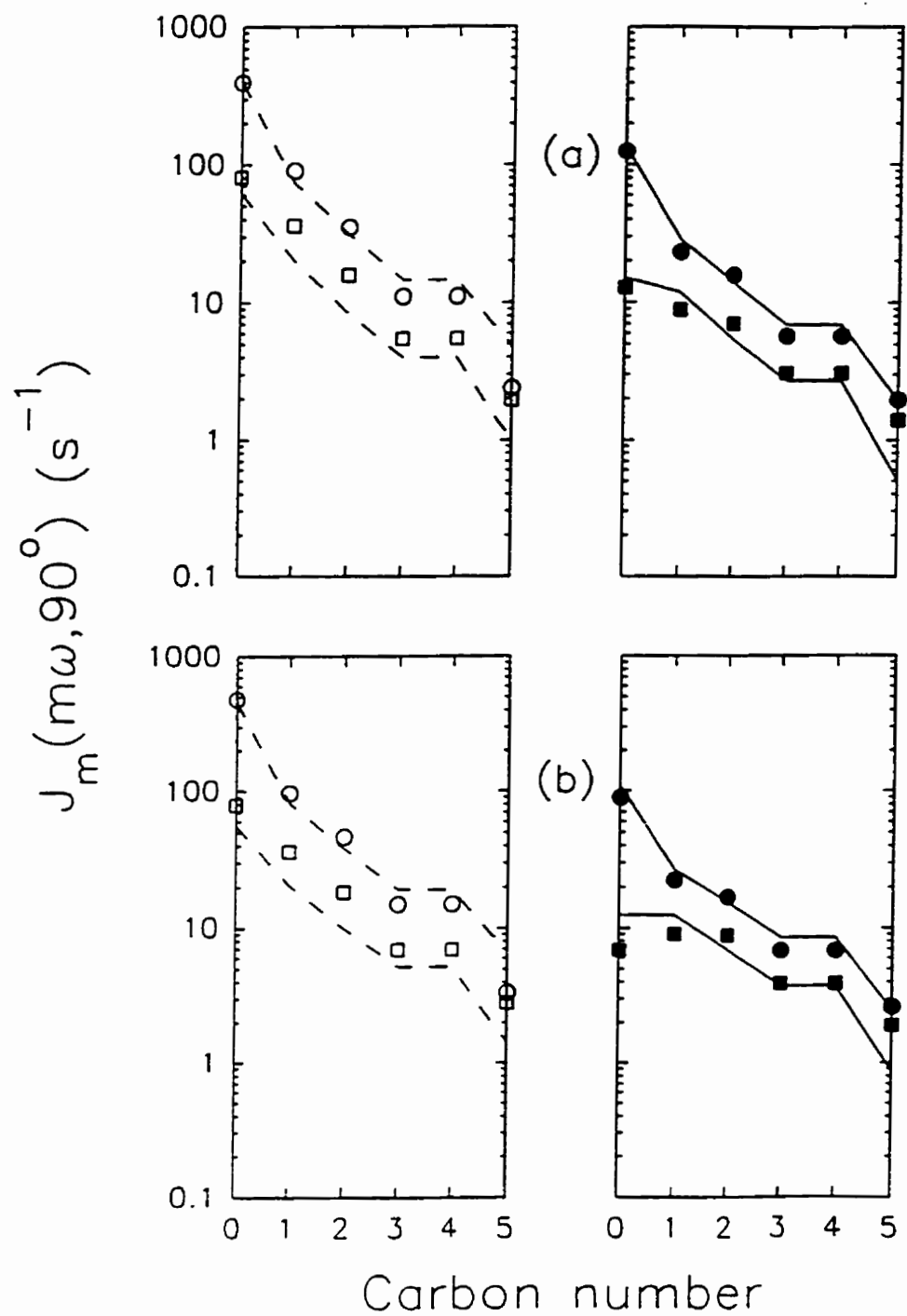
Figure 10.7 Plots of spectral densities as a function of carbon position at (a) 351.6 K and (b) 336.4 K. ◯ denotes $J_1(\omega_0, 90°)$, and □ denotes the corresponding $J_2(2\omega_0, 90°)$. Open and closed symbols denote data at 15.1 and 46 MHz, respectively.

$$D_- = D_-^0 \exp\left[-E_a^-/RT\right] \tag{10.5}$$

$$D_| = D_|^0 \exp\left[-E_a^|/RT\right] \tag{10.6}$$

$$k_2 = k_2^0 \exp\left[-E_a^{k_2}/RT\right] \tag{10.7}$$

In Eqs. (10.5)-(10.7), the global parameters are pre-exponentials D_-^0, $D_|^0$, k_2^0, and their corresponding activation energies E_a^-, $E_a^|$, $E_a^{k_2}$. For convenience, the diffusion and jump rate pre-exponentials are not used as global parameters. Rather Eqs. (10.5)-(10.7) are rewritten in terms of the activation energies and the diffusion and jump constants D_-', $D_|'$, k_2' at $T_{max} = 364.9$ K. When such a relation does not exist for a target parameter like k_1 or k_3, we model them by a linear relation:

$$k_i = k_i' - k_i''(T - T_{max}) \tag{10.8}$$

since its temperature dependence is weak. Here the global parameters k_i', and $k_i''(i = 1 \text{ or } 3)$ are optimized. The diffusion constants D_-', $D_|'$ and the jump constants k_1', k_2', k_3' at T_{max} were first obtained from an individual target analysis. Again AMOEBA was used in our minimization to fit the spectral density data. The sum squared percent error F is given by

$$F = \sum_k \sum_\omega \sum_i \sum_m \left[\frac{J_m^{(i)calc}(m\omega, 90°) - J_m^{(i)}(m\omega, 90°)}{J_m^{(i)}(m\omega, 90°)} \times 100\right]_k^2 \tag{10.9}$$

where the sum over k is for nine temperatures, ω for two frequencies, i for five methylene deuterons (and aromatic deuterons) and $m = 1$ or 2. The fitting quality factor Q is given by the percent mean-squared deviation

$$Q = \frac{\sum_k \sum_\omega \sum_i \sum_m \left[J_m^{(i)calc}(m\omega, 90°) - J_m^{(i)}(m\omega, 90°)\right]_k^2}{\sum_k \sum_\omega \sum_i \sum_m \left[J_m^{(i)}(m\omega, 90°)\right]_k^2} \times 100 \tag{10.10}$$
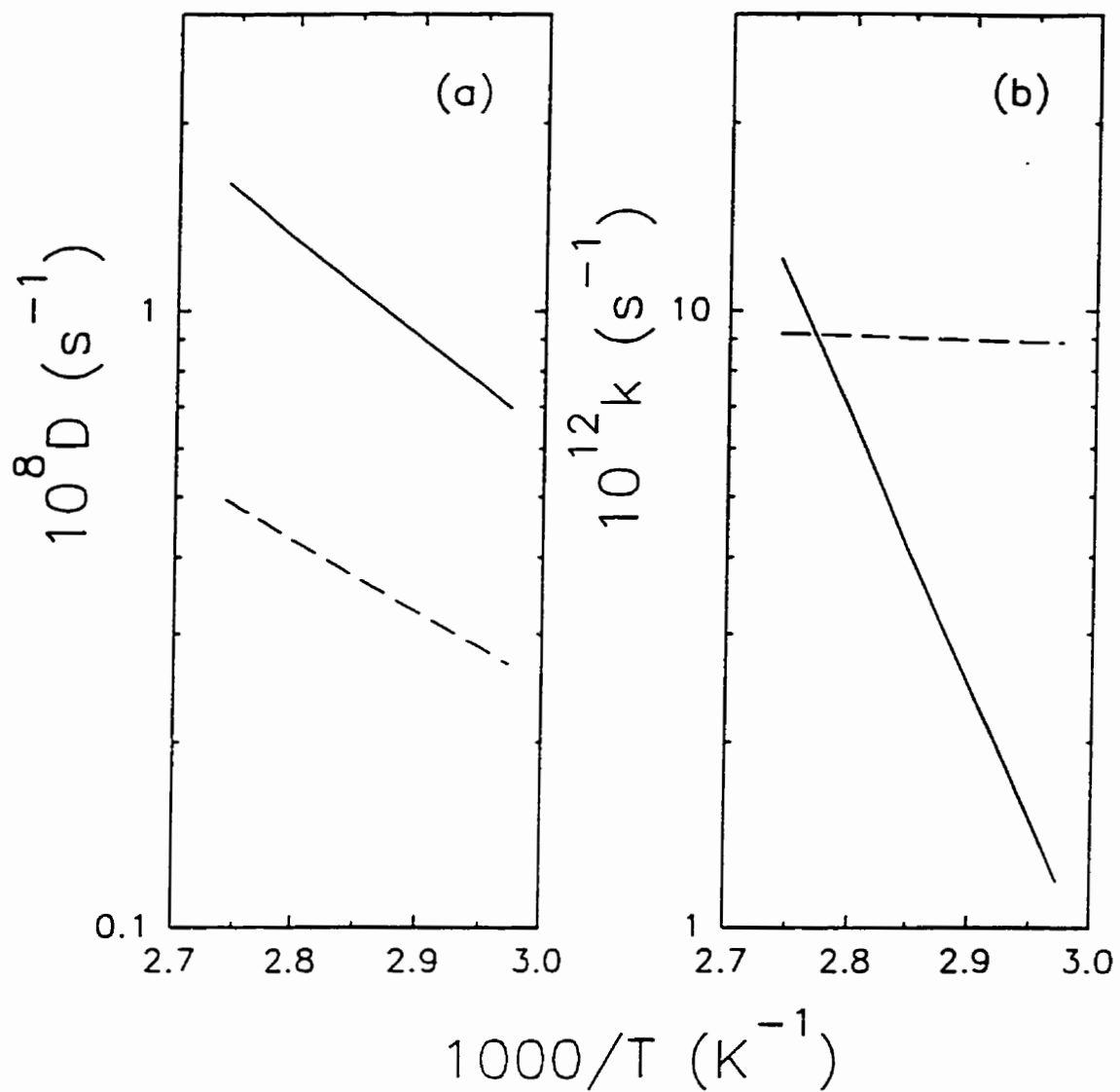
Figure 10.8 Plots of (a) rotational diffusion constants and (b) jump constants as a function of the reciprocal temperature. Solid lines denote $D_\perp$ in (a) and k_2 in (b), while dashed lines denote $D_\parallel$ in (a) and k_3 in (b).

Again the calculated spectral densities for C_3 and C_4 are quite different. However, we have averaged the calculated spectral densities at these two sites in our minimization. Because the ring $J_1(\simeq 90°)$ is larger than all the other spectral densities, we have adopted the strategy to first minimize the sum squared error (i.e. Q). As the global fit appeared to be insensitive to the E_a^- value, we have chosen to derive nine global parameters from a total of 432 spectral densities with several input E_a^- values. There was hardly any change in the Q value when varying E_a^- between 10 and 30 kJ/mol. Thus we have chosen the value $E_a^- = 30$ kJ/mol, simply because it was slightly larger than the derived $E_a^\parallel$ of 22.0 ± 0.6 kJ/mol. By minimizing Q, a better fit of the ring data was achieved. We then used the derived motional parameters for the molecular reorientation, and minimized F using only the methylene data to get the jump constants. We summarize the rotational diffusion constants in Figure 10.8(a). It is interesting to note from this figure that the rotational diffusion constant D_- is larger than $D_\parallel$ in the entire columnar phase of HAT6. This is quite different from calamitic liquid crystals in which the spinning motion is much faster than the tumbling motion. Although, from the first view, the fast tumbling motion in the disc plane would be rather disruptive of the column structure. However, the values of rotational diffusion constants D_- are around 10^8 s^{-1}, an order of magnitude smaller than the diffusion constants of the typical spinning motion of rod-like molecules. This may suggest that the columns are in a dynamic equilibrium state; the tumbling motion of the individual disc may be relatively fast, which impedes and slows down the spinning motion of the disc. The jump constant k_1 is essentially independent of the temperature ($k_1 = 5 \times 10^{12}$ s^{-1}) and describes the fast one-bond motion of the last C-C bond in the chain. The k_2 and k_3 are given as a function of temperature in Figure 10.8(b). As seen in the figure, k_3 decreases very slightly with decreasing temperature. The activation energy for the two-bond motion is $E_a^{k_2} = 83.6$ kJ/mole. Its error limits range between 39 kJ/mol (for 13 % increase in F) to 88.7 kJ/mol. The error limit for a

165

particular global parameter was estimated by varying the one under consideration while keeping all other global parameters identical to those used for the minimum F (or Q), to give an approximate doubling in the Q value (e.g. $E_a^{\parallel}$) or in the F value (e.g. k_1', $E_a^{k_2}$). When the target parameter becomes insensitive in the calculation, a lower % in F was used. Now the pre-exponentials in Eqs. (10.5)-(10.7) are $D_-^0 = 3.17 \times 10^{12}$ s^{-1}, $D_{\parallel}^0 = 7.05 \times 10^{10}$ s^{-1} and $k_2^0 = 1.1 \times 10^{25}$ s^{-1}. The uncertainty in $D_{\parallel}^0$ is 5.6 - 8.5 $\times 10^{10}$ s^{-1} and in D_-^0 is between 5 $\times 10^{11}$ s^{-1} and 1.1 $\times 10^{13}$ s^{-1}. We note that at the low D_-^0 limit, the $D_{\parallel}/D_-$ ratio is about 2. The error limits for k_2^0 are between 1.9 $\times 10^{24}$ s^{-1} and 1 $\times 10^{28}$ s^{-1} (for 13 % increase in F). At T_{max}, $k_1' = 5.0 \times 10^{17}$ s^{-1} and $k_3' = 9.19 \times 10^{12}$ s^{-1}. The error bar for k_3' ranges between 4.25 $\times 10^{12}$ s^{-1} to 2.4 $\times 10^{14}$ s^{-1}. While any larger k_1' value does not affect the fit, its lower limit is found to be 2 $\times 10^{12}$ s^{-1}. Finally, the calculated spectral densities for HAT6 ($Q = 0.67$ %) are indicated by curves in Figures 10.5 and 10.6. Although the final Q value is quite small, there exist systematic deviations between calculated and experimental spectral densities. The predicted site dependences of various spectral densities at two temperatures are also shown in Figure 10.7.

10.4 Conclusion

A consistent interpretation of both the quadrupolar splittings and the spin-lattice relaxation data measured in the columnar phase of two differently deuterated HAT6 molecules have been given . From modeling the splittings with the AP method, the orienting potential needed to describe the reorientational dynamics of molecular disks is obtained. It is clear that the tumbling motion of a disk can be slightly faster than its spinning motion. Both jump constants for one- and three-bond motions are nearly independent of temperature, while the jump constant for two-bond motion is

thermally activated. The relative reorientation of the disc-like cores and their time dependence could play an important role in the charge transport in this type of materials. Given the rotational diffusion constants are of the order of 10^8 s^{-1}, the packing of molecular disks within a column must be viewed as a state of high dynamic mobility. The decoupled model proposed by Dong for correlated internal rotations has been applied for the first time to a discotic liquid crystal. To understand the large mobility anisotropy observed for charge carrier along and perpendicular to the column, one may speculate that the electronic transport through the insulating chain regions is further hampered by the very fast one-bond motion (k_1) at the end of alkyl chains in HAT6.

References

10.1 S. Chandrasekhar and G. S. Raganath, Rep. Prog. Phys. **53**, 57 (1990).

10.2 N. Boden, R. Bissell, J. Clements, and B. Movaghar, Current Science, **71**, 599 (1996).

10.3 R.Y. Dong, D. Goldfarb, M. Moseley, Z. Luz and H. Zimmermann, J. Phys. Chem. **88**, 3118 (1984).

10.4 D. Goldfarb, Z. Luz, and H. Zimmermann, J. Phys. (Paris) **42**, 1303 (1981).

10.5 D. Goldfarb, Z. Luz, and H. Zimmermann, J. Chem. Phys. **78**, 7065 (1983).

10.6 D. Goldfarb, R. Y. Dong, Z. Luz and H. Zimmermann, Mol. Phys., **54**, 1185 (1985).

10.7 P. L. Nordio and P. Busolin, J. Chem. Phys. **55**, 5485 (1971); P. L. Nordio, G. Rigatti, and U. Segre, J. Chem. Phys., **56**, 2117 (1972).

10.8 G. M. Richards and R.Y. Dong, Liq. Crys. **5**, 1011 (1989).

10.9 G. Q. Cheng and R. Y. Dong, J. Chem. Phys. **89**, 3308 (1988).

10.10 R. Y. Dong, Phys. Rev. A **43**, 4310 (1991).

10.11 R. Tarroni and C. Zannoni, J. Chem. Phys. **95**, 4550 (1991).

10.12 P.J. Flory, *Statistical Mechanics of Chain Molecules* (Interscience, New York, 1969).

10.13 R. Y. Dong, "Nuclear Magnetic Resonance of Liquid Crystals", 2nd edition, (Springer-Verlag, N.Y., 1997).

10.14 C. J. R. Counsell, Ph.D. thesis, Southampton (1983).

10.15 C. J. R. Counsell, J. W. Emsley, G. R. Luckhurst, H. S. Sachdev, Mol. Phys. 63, 33 (1988).

Chapter 11

Conclusions

Nuclear spin relaxation measurements can be used to study the molecular dynamics in liquid crystals. The global target analysis approach was used throughout this thesis. It had been shown to produce more reliable model parameters, and was particularly useful when the target model parameters were strongly correlated and/or affected by large statistical errors. The TZ model (proposed by Tarroni and Zannoni) is proven to be very useful in interpreting the deuteron relaxation of biaxial molecules in the uniaxial medium. The director fluctuation, up to second-order contributions, was used where applicable. The molecular mean field theory based on the additive potential (AP) method had been adopted to interpret the order parameter profiles of flexible chains. By modeling the quadrupolar splittings using the AP method, we obtained the orienting potential needed to describe the reorientational dynamics of molecules in the samples studied. In addition, the equilibrium probabilities of all conformers for the flexible chain were determined. These were required in the decoupled model (proposed by Dong) for correlated internal rotations. Both the rod-like and discotic liquid crystals were treated by the decoupled model to give reasonable dynamical parameters.
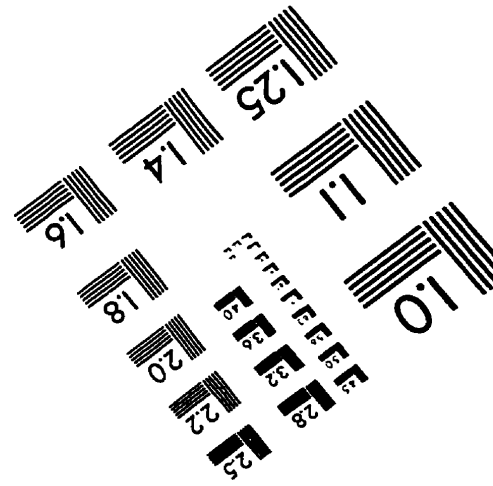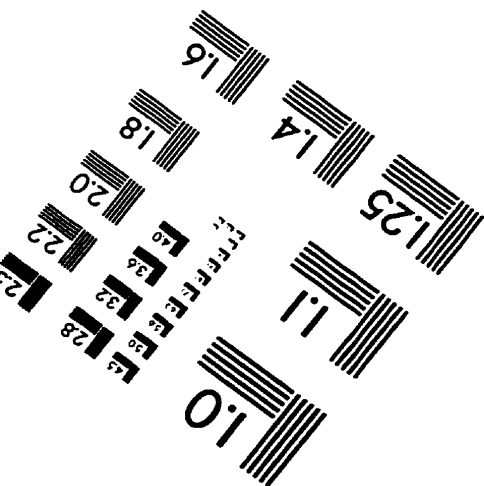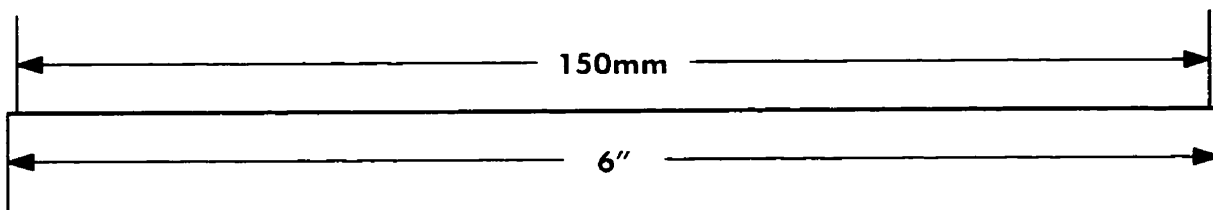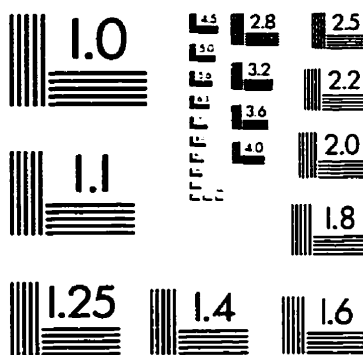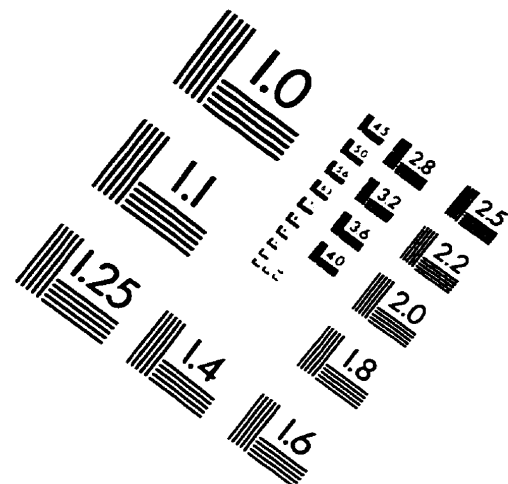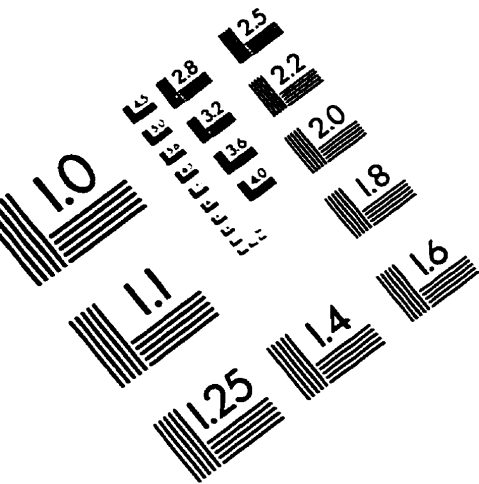
In Chapter 7, it is shown that a model which includes director fluctuations and rotational diffusion of an asymmetric rigid rotor in a biaxial potential of mean torque can efficiently unravel the molecular dynamics of 5O.7 in the nematic and smectic A phases. In addition, the relaxation data allow us to determine the molecular biaxial parameters: ξ, a measure of the deviation from cylindrical symmetry of the molecule, and ϵ, the asymmetry parameter of the rotational diffusion tensor. Both are found negative for the 5O.7 molecule. That the activation energy E_a^- being larger than E_a^i for this molecule is a significant finding from spin relaxation of liquid crystals. It is normally assumed that director fluctuations show a high value for the high-frequency cutoff ($\omega_c \simeq 200$MHz). This high value compared to our Larmor frequencies (15-46 MHz) would result in a significant director fluctuation contribution to $J_1(\omega)$ in the first order approximation, and appears true in the 5O.7 sample. However, this is not the case in the MBBA sample. In Chapter 8, the zero-frequency spectral densities $J_0(0)$ derived from T_1 and T_2 relaxation data in the nematic phase of MBBA support the idea that MBBA has a relatively low value for the high-frequency cutoff (around 3-10 MHz). It is found that director fluctuations have larger effects on $J_0^{(i)}(0)$ (35%-50%) than on $J_1^{(i)}(\omega)$ ($< 10\%$), which is due to the fact that the director fluctuation contribution to $J_0(0)$ has mainly a second-order component, whereas the first-order contribution to $J_1(\omega)$ is suppressed in the limit $\omega_c < \omega$. A consistent interpretation of both the quadrupolar splitting and spin-lattice relaxation data of the pure 6OCB and 6OCB/8OCB mixture is given in Chapter 9. It is shown that the tumbling motion of 6OCB molecule is much slower than its spinning motion, and in comparison with the 6OCB sample, it is strongly hindered in the 6OCB/8OCB mixture. The jump rate k_3 in the S_A/RN region of the mixture is close to that of pure 6OCB, which may indicate that the dimer structure of 6OCB/8OCB mixture is "loose" in the low temperature phases, i.e., similar to

171

"loose" dimer or monomer structure in the pure 6OCB sample. In Chapter 10, a similar study in the columnar phase of discotic HAT6 molecules is presented. It is found the tumbling motion of a disk can be slightly faster than its spinning motion. Given the rotational diffusion constants are of the order of $10^8 \ s^{-1}$, the packing of molecular disks within a column must be viewed as a state of high dynamic mobility. This state of high dynamic mobility within the column has implications to application of HAT6 in developing electric devices.

Finally, we summarize what new findings are obtained from the liquid crystalline samples in the thesis. The molecular reorientation of 5O.7 liquid crystal samples are treated as "rigid" rotors by applying the TZ model, and the fitting is improved in comparison with that using the Nordio's model. Thus, 5O.7 molecules are biaxial rather than uniaxial as assumed by the earlier reports. For MBBA, the high-frequency cutoff was found quite low, around 3-10 MHz. This is a new discovery regarding this sample. In this thesis, it is shown that the zero frequency component $J_0(0)$ from the spin-spin relaxation time measurement provides a means of probing director fluctuations in samples of low high-frequency cutoff. The decoupled model for correlated internal chain motions was used before for shorter molecules like MBBA(1O.4) and 5CB. In the present study, the 6OCB molecule has a slightly longer chain and also an oxygen site, which is different from the carbon site. As a result, the usefulness of the decoupled model is further proven for 6OCB and 6OCB/8OCB mixture. The picture of "loose" dimer in the low temperature phases of 6OCB/8OCB mixture has been qualitatively addressed here using the NMR experiment data. The decoupled model is used for the first time to the columnar liquid crystal phase of a discotic sample. Thus, the decoupled model is not only suitable for rod-like molecules, but also for disk-like molecules. The different forms of interaction tensor for disk-like core and cigar-shaped C-C segment are introduced in this

172

study. and proven valid. Some pre-exponentials for jump constants (e.g. k_1^0 in MBBA. k_2^0 in HAT6) seem too large. since it would be difficult to rationalize these high values in term of the "collision" frequency in the thermal process. Further studies of other liquid crystals are required to shed light on this point. This thesis represents. to our knowledge. a first quantitative study of long flexible molecules in liquid crystals using deuteron NMR spin relaxometry.

IMAGE EVALUATION
TEST TARGET (QA-3)

150mm

6"